Molecular Design, Self-Assembly, and Material Properties of Silk-Like Protein Polymers

Lennart Harm Beun

Thesis committee

Promotor

Prof. Dr M.A. Cohen Stuart

Emeritus Professor of Physical Chemistry & Colloid Science

Wageningen University

Co-promotor

Dr R.J. de Vries

Associate professor, Laboratory of Physical Chemistry & Colloid Science

Wageningen University

Other members

Prof. Dr J.H. Bitter, Wageningen University

Prof. Dr G.H. Koenderink, FOM Institute AMOLF, Amsterdam, The Netherlands

Prof. Dr A.E. Rowan, Radboud University Nijmegen, The Netherlands

Dr I.K. Voets, Eindhoven University of Technology, The Netherlands

This research was conducted under the auspices of the Graduate School VLAG (Advanced studies in Food Technology, Agrobiotechnology, Nutrition and Health Sciences).

Molecular Design, Self-Assembly, and Material Properties of Silk-Like Protein Polymers

Lennart Harm Beun

Thesis

submitted in fulfilment of the requirements for the degree of doctor

at Wageningen University

by the authority of the Rector Magnificus

Prof. Dr M.J. Kropff,

in the presence of the

Thesis Committee appointed by the Academic Board

to be defended in public

on Friday 13th of March 2015

at 4 p.m. in the Aula.

Lennart Harm Beun

Molecular Design, Self-Assembly, and Material Properties of Silk-Like Protein Polymers

166 pages.

PhD thesis, Wageningen University, Wageningen, NL (2015)

With references, with summaries in English and Dutch

ISBN: 978-94-6257-233-1

CONTENTS

Chapter 1

General Introduction

RECOMBINANT PROTEIN POLYMERS

The holy grail of polymer chemistry has always been a perfect control over polymer size, sequence and stereochemistry. This perfect control over size and chemistry leads to a maximum control over the desired properties of the produced polymers. And although the continuing work in the field of polymer chemistry has led to better controlled polymerization methods, any established polymerization method still yields a (more or less) polydisperse population of polymers.

Natural evolution did succeed in producing a polymerization method with virtually perfect control over size and stereochemistry of the polymers. The expression of proteins from a DNA template inside living cells is a process that yields a perfectly monodisperse population of these proteins. These proteins can be considered polymers with amino acids as building blocks. Since the emergence of the field of molecular biology, this cellular machinery can be used to produce proteins with a well-defined size and stereochemistry.

The early developments in the field of genetic engineering led to interspecies transfer of existing genes [1, 2]. The bacterial production of human insulin was the first major commercial success story in this field. This use of existing genes to produce natural proteins in high quantities was followed by the exploration of producing entirely new proteins or polypeptides, by adjusting or combining genes, or by creating entirely new ones. This way, properties of multiple existing proteins could be altered or combined to obtain novel molecules with exciting properties.

Currently, the state of the art technology provides the possibility to create genes that code for any desired amino acid sequence, thus any desired primary protein structure. Most scientists however, choose to make use of the plethora of natural proteins as inspiration for the design of new amino acid based polymers. These bio-inspired recombinant proteins are designed to combine desirable structural, stimulus-responsive and enzymatic parts of existing

proteins. As these new molecules are produced biologically, and are protein based, intuitively they are interesting candidates to be used in biological systems, such as the biomedical field. When only looking at proteins with interesting structural properties, there are many candidates to be used as inspiration. One of these proteins is collagen, an abundant protein in the extracellular matrix (ECM), that is a major element in the mechanical properties of tendons, cartilage and bones [3]. Actin is another structural protein that is abundant in biological systems. It is the key element of the cytoskeleton of cells and therefore dominates the mechanical properties of the cell [4-6]. Fibrin is a protein that is responsible for blood clotting, by forming cross-linked insoluble structures [7]. The protein elastin is an important structural element of connective tissues, giving them elastic properties [8, 9]. Resilin is a highly elastic protein that can be found in many insects [10-15]. Silk proteins from spiders [16, 17] or of silk worms (*Bomby mori*) [18-20] and mussel byssal threads [21-23] are examples of structural proteins that are excreted and perform their roles outside the organism.

These examples of structural natural proteins have been used extensively as inspiration for the development of recombinant proteins [24]. These recombinant versions can either be a modified version of the natural protein or a combination of structural elements of different proteins [25-39]. This way, different structural and stimulus-responsive properties can be combined in one molecule.

In our research, we use silk-like proteins as inspiration for new protein based materials. Natural silk proteins have the interesting property of folding and assembling into supramolecular structures. The production of recombinant silk-like proteins was pioneered by the groups of Ferrari [40] and Tirrell [41-43]. Ferrari introduced the term ‘protein polymer’ to describe these biosynthetic molecules. Tirrell was the first one to produce protein polymers with the silk-like octapeptide (GAGAGAGE) as the building block. The abundant presence of glycine (G) and alanine (A) in this block is responsible for the formation of crystalline

domains in natural silk. The presence of the acidic amino acid glutamic acid (E) makes the block pH-responsive; the pH of the solution determines the charge of the octapeptide.

This octapeptide was incorporated in amphiphilic molecules, by combining it with PEG-chains [27-30]. In our group, this octapeptide repeat was incorporated in fully protein based polymers with triblock conformations [34, 44]. A protein polymer with an amphiphilic nature was created by incorporating a hydrophilic block, that behaves as a random coil under a wide range of aqueous solvent conditions [45, 46]. At pH-conditions where the silk-like block is uncharged, these protein polymers self-assemble into fibrils. At high enough concentrations, these fibrils form the structural elements of a hydrogel [47]. An example of the mechanism of self-assembly of such amphiphilic molecules into ordered structures is presented in Figure 1.1.

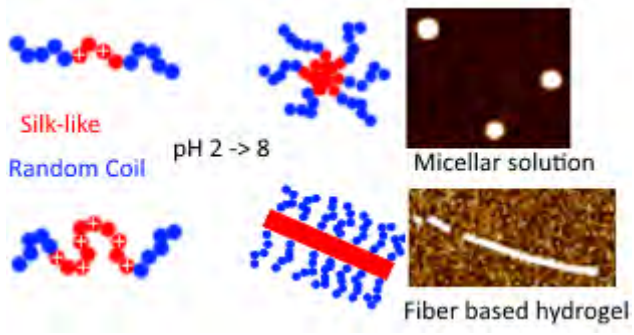

Figure 1.1: Route of self-assembly of protein polymers into ordered structures

PROTEIN BASED HYDROGELS AS ECM MIMICS

Protein based materials, especially the ones that are produced in a biological process, are likely to be biocompatible. These materials are therefore promising candidates for use in biomedical applications, such as tissue engineering or regenerative medicine [48]. One of the key challenges in the biomedical field is to mimic the extracellular matrix (ECM) [49]. The natural ECM is a complex hydrogel that is mainly composed of fibrous protein structures. As silk-like protein polymers self-assemble into fibrous structures that form hydrogels, they are good candidates as structural elements of an ECM mimic.

Just like in the natural ECM, structural support of any ECM mimic should be combined with an open structure, that allows cells to migrate and form 3D tissues. This combination of structural support and porosity is key when designing the basis of an ECM mimic. The role of the natural ECM is not only that of structural support of cells. The ECM is also imperative in signaling, anchoring cells and directing cell functions through specific matrix-cell interactions. Any peptide based interacting element of the protein fiber structures can be incorporated in recombinant protein polymers in a relatively simple way by changing the DNA template.

AIM AND OUTLINE OF THIS THESIS

In this thesis we report on several protein polymers, that all consist of silk-like and random coil blocks. The silk-like block consists of variable numbers of repeats of the octapeptide GAGAGAGX (S^X_n). The amino acid at position X is chosen to be pH-responsive. It is occupied by the acidic glutamic acid (E), or the alkaline histidine (H) or lysine (K). The random coil block has a basic building block (C) that consists of 99 predominantly hydrophilic amino acids. This block can be present as monomer or multimer (C_1, C_2 or C_4). An overview of all protein polymers that we report on is given in Table 1.1.

Table 1.1: Overview of different protein polymers studied in this thesis.

Telechelic (Ch. 2)	Varying Silk-Like Block (Ch. 3 & 4)	Varying Random Coil Block (Ch. 5)
$S^E_{24}C_4S^E_{24}$	$C_2S^H_8C_2$	$C_1S^H_{48}$
$S^H_{24}C_4S^H_{24}$	$C_2S^H_{16}C_2$	$C_2S^H_{48}$
$S^K_{24}C_4S^K_{24}$	$C_2S^H_{24}C_2$	$C_2S^H_{48}C_2$
	$C_2S^H_{48}C_2$	

In chapter 2 and 3 we report on the molecular mechanism of self-assembly of triblock structured protein polymers consisting of these blocks. Chapter 2 deals with self-assembly of telechelic $S^X_{24}C_4S^X_{24}$ protein polymers. We report on three protein polymers that are all pH-responsive, due to acidic or alkaline amino acid residues in the silk-like block. All proteins self-assemble into fibrils at pH-values at which the silk-like block is charge neutral. Interestingly, we find that nucleation of this self-assembly seems to be heterogeneous; initial fast nucleation is followed by elongation of these self-assembling structures without the formation of new fibrils. This mechanism leads to very monodisperse populations of self-

assembled fibrils. In chapter 3 we use super resolution microscopy to study the self-assembly of $C_2S^H_{48}C_2$ protein polymers. Unlike their telechelic counterparts ($S^X_{24}C_4S^X_{24}$), these proteins show a continuous nucleation during self-assembly, leading to a broad size distribution of fibrils. Much to our surprise, the fibrils self-assemble unidirectionally; they only grow from one end. As the building blocks of these fibrils are rather symmetrical, this asymmetrical behavior was unexpected. We further show that the protein polymers, once folded and stacked inside a fibril, are kinetically trapped and don't exchange with protein polymers in the bulk solution on a timescale of days.

In chapters 4 and 5 we report on protein polymers with differently sized silk-like and random coil blocks. In chapter 4, we study 4 protein polymers that have identically sized outer random coil blocks. The size of the central silk-like block is varied. We see that within this series there is a transition from self-assembled fibrils, for the largest silk-like blocks, to micelles for the smallest silk-like blocks. These different microscopic structures have very different secondary structures. Even the smallest silk-like blocks have an intrinsic tendency to self-assemble into fibrils, which we visualize by showing fibril formation after partially degrading the stabilizing random coil block. In chapter 5 we keep the size of the silk-like block constant, but we vary the size of the hydrophilic random coil block. Individual fibril dimensions and secondary structure are very similar for all protein polymers. We do however see a change in mechanical properties of the formed hydrogels. A smaller random coil block promotes attractive fibril-fibril interaction; fibrils start to bundle together. The formed hydrogel is much stiffer; it behaves as a physically cross-linked gel with a strong concentration dependence of the modulus.

In chapter 6 we summarize our work, followed by a discussion on interesting follow-up research on our protein polymers. We finalize our work with an outlook on the applications of biomimetic protein polymers, such as ours, in the biomedical field.

REFERENCES

1. Jackson, D. A.; Berg, P.; Symons, R. H., Biochemical Method for Inserting New Genetic Information into DNA of Simian Virus 40 - Circular Sv40 DNA Molecules Containing Lambda Phage Genes and Galactose Operon of Escherichia-Coli. *P Natl Acad Sci USA* **1972,** 69, (10), 2904-&.
2. Jaenisch, R.; Mintz, B., Simian Virus 40 DNA Sequences in DNA of Healthy Adult Mice Derived from Preimplantation Blastocysts Injected with Viral DNA. *P Natl Acad Sci USA* **1974,** 71, (4), 1250-1254.
3. Traub, W.; Yonath, A.; Segal, D. M., On Molecular Structure of Collagen. *Nature* **1969,** 221, (5184), 914-&.
4. Karakozova, M.; Kozak, M.; Wong, C. C. L.; Bailey, A. O.; Yates, J. R.; Mogilner, A.; Zebroski, H.; Kashina, A., Arginylation of beta-actin regulates actin cytoskeleton and cell motility. *Science* **2006,** 313, (5784), 192-196.
5. Condeelis, J., Direct Role for Actin Cytoskeleton in Mobility of Cell-Surface Receptors. *J Cell Biol* **1978,** 79, (2), 263-263.
6. Gardel, M. L.; Shin, J. H.; MacKintosh, F. C.; Mahadevan, L.; Matsudaira, P.; Weitz, D. A., Elastic Behavior of cross-linked and bundled actin networks. *Science* **2004,** 304, (5675), 1301-1305.
7. Doolittle, R. F., Fibrinogen and Fibrin. *Annu Rev Biochem* **1984,** 53, 195-229.
8. Hoeve, C. A. J.; Flory, P. J., The Elastic Properties of Elastin. *J Am Chem Soc* **1958,** 80, (24), 6523-6526.
9. Gosline, J. M.; French, C. J., Dynamic Mechanical-Properties of Elastin. *Biopolymers* **1979,** 18, (8), 2091-2103.
10. Weisfogh, T., Molecular Interpretation of Elasticity of Resilin, a Rubber-Like Protein. *J Mol Biol* **1961,** 3, (5), 648-&.
11. Elliott, G. F.; Huxley, A. F.; Weisfogh, T., On Structure of Resilin. *J Mol Biol* **1965,** 13, (3), 791-&.
12. Burrows, M.; Sutton, G. P., Locusts use a composite of resilin and hard cuticle as an energy store for jumping and kicking. *J Exp Biol* **2012,** 215, (19), 3501-3512.
13. Renner, J. N.; Cherry, K. M.; Su, R. S. C.; Liu, J. C., Characterization of Resilin-Based Materials for Tissue Engineering Applications. *Biomacromolecules* **2012,** 13, (11), 3678-3685.
14. Li, L.; Kiick, K. L., Resilin-Based Materials for Biomedical Applications. *Acs Macro Lett* **2013,** 2, (8), 635-640.
15. Su, R. S. C.; Kim, Y.; Liu, J. C., Resilin: Protein-based elastomeric biomaterials. *Acta Biomaterialia* **2014,** 10, (4), 1601-1611.
16. Cranford, S. W.; Tarakanova, A.; Pugno, N. M.; Buehler, M. J., Nonlinear material behaviour of spider silk yields robust webs. *Nature* **2012,** 482, (7383), 72-U91.
17. Porter, D.; Guan, J.; Vollrath, F., Spider Silk: Super Material or Thin Fibre? *Adv Mater* **2013,** 25, (9), 1275-1279.
18. Akai, H.; Kobayash.M, Sites of Fibroin Formation in Silk Gland in Bombyx Mori. *Nature* **1965,** 206, (4983), 529-&.
19. Sprague, K. U., Bombyx-Mori Silk Proteins - Characterization of Large Polypeptides. *Biochemistry-Us* **1975,** 14, (5), 925-931.
20. Rockwood, D. N.; Preda, R. C.; Yucel, T.; Wang, X. Q.; Lovett, M. L.; Kaplan, D. L., Materials fabrication from Bombyx mori silk fibroin. *Nat Protoc* **2011,** 6, (10), 1612-1631.
21. Vitellarozuccarello, L.; Debiasi, S.; Bairati, A., The Ultrastructure of the Byssal Apparatus of a Mussel .5. Localization of Collagenic and Elastic Components in the Threads. *Tissue Cell* **1983,** 15, (4), 547-554.

22. Hagenau, A.; Scheibel, T., Towards the Recombinant Production of Mussel Byssal Collagens. *J Adhesion* **2010,** 86, (1), 10-24.
23. Gantayet, A.; Ohana, L.; Sone, E. D., Byssal proteins of the freshwater zebra mussel, Dreissena polymorpha. *Biofouling* **2013,** 29, (1), 77-85.
24. van Hest, J. C. M.; Tirrell, D. A., Protein-based materials, toward a new level of structural control. *Chem Commun* **2001**, (19), 1897-1904.
25. Jin, H. J.; Fridrikh, S. V.; Rutledge, G. C.; Kaplan, D. L., Electrospinning Bombyx mori silk with poly(ethylene oxide). *Biomacromolecules* **2002,** 3, (6), 1233-1239.
26. Altman, G. H.; Diaz, F.; Jakuba, C.; Calabro, T.; Horan, R. L.; Chen, J. S.; Lu, H.; Richmond, J.; Kaplan, D. L., Silk-based biomaterials. *Biomaterials* **2003,** 24, (3), 401-416.
27. Smeenk, J. M.; Ayres, L.; Stunnenberg, H. G.; van Hest, J. C. M., Polymer protein hybrids. *Macromol Symp* **2005,** 225, 1-8.
28. Smeenk, J. M.; Lowik, D. W. P. M.; van Hest, J. C. M., Peptide-containing block copolymers: Synthesis and potential applications of bio-mimetic materials. *Curr Org Chem* **2005,** 9, (12), 1115-1125.
29. Smeenk, J. M.; Otten, M. B. J.; Thies, J.; Tirrell, D. A.; Stunnenberg, H. G.; van Hest, J. C. M., Controlled assembly of macromolecular beta-sheet fibrils. *Angew Chem Int Edit* **2005,** 44, (13), 1968-1971.
30. Schon, P.; Smeenk, J. M.; Speller, S.; Heus, H. A.; van Hest, J. C. M., AFM studies of beta-sheet block copolymers at solid surfaces: High-resolution structures and aggregation dynamics. *Aust J Chem* **2006,** 59, (8), 560-563.
31. Daamen, W. F.; Veerkamp, J. H.; van Hest, J. C. M.; van Kuppevelt, T. H., Elastin as a biomaterial for tissue engineering. *Biomaterials* **2007,** 28, (30), 4378-4398.
32. Huang, J.; Foo, C. W. P.; Kaplan, D. L., Biosynthesis and applications of silk-like and collagen-like proteins. *Polym Rev* **2007,** 47, (1), 29-62.
33. Werten, M. W. T.; Moers, A. P. H. A.; Vong, T.; Zuilhof, H.; van Hest, J. C. M.; de Wolff, F. A., Biosynthesis of an amphiphilic silk-like polymer. *Biomacromolecules* **2008,** 9, (7), 1705-1711.
34. Martens, A. A.; Portale, G.; Werten, M. W. T.; de Vries, R. J.; Eggink, G.; Stuart, M. A. C.; de Wolf, F. A., Triblock Protein Copolymers Forming Supramolecular Nanotapes and pH-Responsive Gels. *Macromolecules* **2009,** 42, (4), 1002-1009.
35. Skrzeszewska, P. J.; de Wolf, F. A.; Werten, M. W. T.; Moers, A. P. H. A.; Stuart, M. A. C.; van der Gucht, J., Physical gels of telechelic triblock copolymers with precisely defined junction multiplicity. *Soft Matter* **2009,** 5, (10), 2057-2062.
36. Nettles, D. L.; Chilkoti, A.; Setton, L. A., Applications of elastin-like polypeptides in tissue engineering. *Adv Drug Deliver Rev* **2010,** 62, (15), 1479-1485.
37. Koria, P.; Yagi, H.; Kitagawa, Y.; Megeed, Z.; Nahmias, Y.; Sheridan, R.; Yarmush, M. L., Self-assembling elastin-like peptides growth factor chimeric nanoparticles for the treatment of chronic wounds. *P Natl Acad Sci USA* **2011,** 108, (3), 1034-1039.
38. Schipperus, R.; Eggink, G.; de Wolf, F. A., Secretion of elastin-like polypeptides with different transition temperatures by Pichia pastoris. *Biotechnol Progr* **2012,** 28, (1), 242-247.
39. Silva, C. I. F.; Skrzeszewska, P. J.; Golinska, M. D.; Werten, M. W. T.; Eggink, G.; de Wolf, F. A., Tuning of Collagen Triple-Helix Stability in Recombinant Telechelic Polymers. *Biomacromolecules* **2012,** 13, (5), 1250-1258.
40. Cappello, J.; Crissman, J.; Dorman, M.; Mikolajczak, M.; Textor, G.; Marquet, M.; Ferrari, F., Genetic-Engineering of Structural Protein Polymers. *Biotechnol Progr* **1990,** 6, (3), 198-202.
41. Krejchi, M. T.; Atkins, E. D. T.; Waddon, A. J.; Fournier, M. J.; Mason, T. L.; Tirrell, D. A., Chemical Sequence Control of Beta-Sheet Assembly in Macromolecular Crystals of Periodic Polypeptides. *Science* **1994,** 265, (5177), 1427-1432.

42. Krejchi, M. T.; Atkins, E. D. T.; Fournier, M. J.; Mason, T. L.; Tirrell, D. A., Observation of a silk-like crystal structure in a genetically engineered periodic polypeptide. *J Macromol Sci Pure* **1996,** A33, (10), 1389-1398.
43. Krejchi, M. T.; Cooper, S. J.; Deguchi, Y.; Atkins, E. D. T.; Fournier, M. J.; Mason, T. L.; Tirrell, D. A., Crystal structures of chain-folded antiparallel beta-sheet assemblies from sequence-designed periodic polypeptides. *Macromolecules* **1997,** 30, (17), 5012-5024.
44. Martens, A. A.; van der Gucht, J.; Eggink, G.; de Wolf, F. A.; Stuart, M. A. C., Dilute gels with exceptional rigidity from self-assembling silk-collagen-like block copolymers. *Soft Matter* **2009,** 5, (21), 4191-4197.
45. Werten, M. W. T.; Van den Bosch, T. J.; Wind, R. D.; Mooibroek, H.; De Wolf, F. A., High-yield secretion of recombinant gelatins by Pichia pastoris. *Yeast* **1999,** 15, (11), 1087-1096.
46. Werten, M. W. T.; Wisselink, W. H.; van den Bosch, T. J. J.; de Bruin, E. C.; de Wolf, F. A., Secreted production of a custom-designed, highly hydrophilic gelatin in Pichia pastoris. *Protein Eng* **2001,** 14, (6), 447-454.
47. Golinska, M. D.; Wlodarczyk-Biegun, M. K.; Werten, M. W. T.; Stuart, M. A. C.; de Wolf, F. A.; de Vries, R., Dilute Self-Healing Hydrogels of Silk-Collagen-Like Block Copolypeptides at Neutral pH. *Biomacromolecules* **2014,** 15, (3), 699-706.
48. Maskarinec, S. A.; Tirrell, D. A., Protein engineering approaches to biomaterials design. *Curr Opin Biotech* **2005,** 16, (4), 422-426.
49. Geckil, H.; Xu, F.; Zhang, X. H.; Moon, S.; Demirci, U., Engineering hydrogels as extracellular matrix mimics. *Nanomedicine-Uk* **2010,** 5, (3), 469-484.

Chapter 2

Self-Assembly of Silk-Collagen-Silk-Like Triblock Copolymers Resembles a Supramolecular Living Polymerization

This chapter is published as: Beun, L. H.; Beaudoux, X. J.; Kleijn, J. M.; de Wolf, F. A.; Cohen Stuart, M. A., *Acs Nano* **2012,** 6, (1), 133-140.

ABSTRACT

We produced several pH-responsive silk-collagen-like protein polymers, one acidic and two alkaline. At pH-values where the silk-like block is uncharged the protein polymers self-assemble into fibrils. The pH-induced self-assembly was examined by atomic force microscopy, light scattering and circular dichroism. The populations of fibrils were found to be very monodisperse, indicating that the fibrils start to grow from already present nuclei in the sample. The growth then follows pseudo-first order kinetics for all examined proteins. When normalized to the initial concentration, the growth curves of each type of protein polymer overlap, showing that the self-assembly is a generic process for silk-collagen-silk triblock structured protein polymers, regardless of the nature of their chargeable groups. The elongation rate of the fibrils is slow, due to the presence of repulsive collagen-like blocks and the limited number of possibilities for an approaching protein polymer to successfully attach to a growing end. The formation of fibrils is fully reversible. Already present fibrils can start growing again by addition of new protein polymers in solution. The structure of all fibrils is very rich in β-turns, resulting in β-rolls. The silk-like core only attains this structure when attaching to a growing fibril.

INTRODUCTION

Fibrillar protein structures are widely studied and are important in many fields of research. They are crucial for several biological functions, [1, 2] play an important role in certain diseases [3, 4] and have a major influence on food structures.[5-7] Understanding the process of fibril formation is essential to be able to control their final size and shape and therefore their function. We developed a new class of stimulus-responsive biopolymers that can self-assemble into fibrillar structures. These biologically synthesized protein polymers form a monodisperse system with an exactly defined length and sequence, stored in one genetic template. These properties are superior to those achieved with any established chemical polymerization method.

In this chapter we present our experimental work on the self-assembly behavior of silk-collagen-like protein polymers into fibrillar structures. These protein polymers consist of a hydrophilic and inert random coil part (C_n), which is a multimer of a basic 99 amino acids long block; this block is very rich in glutamine, arginine, proline and serine. The chemical composition and the amino acid order (PXY triplets) resembles that of natural collagen. The block does not attain any secondary structure like natural collagen: it acts as a random coil under a variety of solvent conditions [8]. The second block is a silk-based part (S^X_n) that consists of repeats of an octapeptide $(GAGAGAGX)_n$. This repeat is known to self-assemble under certain conditions into a highly structured compact crystalline core. We use three different silk-like blocks, where the X position in the glycine- and alanine-rich octapeptide is taken by either glutamic acid (E), histidine (H) or lysine (K). This way we have three different silk-like blocks that are all pH-responsive, of which one is acidic (S^E) and two are alkaline (S^H and S^K). We produced triblock structured protein polymers, with silk blocks at the outside and the random coil block at the inside ($S^X_{24}C_4S^X_{24}$). Together with the three variants in silk-like

blocks, this gives us six different proteins. This chapter shows experimental results on the three silk-collagen-silk-like protein polymers, indicated in Table 2.1.

Table 2.1: Overview of different protein polymers described in this chapter.

	Silk-Collagen-Silk	pKa
Acidic	$S^{E}_{24}C_4S^{E}_{24}$	~4.1
Alkaline	$S^{H}_{24}C_4S^{H}_{24}$	~6.0
Alkaline	$S^{K}_{24}C_4S^{K}_{24}$	~10.5

Previous work showed that the histidine bearing protein polymer ($S^{H}_{24}C_4S^{H}_{24}$) self-assembles upon increasing the pH to a value higher than the pKa of histidine [9]. The glutamic acid bearing protein polymers show similar behavior at a pH below the pKa of the side group. The self-assembled protein polymers have a fibrillar structure with stacked β-rolls made up from the uncharged silk-like block and a dilute hydrophilic corona (loop) of the C-block [9]. These β-rolls are composed of two parallel β-sheets, oriented in opposite directions and connected *via* β-turns. This way hydrogen bonds can be formed within each parallel β-sheet and between the oppositely oriented β-sheets. These β-rolls differ from the anti-parallel β-sheets that are formed when crystallizing the silk-like domains in methanol or formic acid [10-13]. The combination of a silk-like domain and a random coil one can yield interesting properties. These bio-inspired protein polymers make use of the unique combination of flexibility and strength of silk [13-18] and the excellent biocompatibility of the collagenous random coil block, which has been widely studied as a basis for tissue engineering [19-22].

In this chapter we elucidate the self-assembly kinetics of three different silk-collagen-silk-like protein polymers. Using microscopy, light scattering and circular dichroism we

investigate the formation of supramolecular fibrils after charge neutralization. We use both acidic and alkaline pH-responsive protein polymers to study the self-assembly of the neutralized polymer under different pH-conditions. We look at the concentration dependence of the self-assembly process and at the structure of the different protein polymers in the self-assembled state. Furthermore, we look into the reversibility of the pH-induced self-assembly.

RESULTS AND DISCUSSION

Atomic Force Microscopy

Samples that contained fibrils after self-assembly of individual proteins were analyzed by tapping mode AFM. An example can be seen in Figure 2.1. Interestingly, the fibrils visible in this image have a remarkably narrow length distribution.

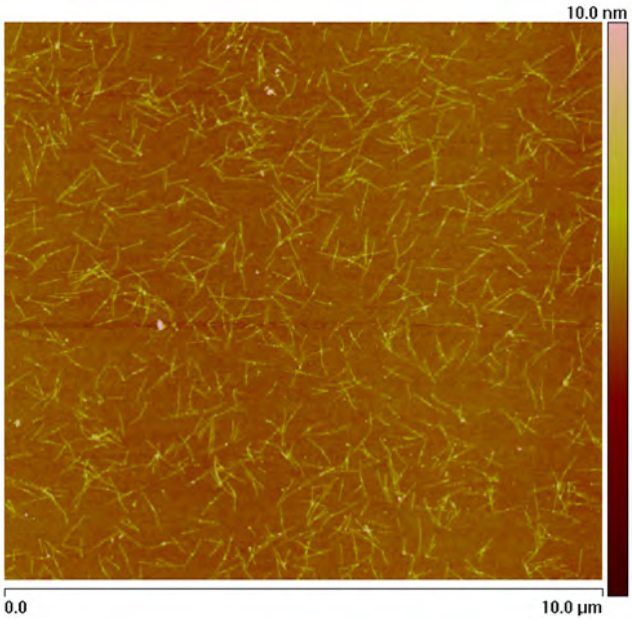

Figure 2.1: AFM tapping mode image of $S^{E}_{24}C_4S^{E}_{24}$ fibrils formed at pH 2.3 and adsorbed on a silica surface.

For different times after the start of the self-assembly, we imaged the adsorbed and dried fibrils and measured their contour length. Results are shown in Figure 2.2. As can be seen, in the initial phase the average length increases linearly in time; from the slope a value for the elongation rate of the growing fibrils can be obtained (Table 2.2).

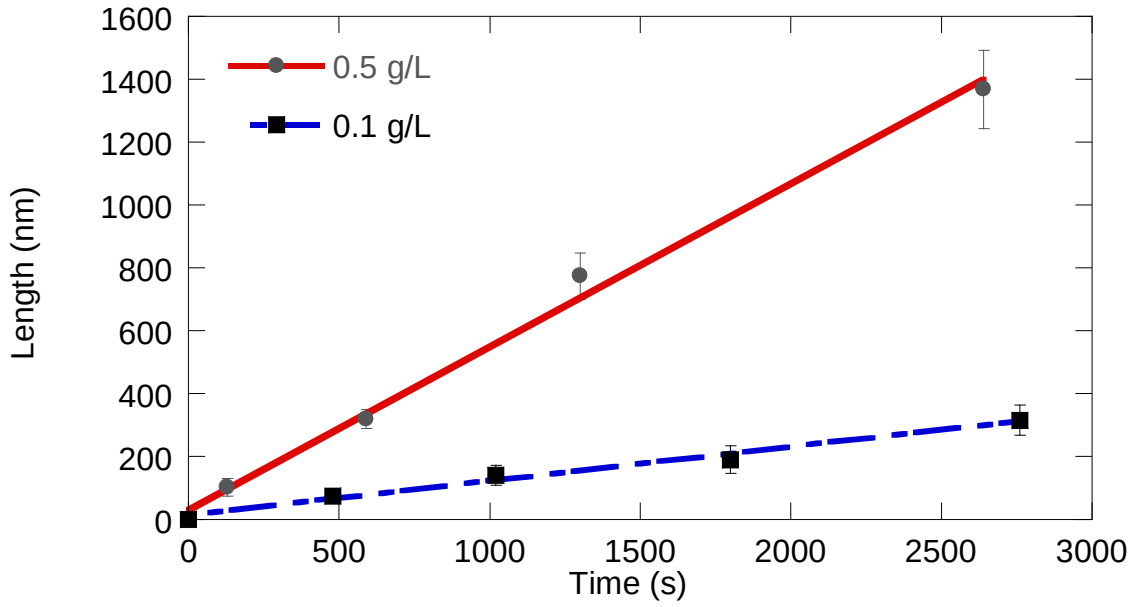

Figure 2.2: Elongation of growing fibrils of $S^{E}_{24}C_4S^{E}_{24}$ measured with AFM tapping mode for different protein concentrations. Error bars represent standard deviations of 20 measured fibrils per time step. The lines represent calculated values according to Equation 4.

Table 2.2: Initial fibril elongation rate of $S^{E}_{24}C_4S^{E}_{24}$ at pH 2.3

Protein concentration	Elongation rate
0.10 g/L (1.5 μM)	0.11 nm/s
0.50 g/L (7.5 μM)	0.58 nm/s

The presence of a very monodisperse system of fibrils at all times shows that an initial fast nucleation step is followed by elongation by the attachment of new protein polymers. This experiment shows that the individual fibrils have a growth rate that has a first order dependency on the protein concentration $c(t)$.

$$\frac{dL}{dt} = k_a c(t)$$

From Figure 2.2, the value of the rate constant k_a can be determined as being 7.7 x 10^{-8} m^4 mol^{-1} s^{-1}.

The monodisperse population of fibrils, which is visible in Figure 2.2, suggests a nucleated growth mechanism with a fixed number of initial nuclei n ($mol\ m^{-3}$). The same is found for the two alkaline protein polymers that were examined. These nuclei could be impurities that were not removed during the purification or partially digested protein polymers. As for a certain protein polymer, per batch, the length of the fibrils that are visible on AFM-pictures after completion of the self-assembly does not depend on concentration, we conclude that the ratio of the concentration of nuclei (n) to the initial concentration of proteins is a constant. This aggregation number N also corresponds to the average number of protein molecules in one fibril after completion of the self-assembly:

$$N = \frac{c(0)}{n} \tag{2}$$

The concentration of free protein polymers that determines the growth rate of the fibrils can be expressed as a function of the total concentration of protein $c(0)$ and the concentration of proteins in the fibrils.

$$c(t) = c(0) - \frac{c(0)}{Nl} L(t) \tag{3}$$

with $n = c(0)/N$ the concentration and $L(t)$ the contour length of the fibrils, and l the length per protein molecule in the fibril.

Substituting this equation for $c(t)$ in Equation 1 gives us a differential equation which can be solved into:

$$L(t) = \frac{c(0)l}{n}[1 - \exp(-k_a \frac{c(0)}{Nl} t)] \tag{4}$$

This equation gives an excellent match with the measured data presented in Figure 2.2.

If we compare the elongation rate of the growing fibrils with the flocculation of Brownian particles according to Smoluchowski, we can compare the elongation rate with that of a

diffusion limited case. The Smoluchowski equation for our case gives the decrease of the concentration of free proteins in solution *dc/dt* as a function of the concentration of the proteins *c*, the concentration of fibrils *n*, Avogadro's number N_A and the kinetic parameter $K_{Brown.}$

$$-\frac{dc}{dt} = K_{Brown} c n N_A \tag{5}$$

The parameter K_{Brown} is a function of the absolute temperature *T*, the viscosity of the solution η and Boltzmann constant k_b:

$$K_{Brown} = \frac{4k_b T}{3\eta} \tag{6}$$

We can express *dc/dt* in terms of the elongation rate *dL/dt*, the concentration of fibrils *n* and the length per protein molecule in the fibril *l*.

$$-\frac{dc}{dt} = \frac{dL}{dt}\frac{n}{l} \tag{7}$$

Combining these equations gives a value for *dL/dt* :

$$\frac{dL}{dt} = K_{Brown} c l N_A \tag{8}$$

For the solution of $S^E_{24}C_4S^E_{24}$ of 1.5 μM and a value for *l* of 0.95 nm [23] this leads to a value for *dL/dt* of 4.6 μm/s, which is more than four orders of magnitude higher than experimentally found and shown in Table 2.2. We have several explanations for this difference. First of all the Smoluchowski equation does not account for the limited part of the growing fibril that is available for aggregation. Only a collision between a growing end of a fibril and a free protein can lead to the elongation of that fibril. Furthermore, the steric nature of the glutamic acid leads to a lower number of succesful collisions. There must be a parallel stacking of the proteins in order for the glutamic acid groups not to overlap.[23-25] As a consequence, the conformation and orientation of the protein polymer when approaching a growing end is essential for attachment to the fibril. An unfavourable conformation will thus not lead to the

attachment of the new protein polymer. Finally, the good solubility of the random coil part induces a repulsive interaction between the fibril and the approaching protein polymer that leads to an energy barrier to be overcome, which would lead to a lower growth rate.

Static light scattering

According to the Rayleigh theory the light scattered by a solution is given by the sum of the scattered intensity of all particles in solution. The light scattered is usually given as the Rayleigh ratio *R* and can be written as the sum of the scattering by the individual particles in solution:

$$R = K\sum_i c_i M_i^2 P_i(q) S(q) \tag{9}$$

where *c* is the concentration, *M* the molar mass, *P*(*q*) the form factor that accounts for interference of scattered light within one particle and *S*(*q*) is the structure factor that accounts for interference of scattered light from different particles in the solution. The optical constant *K* is given by:

$$K = 4\pi^2 n_0^2 (\frac{dn}{dc})^2 / N_A \lambda^4 \tag{10}$$

Where n_0 is the refractive index of the solvent, *dn/dc* is the refractive index increment of the solute (0.18 cm^3/g for our proteins), N_A is Avogadro's number and λ the wavelength of the light *in vacuo*.

The Rayleigh ratio *R* can be determined by measuring the scattered intensity of a sample, the pure solvent and a reference sample of which the Rayleigh ratio is known:

$$R_{sam} = \frac{I_{sam} - I_{sol}}{I_{ref}} * R_{ref} * \frac{n_{sam}^2}{n_{ref}^2} \tag{11}$$

As a reference toluene was taken, which has a known Rayleigh ratio of 1.98 x 10^{-5} cm^{-1} at the used wavelength [26].

Figure 2.3 shows the development of *R/c* for a solution of $S^{E}_{24}C_4S^{E}_{24}$ after decreasing the pH to 2.3.

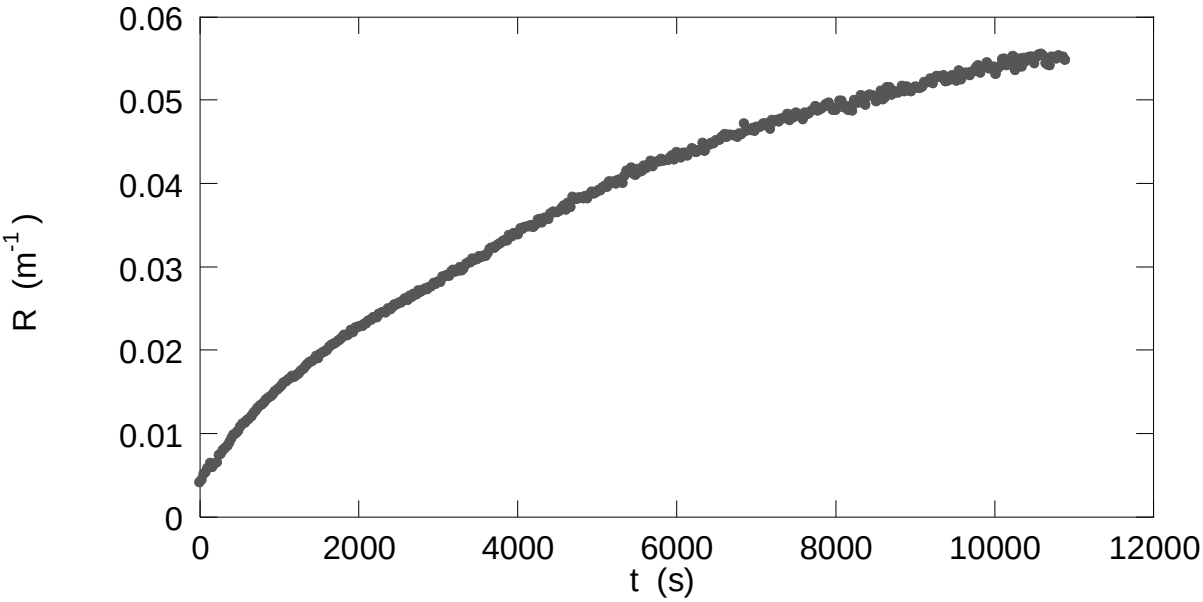

Figure 2.3: Static light scattering data of a 1.5 μM $S^{E}_{24}C_4S^{E}_{24}$ solution at pH 2.3 during self-assembly.

We see that directly after acidification of the sample, there is a steady increase of the scattered light intensity, showing that the size of the particles in solution is increasing continuously. From the rate of increase we can obtain information about the kinetics of the self-assembly process.

For a monodisperse population of linear particles in a dilute solution as in our study, we can assume $S(q) = 1$ and equation 9 can be rewritten as:

$$R = Kn\frac{M_w^2 L^2}{l^2}P(qL) \qquad (12)$$

with n the fibril concentration, M_w the molar mass of the individual protein polymer, l the length per protein in the fibril and L the contour length of the scattering particles.

Combining Equations 4 and 12 gives an expression for *R(t)* for a monodisperse population of growing fibrils:

$$R(t) = \frac{KM_w^2 c(0)^2}{n}[1 - \exp(-k_a \frac{c(0)}{Nl} t)]^2 P(qL) \quad (13)$$

Rewriting this equation shows that for a system that displays pseudo-first order kinetics, plotting $R/c(0)$ against $c(0)t$ for different concentrations of protein polymer gives graphs that will overlap if the shape of the fibrils and thus the form factor $P(qL)$ develops in the same way. Equation 4 shows that the length of the fibrils $L(t)$ is a function of the combined variable $c(0)t$. The wavevector q is constant, which means that the form factor $P(qL)$ is also a function of $c(0)t$. Dividing Equation 13 by $c(0)$ leads to the expression below (14) that contains the values K, N, l and k_a, which are all constants for a given protein polymer. The only variables in the equation are $c(0)$, t and $P(qL)$.

$$\frac{R(t)}{c(0)} = KM_w^2 N[1 - \exp(\frac{-k_a c(0)t}{Nl})]^2 P(qL) \quad (14)$$

From the AFM-pictures it is clear that the shape of the fibrils does not depend on the concentration of protein polymers in a sample. The development of the form factor $P(qL)$ only depends on $L(t)$ which according to Equation 4 scales with $c(0)t$. Figure 2.4 shows plots in which the Rayleigh ratio per concentration of protein $R/c(0)$ is plotted against $c(0)t$.

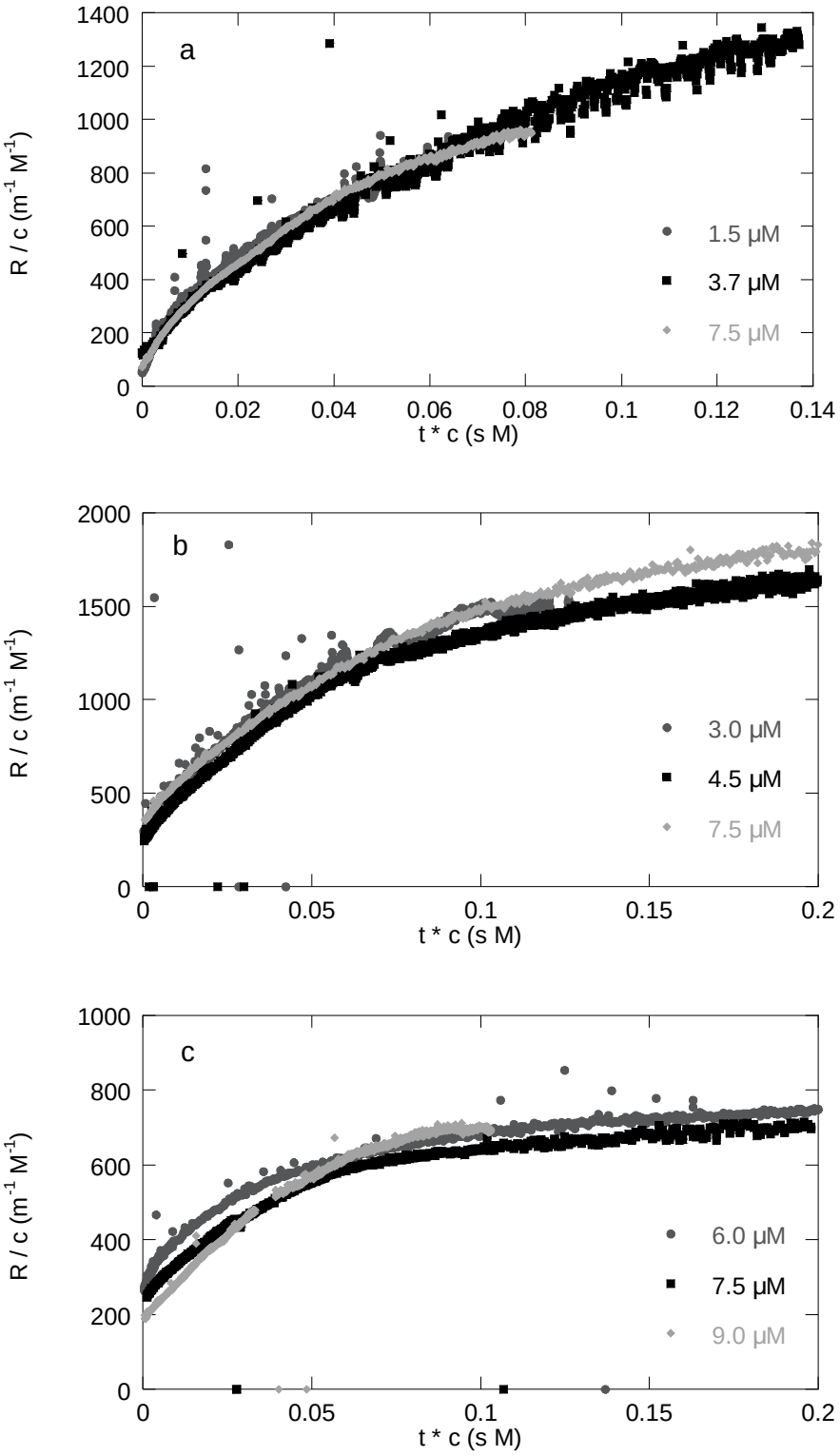

Figure 2.4: Static light scattering data for self-assembly of different protein polymers. (a) $S^{E}_{24}C_4S^{E}_{24}$ solutions of different concentrations at pH 2.3. (b) $S^{H}_{24}C_4S^{H}_{24}$ solutions of different concentrations at pH 11. (c) $S^{K}_{24}C_4S^{K}_{24}$ solutions of different concentrations at pH 12.

Figure 2.4 shows that indeed for every separate protein polymer, plots of $R/c(0)$ against $c(0)t$ for different concentrations overlap. This confirms our hypothesis that the self-assembly process follows pseudo-first order kinetics. It also shows that this behaviour is generic for silk-collagen-silk structured protein polymers, regardless of the nature of the chargeable group.

After completion of the self-assembly process it is possible to restart the growth of the fibrils by adding a solution of molecularly dissolved protein polymers, similar as in a living polymerization process [27]. This is shown in Figure 2.5 for a solution of 7.5 μM of $S^{E}_{24}C_4S^{E}_{24}$ at pH 2.3. The first part of the plot shows an increase in Rayleigh ratio by the self-assembly of individual protein molecules into fibrils. The solution was left until the scattered light intensity was stable, so no net self-assembly was taking place anymore. Then half of the solution was removed and new protein polymers and acid was added to obtain the same concentration and pH. As expected, this resulted in a Rayleigh ratio that is exactly the average of that of both solutions. The Rayleigh ratio immediately starts to increase again, indicating that self-assembly is started again. The final value of the Rayleigh ratio is higher than the first plateau value. Therefore, we conclude that the already present fibrils start growing again once new proteins are added to the solution. If only new fibrils would be formed, the second plateau would be the same as the first as a monodisperse population of fibrils of size L would be formed. Due to the quadratic dependence of the scattered intensity on particle size, the bidisperse population that consists half of fibrils of size L-x and half of fibrils of size L+x has a higher total scattered intensity as shown in Figure 2.5.

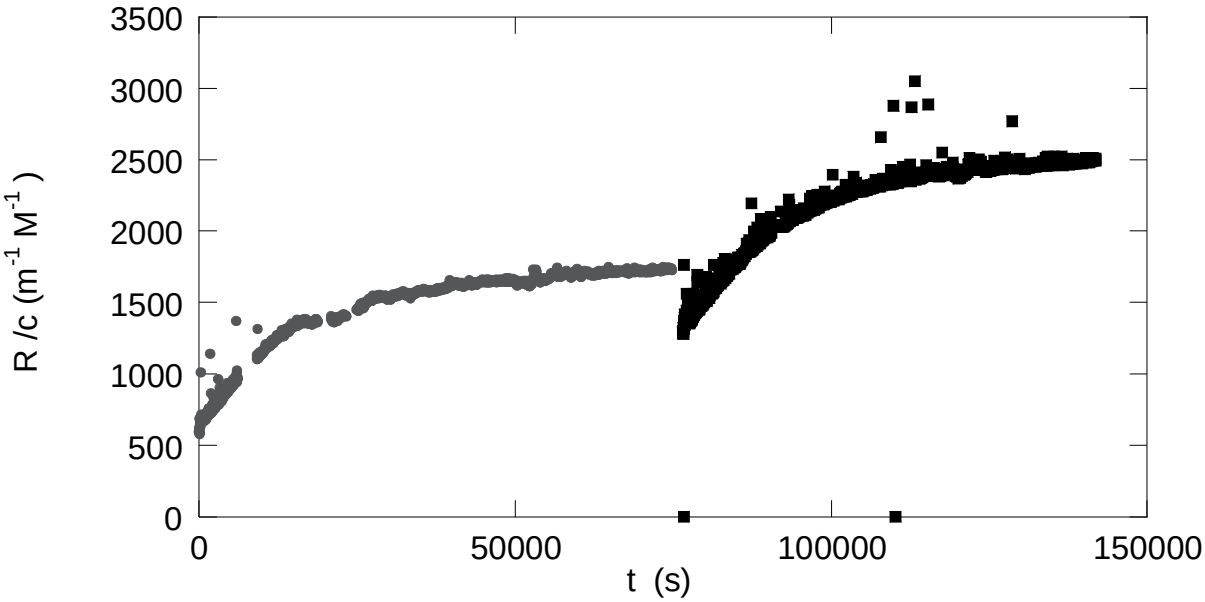

Figure 2.5: Static light scattering data for the self-assembly of a 7.5 μM solution of $S^{E}_{24}C_4S^{E}_{24}$ at pH 2.3. At t=75000 s half of the solution was removed and a fresh solution of molecularly dissolved $S^{E}_{24}C_4S^{E}_{24}$ and acid was added to reach the same concentration, volume and pH as before.

When the pH of a solution with fibrils is changed to a value well above the pK_a for the acidic protein polymer or below the pK_a for the alkaline ones, we observe an instant drop in scattered light intensity to a value that corresponds to the scattering of proteins in their unassembled state. This indicates the breakup of fibrils into individual charged proteins. After this, self-assembly into fibrils can be induced again by changing the pH to an appropriate value. In Figure 2.6 we show static light scattering data for a solution of $S^{E}_{24}C_4S^{E}_{24}$ that was acidified for a second time to a pH of 2.3 after breaking up the fibrils by adding NaOH. Previous work shows that the critical pH at which these fibrils break up is 5.4 [28].

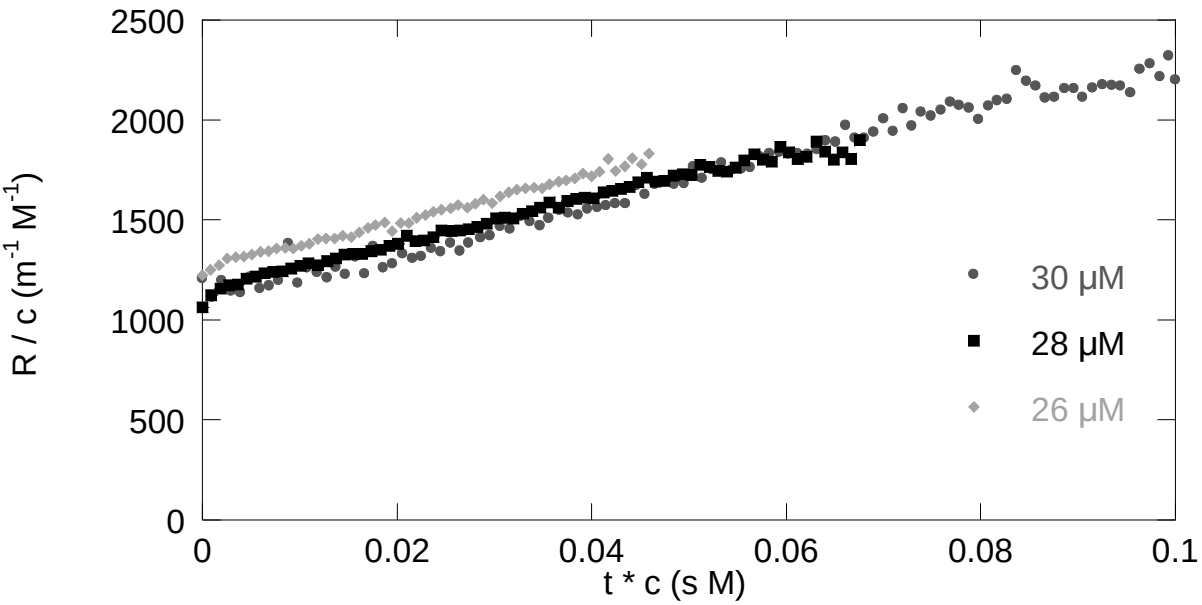

Figure 2.6: Static light scattering data for $S^{E}_{24}C_4S^{E}_{24}$ directly after lowering the pH to 2.3 (30 µM). The two other graphs show data obtained after increasing the pH to 10 again and acidifying to pH 2.3 a second time (28 µM), and repeating this procedure once more (26 µM).

In Figure 2.6 we see that lowering the pH to 2.3 again, gives us the same development of the signal *R/c*(*0*), after correction for the dilution by the extra added acid and base. Repeating this procedure again gives us a corresponding development of *R/c*(*0*). These data show that the self-assembly of these protein polymer is a fully reversible process. It also confirms that the concentration of nuclei is proportional to the concentration of proteins in the sample. We attribute the small vertical shifts of the plots to the increase of salt due to the addition of acid and base.

Circular Dichroism

CD-measurements were used to compare the secondary structure of the three protein polymers $S^{E}_{24}C_4S^{E}_{24}$, $S^{H}_{24}C_4S^{H}_{24}$ and $S^{K}_{24}C_4S^{K}_{24}$. For each protein we recorded a spectrum in the charged molecularly dissolved state and in the self-assembled state. We left the solutions for 24h for the self-assembly to complete.

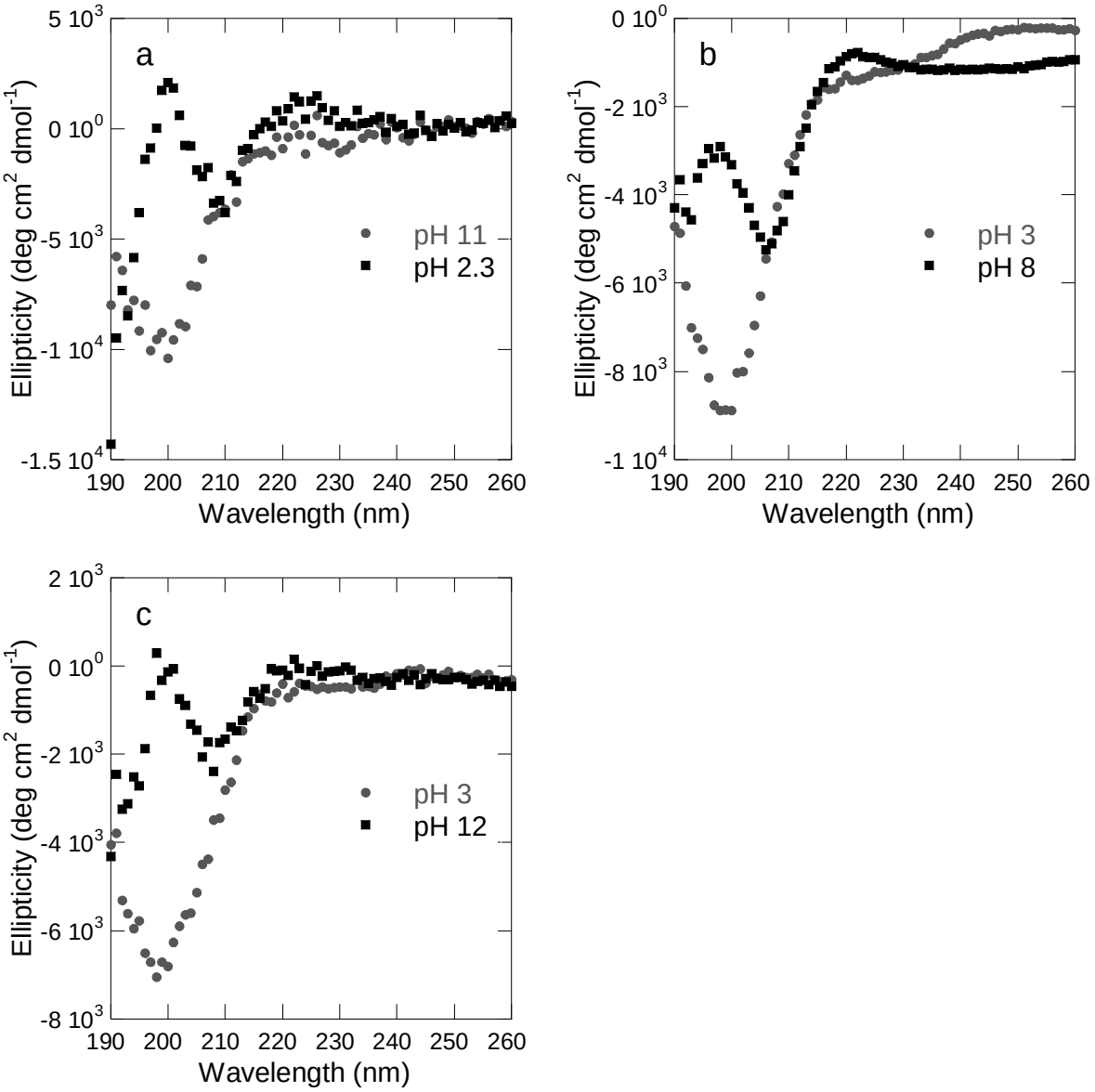

Figure 2.7: Molar ellipiticies per amino acid of three different protein polymers in their charged state and after self-assembly into fibrils. (a) A 1.5 μM solution of $S^{E}_{24}C_4S^{E}_{24}$ at pH 11 and 24h after acidification to pH 2.3. (b) A 1.5 μM solution of $S^{H}_{24}C_4S^{H}_{24}$ at pH 3 and 24h after changing the pH to 8. (c) A 4.5 μM solution of $S^{K}_{24}C_4S^{K}_{24}$ at pH 3 and 24h after changing the pH to 12.

It has already been shown that the glutamic acid bearing protein polymers are very rich in β-turns once fibrils are formed.[9] These β-turns are present in so called β-rolls as demonstrated by molecular dynamics simulations. The data on $S^{H}_{24}C_4S^{H}_{24}$ and $S^{K}_{24}C_4S^{K}_{24}$ presented in Figure 2.7, show spectra that are very similar to that of $S^{E}_{24}C_4S^{E}_{24}$. In the charged state (pH 3) they both show a clear negative ellipticity around 197 nm. After the formation of fibrils this negative ellipticity almost disappears, very much alike the spectrum of $S^{E}_{24}C_4S^{E}_{24}$. The most significant difference is that the spectra for the self-assembled $S^{K}_{24}C_4S^{K}_{24}$ and $S^{H}_{24}C_4S^{H}_{24}$ have a slightly lower peak at 197 nm compared to that of $S^{E}_{24}C_4S^{E}_{24}$. The former spectra look like an intermediate form of the random coil spectrum and the β-roll structure. This can be a result of the bulky and hydrophobic nature of the histidine and lysine sidechains. The bulky nature of these sidechains at the turn can disturb this structure and decrease its impact on the CD-spectrum. The hydrophobic character of the uncharged sidechains could lead to the incorporation of improperly folded proteins in the fibril. These molecules are then kinetically trapped and don't contribute to the signal of the β-roll structure, but are visible as random coiled structures in the CD-spectrum.

We also measured the spectrum of a 1.5 μM solution of $S^{E}_{24}C_4S^{E}_{24}$ in time to determine the evolution of the secondary structure during the self-assembly into fibrils. We observed no clear shift in the spectrum directly after lowering the pH to 2.3. The shift from random coil to β-roll structure is slow and occurs on the same time scale as the formation of the fibrils. Therefore we conclude that the protein polymer attains the β-roll structure only when attaching to a growing end of a fibril. In Figure 2.8 we fraction of unfolded (and thus molecularly dissolved) proteins in time. This fraction is calculated as:

$$f = 1 - \frac{\theta(t) - \theta(0)}{\theta(\infty) - \theta(0)} \qquad (15)$$

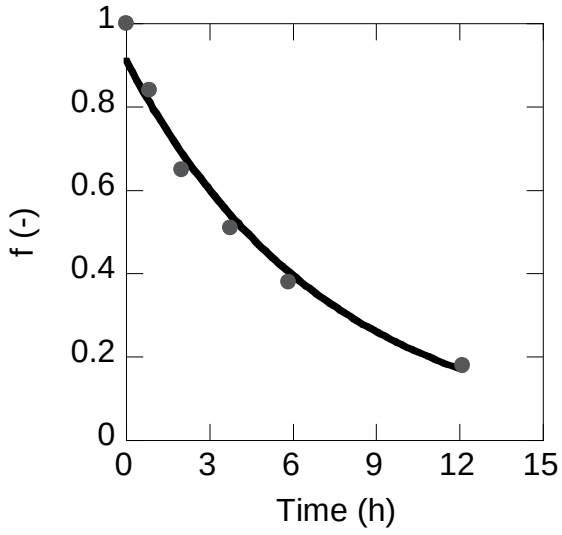

Figure 2.8: Fraction of unfolded protein of in a 1.5 μM solution of $S^{E}_{24}C_4S^{E}_{24}$ during the self-assembly process at pH 2.3. The fit shows a monoexponential decay of the fraction of protein polymers in the unassembled state.

The plot in Figure 2.8 shows a monoexponential decay of this fraction, which is consistent with pseudo-first order kinetics. This supports our conclusion that the protein polymer attains a β-roll structure during self-assembly into fibrils.

CONCLUSIONS

Silk-collagen-silk-like protein polymers follow pseudo-first order kinetics during self-assembly in dilute solutions. The slow growth in these dilute solutions enabled us to follow the length development of populations of fibrils in time. Using light scattering we could investigate the growth kinetics in a dilute system without dealing with a steep increase in viscosity during gel formation. The formation of fibrils after charge neutralization shows generic behaviour for the acidic ($S^{E}_{24}C_4S^{E}_{24}$) and alkaline ($S^{H}_{24}C_4S^{H}_{24}$ and $S^{K}_{24}C_4S^{K}_{24}$) protein polymers. Each protein polymer forms ribbon-like fibrils after the pH is adjusted to a value at which the silk-like block is uncharged. The narrow length distribution of the populations of fibrils suggests a nucleated growth mechanism from already present nuclei in the sample. The consecutive elongation of the growing fibrils shows a first-order concentration dependence. Elongation can be restarted by addition of new molecularly dissolved proteins. The elongation rate is much slower than expected for a random aggregation mechanism. This is attributed to the repulsive nature of the collagen block, the limited size and availability of the growing end of a fibril, and the orientation and conformation that is needed for an approaching protein to successfully attach to a growing fibril. Charging up the fibrils by altering the pH causes the fibrils to disassemble immediately due to multiple charge-charge interactions. The self-assembly into fibrils can then be triggered again by altering the pH to a value at which the protein polymers are uncharged. The kinetic properties of this repeated self-assembly, when corrected for dilution, are identical to those of the freshly prepared solution. Therefore, we conclude that the nuclei present in the sample stay intact and the pH-induced self-assembly is reversible. The structure of the fibrils of all three types of protein polymers is very rich in β-turns, forming β-rolls. Surprisingly, the formation of these β-rolls does not occur directly after charge neutralization, but only upon attachment to a fibril, illustrated by the slow evolution of the CD-spectrum from random coil to β-rolls. The kinetic properties of the self-assembly

process are very similar to those of a living polymerization reaction, with the exception that the self-assembly is a reversible supramolecular process.

EXPERIMENTAL SECTION

Protein sequence and synthesis

The amino acid sequences of $S^{E}_{24}C_4S^{E}_{24}$ and $S^{H}_{24}C_4S^{H}_{24}$ have been described previously [29]. The $S^{K}_{24}C_4S^{K}_{24}$ protein polymer only differs from the $S^{E}_{24}C_4S^{E}_{24}$ and $S^{H}_{24}C_4S^{H}_{24}$ polymers in the silk-like part, where the GAGAGAGX repeat bears a lysine (K) in the X position instead of glutamic acid (E) or histidine (H) respectively. All protein polymers were produced in a fed batch fermentation of *Pichia pastoris* as previously described for the glutamic acid and histidine bearing proteins. $S^{K}_{24}C_4S^{K}_{24}$ was produced and purified in the same way as $S^{H}_{24}C_4S^{H}_{24}$.

Static Light Scattering

Static light scattering data were all obtained at a 90° angle using an ALV-SP/86 goniometer with an ALV7002 external correlator and a Thorn RFIB263KF Photo Multiplier Detector with 200/400 μm pinhole detection system. It was operated using a 300 mW Cobolt Samba-300 DPSS Laser at a wavelength of 532 nm. The setup corresponds to a wavevector of 0.022 nm^{-1}. All samples were measured in round quartz cuvettes, including solvent blanks, for which water was used. As a reference sample we used toluene. Samples were prepared by mixing the appropriate amount of protein stock solution and demineralized water. After adding a 50 mM HCl or NaOH solution to reach a final concentration of 10 mM the sample was immediately shaken and filtered with a Nalgene 200 nm syringe filter. Subsequently the solution was transferred to the quartz cuvette and the measurement was started. The average time between the start of the experiment and the start of the measurement was 1 minute. After the experiment had finished, we measured the pH of each sample.

AFM imaging

AFM samples were made by dipping a 10x10 mm hydrophilic silicon wafer bearing a thin oxide layer into the protein solution, rinsing with demineralized water to remove any non-adsorbed material and drying it under a stream of nitrogen. The samples were analyzed using a Digital Instruments Nanoscope III in tapping mode with NANOSENSORS SSS-NCH-20 silicon tips with a typical tip radius of 2 nm.

Circular dichroism

CD measurements were performed on a Jasco J-715 spectropolarimeter at room temperature. The spectra were recorded between 190 and 260 nm with a resolution of 0.2 nm and a scanning speed of 1 nm/s. Spectra were recorded for three different protein polymers: $S^{E}_{24}C_4S^{E}_{24}$, $S^{H}_{24}C_4S^{H}_{24}$ and $S^{K}_{24}C_4S^{K}_{24}$. First spectra were recorded for each protein polymer in the unassembled state. For $S^{E}_{24}C_4S^{E}_{24}$ we used a 1.5 μM solution in 1 mM NaOH, for $S^{H}_{24}C_4S^{H}_{24}$ we used a 1.5 μM solution in 1 mM HCl and for $S^{K}_{24}C_4S^{K}_{24}$ we used a 4.5 μM solution in 1 mM HCl. Measurements of the three protein polymers in the self-assembled state were performed as follows: For the acidic $S^{E}_{24}C_4S^{E}_{24}$ a 1.5 μM solution in 10 mM HCl was prepared (final pH of 2.3), for $S^{H}_{24}C_4S^{H}_{24}$ a 1.5 μM solution in 20mM phosphate buffer (final pH 7.9) was used and measurements with $S^{K}_{24}C_4S^{K}_{24}$ were performed with a 4.5 μM solution in 20 mM NaOH (final pH 12.1). The solutions were left overnight to complete the self-assembly process before measuring the spectrum. The spectrum of a 1.5 μM solution of $S^{E}_{24}C_4S^{E}_{24}$ was recorded during the self-assembly process at different time intervals to examine the evolution of the secondary structure in time. Each measurement was performed in a 1 mm quartz cuvette.

REFERENCES

1. Shvetsov, A.; Galkin, V. E.; Orlova, A.; Phillips, M.; Bergeron, S. E.; Rubenstein, P. A.; Egelman, E. H.; Reisler, E., Actin Hydrophobic Loop 262-274 and Filament Nucleation and Elongation. *J. Mol. Biol.* **2008,** 375, (3), 793-801.
2. Guthold, M.; Liu, W.; Sparks, E. A.; Jawerth, L. M.; Peng, L.; Falvo, M.; Superfine, R.; Hantgan, R. R.; Lord, S. T., A Comparison of the Mechanical and Structural Properties of Fibrin Fibers with Other Protein Fibers. *Cell Biochem. Biophys.* **2007,** 49, (3), 165-181.
3. Goldsbury, C.; Baxa, U.; Simon, M. N.; Steven, A. C.; Engel, A.; Wall, J. S.; Aebi, U.; Muller, S. A., Amyloid Structure and Assembly: Insights from Scanning Transmission Electron Microscopy. *J. Struct. Biol.* **2011,** 173, (1), 1-13.
4. Labeit, S.; Ottenheijm, C. A. C.; Granzier, H., Nebulin, a Major Player in Muscle Health and Disease. *FASEB J.* **2011,** 25, (3), 822-829.
5. Arnaudov, L. N.; de Vries, R., Thermally Induced Fibrillar Aggregation of Hen Egg White Lysozyme. *Biophys. J.* **2005,** 88, (1), 515-526.
6. Arnaudov, L. N.; de Vries, R.; Ippel, H.; van Mierlo, C. P. M., Multiple Steps During the Formation of Beta-lactoglobulin Fibrils. *Biomacromolecules* **2003,** 4, (6), 1614-1622.
7. Pearce, F. G.; Mackintosh, S. H.; Gerrard, J. A., Formation of Amyloid-like Fibrils by Ovalbumin and Related Proteins under Conditions Relevant to Food Processing. *J. Agric. Food. Chem.* **2007,** 55, (2), 318-322.
8. Werten, M. W. T.; Wisselink, W. H.; van den Bosch, T. J. J.; de Bruin, E. C.; de Wolf, F. A., Secreted production of a custom-designed, highly hydrophilic gelatin in Pichia pastoris. *Protein Eng* **2001,** 14, (6), 447-454.
9. Martens, A. A.; Portale, G.; Werten, M. W. T.; de Vries, R. J.; Eggink, G.; Stuart, M. A. C.; de Wolf, F. A., Triblock Protein Copolymers Forming Supramolecular Nanotapes and pH-Responsive Gels. *Macromolecules* **2009,** 42, (4), 1002-1009.
10. Krejchi, M. T.; Atkins, E. D. T.; Waddon, A. J.; Fournier, M. J.; Mason, T. L.; Tirrell, D. A., Chemical Sequence Control of Beta-Sheet Assembly in Macromolecular Crystals of Periodic Polypeptides. *Science* **1994,** 265, (5177), 1427-1432.
11. Krejchi, M. T.; Atkins, E. D. T.; Fournier, M. J.; Mason, T. L.; Tirrell, D. A., Observation of a silk-like crystal structure in a genetically engineered periodic polypeptide. *J Macromol Sci Pure* **1996,** A33, (10), 1389-1398.
12. Krejchi, M. T.; Cooper, S. J.; Deguchi, Y.; Atkins, E. D. T.; Fournier, M. J.; Mason, T. L.; Tirrell, D. A., Crystal structures of chain-folded antiparallel beta-sheet assemblies from sequence-designed periodic polypeptides. *Macromolecules* **1997,** 30, (17), 5012-5024.
13. Smeenk, J. M.; Otten, M. B. J.; Thies, J.; Tirrell, D. A.; Stunnenberg, H. G.; van Hest, J. C. M., Controlled assembly of macromolecular beta-sheet fibrils. *Angew Chem Int Edit* **2005,** 44, (13), 1968-1971.
14. Smeenk, J. M.; Schon, P.; Otten, M. B. J.; Speller, S.; Stunnenberg, H. G.; van Hest, J. C. M., Fibril Formation by Triblock Copolymers of Silklike Beta-sheet Polypeptides and Poly(ethylene glycol). *Macromolecules* **2006,** 39, (8), 2989-2997.
15. Muller, M.; Krasnov, I.; Ogurreck, M.; Blankenburg, M.; Pazera, T.; Seydel, T., Wood and Silk: Hierarchically Structured Biomaterials Investigated In Situ With X-Ray and Neutron Scattering. *Adv. Eng. Mater.* **2011,** 13, (8), 767-772.
16. Nogueira, G. M.; de Moraes, M. A.; Rodas, A. C. D.; Higa, O. Z.; Beppu, M. M., Hydrogels from Silk Fibroin Metastable Solution: Formation and Characterization from a Biomaterial Perspective. *Materials Science & Engineering C-Materials for Biological Applications* **2011,** 31, (5), 997-1001.

17. Byette, F.; Bouchard, F.; Pellerin, C.; Paquin, J.; Marcotte, I.; Mateescu, M. A., Cell-culture Compatible Silk Fibroin Scaffolds Concomitantly Patterned by Freezing Conditions and Salt Concentration. *Polym. Bull.* **2011,** 67, (1), 159-175.
18. Tiyaboonchai, W.; Chomchalao, P.; Pongcharoen, S.; Sutheerawattananonda, M.; Sobhon, P., Preparation and Characterization of Blended Bombyx mori Silk Fibroin Scaffolds. *Fibers and Polymers* **2011,** 12, (3), 324-333.
19. Ferguson, M. W. J.; Metcalfe, A. D., Tissue Engineering of Replacement Skin: The Crossroads of Biomaterials, Wound Healing, Embryonic Development, Stem Cells and Regeneration. *Journal of the Royal Society Interface* **2007,** 4, (14), 413-437.
20. Guille, M. M. G.; Helary, C.; Vigier, S.; Nassif, N., Dense Fibrillar Collagen Matrices for Tissue Repair. *Soft Matter* **2010,** 6, (20), 4963-4967.
21. Brown, R. A.; Wiseman, M.; Chuo, C. B.; Cheema, U.; Nazhat, S. N., Ultrarapid Engineering of Biomimetic Materials and Tissues: Fabrication of Nano- and Microstructures by Plastic Compression. *Adv. Funct. Mater.* **2005,** 15, (11), 1762-1770.
22. Lee, C. H.; Singla, A.; Lee, Y., Biomedical Applications of Collagen. *Int. J. Pharm.* **2001,** 221, (1-2), 1-22.
23. Schor, M.; Martens, A. A.; de Wolf, F. A.; Cohen Stuart, M. A.; Bolhuis, P. G., Prediction of solvent dependent beta-roll formation of a self-assembling silk-like protein domain. *Soft Matter* **2009,** 5, (13), 2658-2665.
24. Schor, M.; Ensing, B.; Bolhuis, P. G., A simple coarse-grained model for self-assembling silk-like protein fibers. *Faraday Discuss* **2010,** 144, 127-141.
25. Schor, M.; Bolhuis, P. G., The Self-assembly Mechanism of Fibril-forming Silk-based Block Copolymers. *Phys. Chem. Chem. Phys* **2011,** 13, 10457-10467.
26. Wu, H., Correlations between the Rayleigh Ratio and the Wavelength for Toluene and Benzene. *Chem. Phys.* **2010,** 367, (1), 44-47.
27. Hadjichristidis, N.; Iatrou, H.; Pitsikalis, M.; Mays, J., Macromolecular Architectures by Living and Controlled/Living Polymerizations. *Prog. Polym. Sci.* **2006,** 31, (12), 1068-1132.
28. Martens, A. A. Silk-Collagen-like Block Copolymers with Charged Blocks. Wageningen University, Wageningen, 2008.
29. Li, F.; Martens, A. A.; Aslund, A.; Konradsson, P.; de Wolf, F. A.; Stuart, M. A. C.; Sudholter, E. J. R.; Marcelis, A. T. M.; Leermakers, F. A. M., Formation of nanotapes by co-assembly of triblock peptide copolymers and polythiophenes in aqueous solution. *Soft Matter* **2009,** 5, (8), 1668-1673.

Chapter 3

Super Resolution Microscopy Shows Asymmetrical Self-Assembly of Highly Symmetrical Protein-Based Building Blocks.

ABSTRACT

We have used super resolution microscopy (STORM) and atomic force microscopy (AFM) to study the growth and exchange dynamics of 1D fibril-forming recombinant triblock protein polymers. The protein polymers consist of a central pH-responsive silk-like block, flanked by two hydrophilic collagen-inspired random coil blocks. Analysis of the kinetics of growth using AFM shows that self-assembly of the pH-responsive triblock protein polymers into fibrils involves continuous nucleation. Super resolution microscopy (STORM) of differently labelled proteins is used to study exchange dynamics. We find that once assembled, there is essentially no exchange of protein subunits. By sequential growth of differently labelled proteins, we have created fibrils with a blocked distribution of different fluorophores. Surprisingly, we find that fibrils grow only in one direction, despite the symmetrical nature of the protein building blocks. Our findings pave the way for the engineering of protein nanofibrils with structures along the fibril axis at larger length scales. It also highlights the power of super resolution microscopy as a method for studying the growth and exchange dynamics of protein fibrils.

INTRODUCTION

Bio-inspired protein polymers[1] are a promising class of new materials with potential biomedical applications, such as tissue engineering [2-4], drug or gene delivery [5,6] or self-healing materials [1]. One of the advantages of using recombinant protein based polymers over synthetic ones is the use of the virtually defect free cellular machinery for the production of these protein polymers. The route of genetic engineering provides a near perfect control over size, amino acid sequence and chirality of the protein polymer. As a result, one can obtain a much better defined and tunable set of properties compared to any synthetic polymer, produced by chemical polymerization methods. The building blocks of these protein polymers, amino acids, are the same in any naturally occurring protein. This gives the option of including and combining any naturally occurring amino acid sequences, that have desirable properties, in the designed protein polymer. Among the amino acid sequences that have been used to make these biomimetic protein polymers in recent years, many have been inspired by, or based on structural proteins known for their superior stimulus-responsive, mechanical, biocompatible and structural properties. These domains include natural silk [7-15], collagen [10,16-18], elastin [3,13,19-21] and resilin [22-24].

One of the main challenges when working with biomimetic materials is to mimic the extracellular matrix (ECM) for use as a scaffold in tissue engineering. This matrix is a mixture of mainly glycoproteins and fibrous proteins. The basic structure of these fibrous proteins is a self-assembled, one dimensional aggregate [25]. A common approach to mimic the ECM involves building blocks that form a similar fiber-based matrix, in the form of a hydrogel. These building blocks can be synthetic, natural, or a hybrid of these.

When aiming for a well-controlled recreation of this basic structure of the ECM, one requires a detailed knowledge on the mechanism of self-assembly of the building blocks of these aggregates. Although numerous models on kinetics of the self-assembly of 1D

aggregates exist, it has proven very challenging to probe self-assembly and exchange dynamics on the molecular scale. Kinetic models of 1D aggregates generally assume depolymerization-polymerization or fragmentation-recombination as exchange mechanisms. Experimental validation of these assumptions is essential for an increased validity of these models.

Super resolution techniques are on the rise as tools to image structures with spatial resolutions that go beyond the diffraction limit [26]. As one of these techniques, STORM, has proven to hold the potential to extract quantitative information about structure and dynamics of organized biological [27-32] or synthetic structures [33]. The ability of multicolor imaging, together with an enhanced resolution, provides the possibility of elucidating structures at the sub-fibril level as well as the fate of individual molecules making up these structures.

Recently, it was shown by means of super resolution microscopy, that an entirely different exchange pathway is possible, namely a homogeneous exchange along the aggregate backbone, which stresses the need to re-evaluate existing kinetic models on self-assembled 1D aggregates [33]. In this recent work, the high resolution of Stochastic Optical Reconstruction Microscopy (STORM) is combined with sophisticated analytical tools to extract quantitative data from these microscopy images. This powerful combination has opened up the possibility to probe self-assembly and exchange kinetics of these 1D aggregates on the molecular scale.

In this chapter we use super resolution microscopy to acquire details on self-assembled protein fibrils on the molecular scale. We study a biomimetic protein polymer with a triblock structure, that combines a central silk-like block, which enables highly structured self-assembly, with flanking random coil blocks. We name this protein $C_2S^H_{48}C_2$. The pH-responsive middle domain is silk-inspired and consists of 48 repeats of the octapeptide GAGAGAGH (S^H). The alkaline nature of the amino acid histidine (H) gives it a positive charge at low pH (pKa ~ 6), which prevents self-assembly. At higher pH the silk-like block is

neutral and can self-assemble into a fibrous structure that is a stack of beta-rolls [12,34,35]. The two identical outer blocks are dimers of a 99 amino acid long C-block. This block is rich in the hydrophilic amino acids glutamine, asparagine and serine. Its sequence has similarities to that of natural collagen (GXY triplets), but it does not attain any secondary structure under a wide range of aqueous solvent conditions [12,36]. The C_2-blocks provide colloidal stability to the self-assembled fibrils by exposing a hydrophilic polymer brush on the outside of the fibrils. Without these hydrophilic blocks the self-assembled fibrils aggregate and precipitate [11]. This $C_2S^H_{48}C_2$ protein polymer is known to form weak fibril based hydrogels [37] at neutral or higher pH (e.g., under physiological conditions). The collagenous nature of the side-blocks (PXY triplets) assures that the fibril exterior resembles to some extent the chemical composition of natural collagen. This collagenous fibril-based hydrogel could be an important element in mimicking the extracellular matrix.

Although gel properties of this protein polymer on the macroscopic level (gelation time, strength, recovery after breaking) have been studied extensively [12,37,38], there is little known about the mechanism of self-assembly into fibrils on the molecular level. We have found that the self-assembly of a similar protein polymer, with an inverted block sequence, $S^E_{24}C_2C_2S^E_{24}$, exhibits a pseudo-first order nucleation and growth mechanism with living fibril ends [34]. This protein polymer has the acidic glutamic acid as pH-responsive amino acid. It is charged at neutral or high pH and is neutral at low pH (pKa ~4) and self-assembles into fibrils at low pH. In contrast, the protein polymer $C_2S^H_{48}C_2$ self-assembles at a pH as low as 5, and the rate of self-assembly increases with increasing pH [37]. The techniques used in these studies (atomic force microscopy, light scattering, circular dichroism, electron microscopy) provide valuable information on the kinetics of self-assembly, but fail to extract details on the molecular level.

Here we use STORM to probe the molecular exchange dynamics in self-assembled protein fibrils, using previously reported analytical tools [33]. We also employ this technique to assess

the creation of block structures within fibrils. Both fibril properties are essential when introducing proteins with different (bio-)functional moieties (e.g., cell-binding RGD-domains) in a fibril based hydrogel as block structure and exchange dynamics of fibrils determine local densities and domain sizes of these moieties. We complement this work with extensive quantitative data obtained with AFM. We quantify the rate of fibril self-assembly as well as final fibril dimensions as a function of total protein concentration. The combination of these two techniques provides detailed knowledge on the fate of individual molecules as well as dimensions and properties on the scale of individual fibrils. An increased understanding of growth and exchange dynamics on these two length scales leads to a better control over tailoring macroscopic properties of hydrogels formed by these protein polymers.

RESULTS & DISCUSSION

Atomic Force Microscopy

The high spatial resolution of Atomic Force Microscopy (AFM) makes it an excellent tool to assess the dimension of structures on the (sub-)micrometer scale. An advantage of the technique is that it does not require any chemical modification of the component of interest. We determined the length of individual fibrils during the self-assembly process as well as a size distribution after completion of self-assembly. As fibril dimensions are one of the principal features that determine the properties of a fibril based hydrogel, it is essential to probe and control them. Figure 3.1a shows the average length of an ensemble of self-assembled fibrils (n = 50 – 70) at different times after the pH-induced start of fibril growth. The increase of the standard deviation over time for all samples indicates an increasing polydispersity over time. This implies a continuous nucleation of new fibrils accompanying the elongation of existing ones. Figure 3.1b shows a clear dependence of the growth rate on total protein polymer concentration, according to: $d\langle L\rangle/dt \sim C^{0.74}$

The initial increase of the average fibril length in time goes up at higher protein concentrations. A scaling exponent smaller than one is expected for a process of continuous nucleation. Continuous nucleation not only leads to a very polydisperse fibril length distribution, it also leads to a decrease in final average fibril length as the number of fibrils increases. Suppressing nucleation after an initial phase of fibril genesis could therefore be a promising, yet challenging, route to obtain longer individual fibrils and thus more dilute hydrogels.

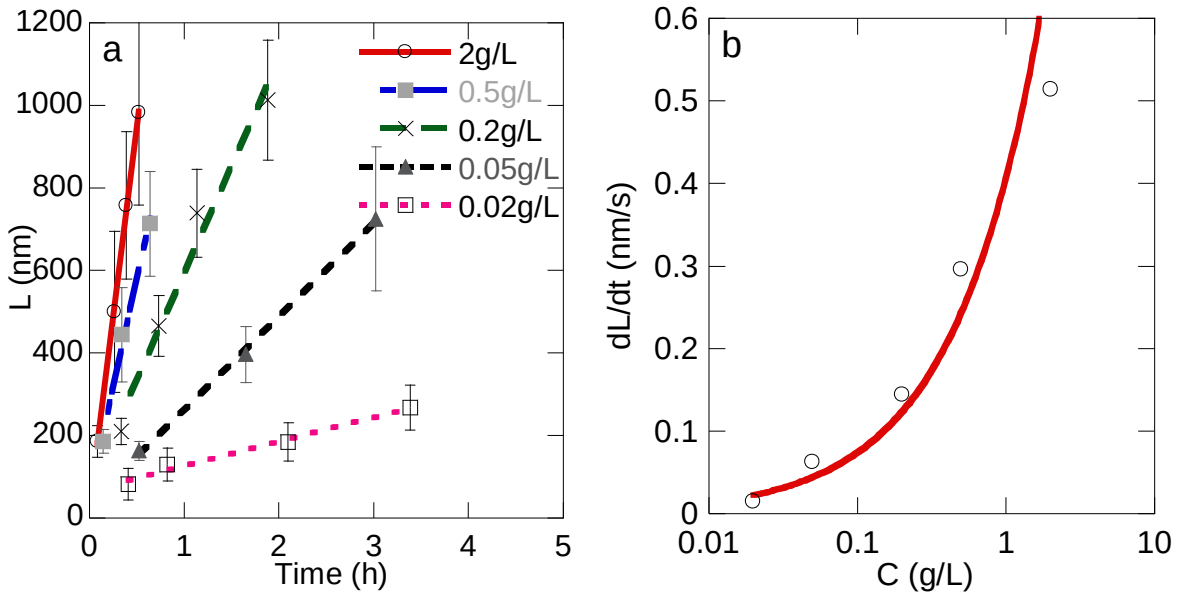

Figure 3.1: Average fibril contour length (n=50-70) at different times for two decades of total protein polymer concentration, error bars represent standard deviations (a) and the initial fibril elongation speed as a function of concentration (b). Figure b is fitted with a power law with exponent 0.74.

We also determined the sizes of the protein fibril after 14 days of self-assembled fibril formation. We measured sizes over a concentration range of two decades as shown in Figure 3.2a. This figure shows that for all concentrations the polydispersity of the final fibril population is rather high, with relative standard deviations of almost 100%. The two samples with the lowest concentrations, 0.05 g/L and 0.2 g/L, have an average fibril length of approximately 1 µm, while the three highest concentrations have an average fibril length twice that size. All samples except the two lowest concentrations contained fibrils of several micrometers length (up to 10 µm), but these were outnumbered by numerous sub-micron sized fibrils, as we show in Figure 3.2b-f. One might naively have expected that nucleation of fibrils is a multimolecular event that is strongly concentration dependent. As this would have resulted in a decreasing fibril length with increasing protein concentration, this is clearly not

the case. Instead this results leads us to believe the nucleation is a heterogeneous process that is slow compared to fibril elongation.

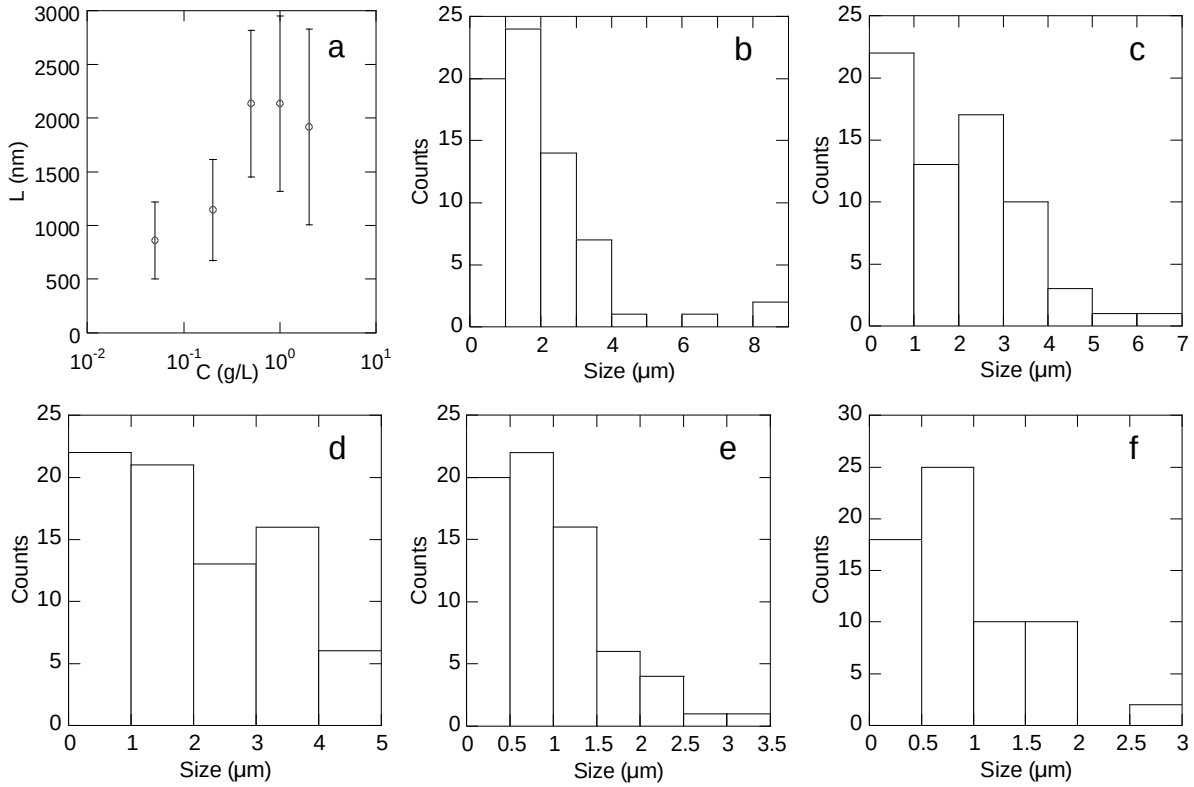

Figure 3.2: Average contour length with standard deviation (a) and size distributions (b-f) of self-assembled protein fibrils after two weeks of incubation at pH 8.0 (50 mM phosphate buffer) as a function of total protein polymer concentration. Protein concentrations of the samples were 2 g/L (b), 1 g/L (c), 0.5 g/L (d), 0.2 g/L (e) or 0.05 g/L (f).

STORM

The high resolution and the use of multiple colors in STORM give us the possibility to observe self-assembled fibrils on the molecular level. STORM has proven very suitable to probe exchange dynamics by mixing fibrils of different colors and analyzing the distribution of different labels along these fibers in time [33]. It can also probe fibril growth direction and kinetics [27], and the existence of living fibril ends in solution. The analytical method to extract quantitative data from STORM images has been described in detail [33]. We demonstrate the increased resolution of STORM compared to conventional fluorescence microscopy (TIRF) for our fibrils in Figure 3.3. The imaged sample contains self-assembled protein polymers (at pH 8.0) that are labelled with Alexa 647 dye.

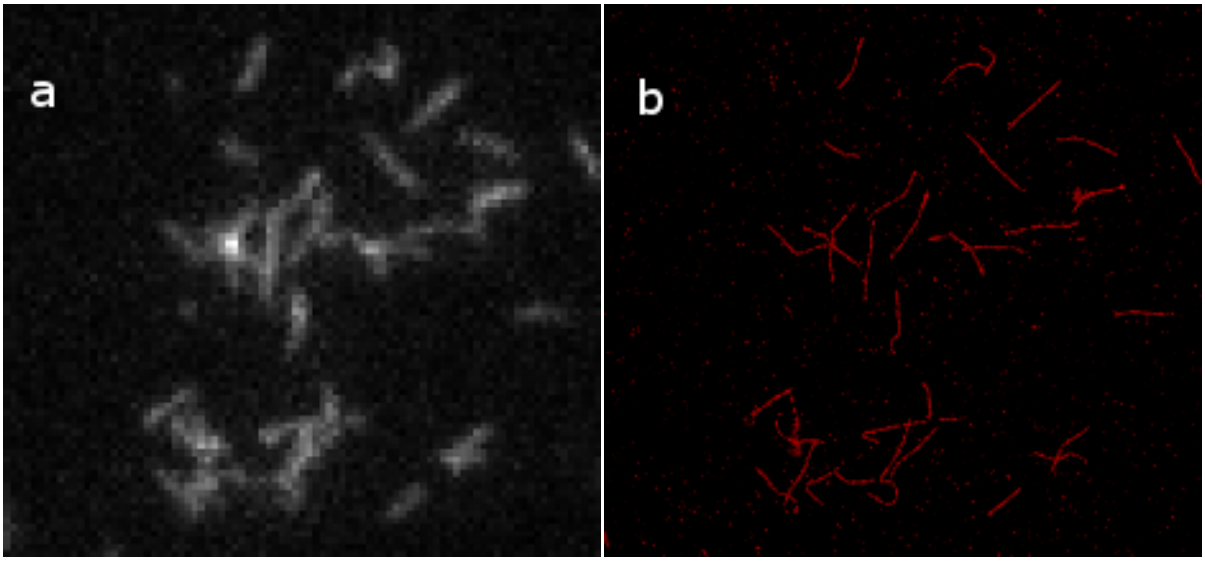

Figure 3.3: Conventional TIRF-image (a) and STORM-image (b) of self-assembled Alexa 647-labelled protein polymers. The sample contained 0.1 g/L of protein in 50 mM phosphate buffer (pH 8.0) during self-assembly and was diluted 10x before imaging.

To probe exchange dynamics of the self-assembled fibrils we used two fluorescently labelled protein polymers. We chose Alexa Fluor 488 and Alexa Fluor 647 as dyes, one of which was N-terminally covalently attached to a sample of the protein polymer. The labelling degree dye:protein for both fluorescent labels was 0.4. We used two separate solutions that contained one label each, and let the labelled protein polymers self-assemble into fibrils. After completion of the self-assembly (3 days) we mixed both samples to obtain a mixture of 488-labelled fibrils and 647-labelled fibrils. After 3 days we analyzed the mixture by STORM to observe the fate of individual protein molecules inside the fibrils. A schematic drawing of this method is given in Figure 3.4.

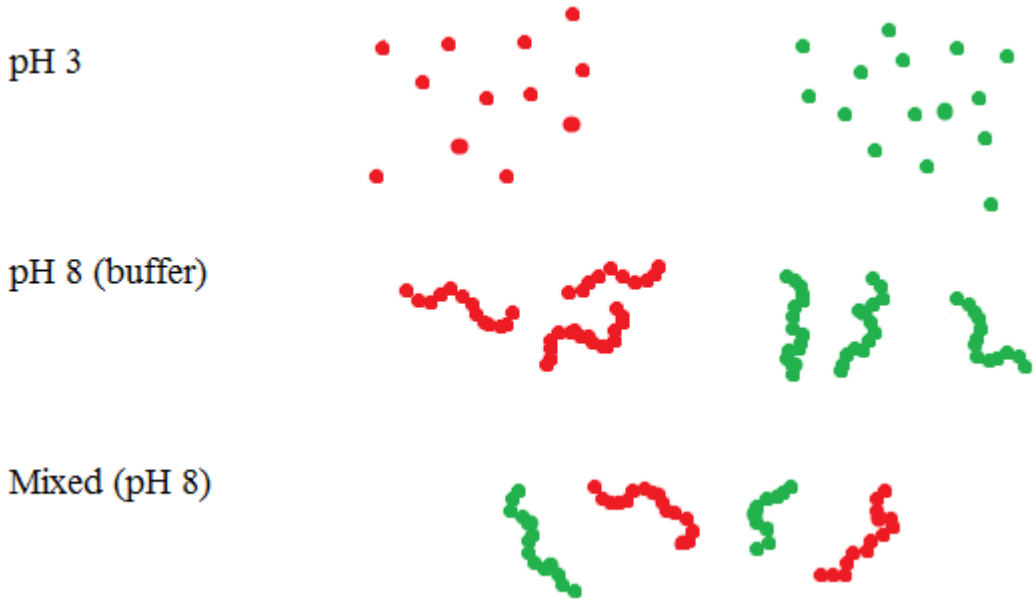

Figure 3.4: Schematic drawing of method to probe exchange dynamics of self-assembled protein fibrils. Green (488-labelled) and red (647-labelled) protein fibrils are created separately and subsequently mixed. After 3 days the sample was analyzed by means of STORM.

The result was a series of images of separate, either purely 488-labelled (green) fibrils or 647-labelled (red) fibrils (Fig 3.5). A STORM image of this sample is presented in Figure A3.1. We did not observe any cross talk between the channels. No exchange of labelled

monomers had occurred between fibrils; each fibril only contained one kind of fluorescent label (the very few single counts of the opposite label in each fibril are negligible). This means that individual protein polymer molecules are kinetically trapped inside the fibril; on this timescale they do not exchange with single protein polymer molecules left in solution. This behavior differs from the previously reported exchange mechanism of BTA supramolecular polymers [33]. That study also reported purely red and purely green labelled aggregates directly after mixing them. However, in a timeframe of hours these BTA assemblies exchanged their monomers with the bulk solution and became mixtures of red and green labelled monomers. Our study extends this work by probing aggregates that lack molecular exchange on this timescale, and well beyond.

We also conclude that no end-to-end connection of individual fibrils occurs; this would have resulted in bi-colored block structures. As a consequence, it is possible to create stable mixtures in which self-assembled fibrils with different (bio-)chemical moieties co-exist. Fast exchange dynamics would result in a rapid dilution of any moiety throughout the mixture, but we do not observe this. The lack of exchange dynamics leaves the possibility open to make spatially heterogeneous hydrogels with locally varying densities of specific moieties (e.g. cell binding domains, hormonal domains, etc.).

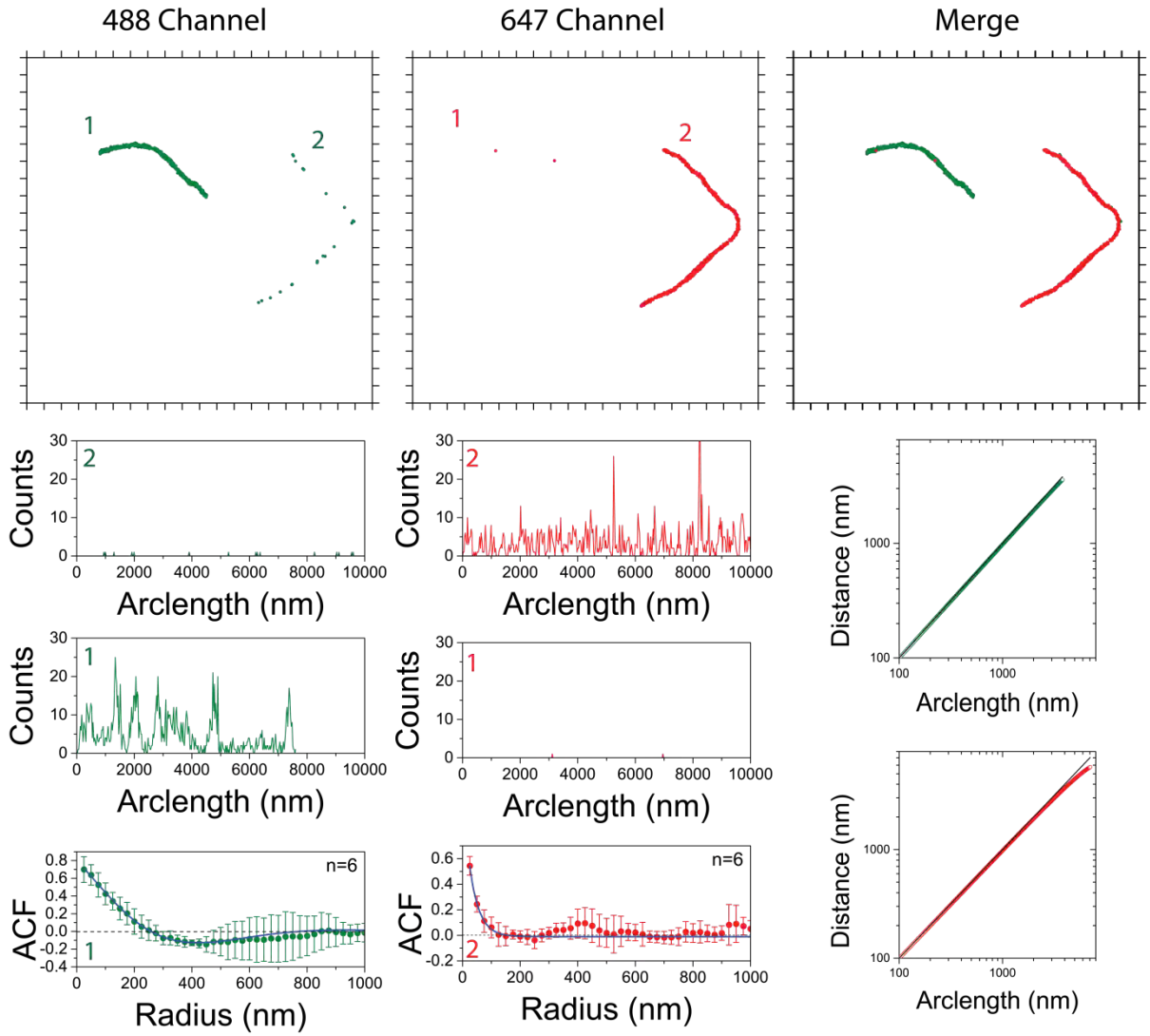

Figure 3.5: Analysis of STORM images of sample containing green (488-labelled) and red (647-labelled) self-assembled protein fibrils. The sample contained a mixture of separately self-assembled red (647-labelled) fibrils and green (488-labelled) fibrils (both self-assembled for one week at pH 8.0 in 50mM phosphate buffer at 0.1 g/L of protein). Both samples were mixed in a 1:1 ratio and the mixed sample was diluted 10x prior to measuring.

Figure 3.5 shows histograms of the localizations of the two labels along the fibrils. The 647 channel shows a homogeneous (random) distribution while the profile on the 488 channel seems a bit patchy. This is confirmed by the autocorrelation analysis (ACF plot) that shows a long-range correlation for the green 488 channel, due to the patchiness, while this trend is absent in the red 647 channel. This may be due to the clustering of 488-labelled protein

polymers within one fibril. The autocorrelation functions have been fitted (solid lines in ACF diagrams) with a model for a patchy distribution (green) and a homogeneous distribution (red).

We used scaling analysis to determine the rigidity of the protein fibrils [39]. We measured the end-to-end distance as well as the contour length of the fibrils. For lengths well below the persistence length, the fibril behaves as a stiff rod: end-to-end distance and contour length are the same (the scaling exponent is 1). When the contour length of the fibril significantly exceeds its persistence length, the scaling behavior resembles that of a random walk (an exponent of 0.5). Our analysis of end-to-end distance and contour length of the fibrils shows a persistence length that exceeds 1 μm. Below this length, the scaling exponent equals 1, while only at larger length scales the scaling exponent starts to drop. The contour length of the fibrils is too short to determine the persistence length in more detail. We do see that contour length and persistence length of the fibrils are of the same order of magnitude (~ 1 μm). For a solution of stiff fibrils of L = 1 μm of this protein, the overlap concentration (scaling with L^{-2}) is 0.11 g/L. An increase in length of the fibrils would lead to a sharp decrease in the overlap concentration, and thus much more dilute hydrogels. If, however, this increase in length leads to (semi-)flexible fibrils, the decrease of the overlap concentration would be less. If extension of fibril length can be accompanied by increasing the persistence length, e.g. by controlled bundling into thicker fiber structures, these structures might form very dilute hydrogels.

Finally, we use STORM to probe the existence of living ends of the self-assembled fibrils. In previous work we used light scattering to prove the existence of at least one living end for self-assembled fibrils of similar protein polymers [34]. The use of two fluorescent labels in STORM provides the possibility of establishing whether there is only one living end, or whether there are two. We attempted to produce multi-colored fibrils as follows: We first

prepared a sample containing 647 labelled (red) protein polymers and allowed these to self-assemble into fibrils at pH 8.0 (50 mM phosphate buffer) for one week (a similar sample as presented in Figure 3.3). After one week we had a solution consisting of 647-labelled protein fibrils and very few molecularly dissolved protein polymers [40]. We then added to this solution a batch of 488-labelled, molecularly dissolved protein polymers. The latter start to self-assemble due to the pH (8.0) of the buffered solution containing 647-labelled fibrils. This method is graphically presented in Figure 3.6.

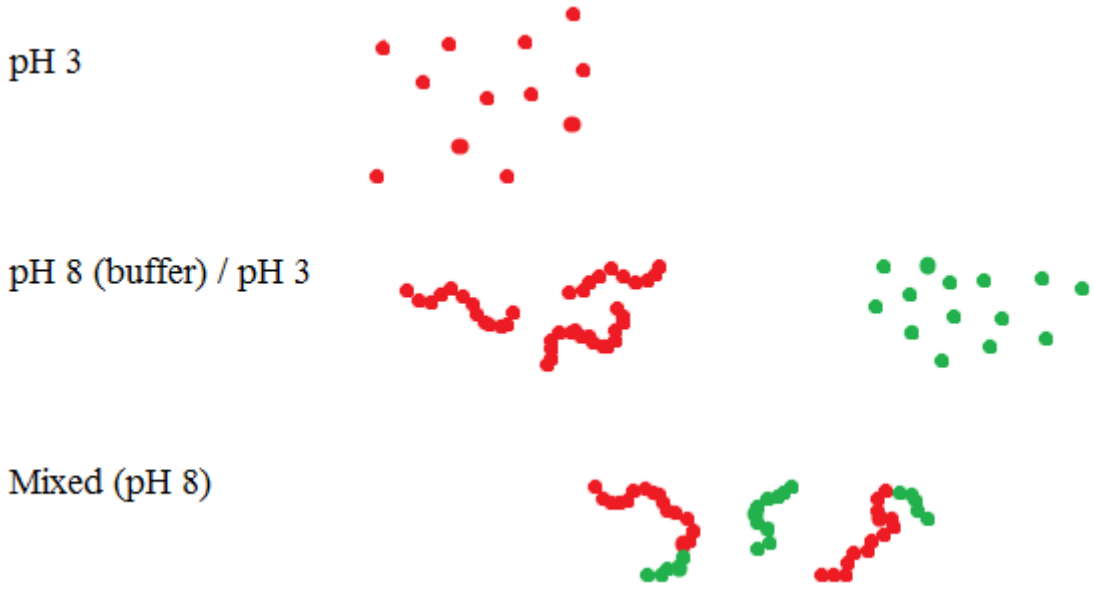

Figure 3.6: Schematic drawing of method to probe living ends of self-assembled protein fibrils. Red (647-labelled) protein fibrils are created separately and subsequently green (488-labelled) protein polymers were added to the buffered solution.

The result is a mixture of two populations. We observe fibrils that are a result of self-assembly of the 488-labelled newly added protein polymers: these fibrils are purely green. The second population consists of diblock structured fibrils with a red (647) and a green (488) block, resulting from the assembly of green molecules on one end of a red fibril. We present a processed image and its analysis of a diblock fibril in Figure 3.7. A STORM image of this sample is presented in Figure A3.2. The autocorrelation analysis presented in this

figure of these two-colored fibrils shows a bi-exponential decay, which is consistent with a pure diblock structure. As expected for the diblock structure, we see a negative cross correlation for short range and a positive cross correlation for long range. Remarkably, we exclusively observe diblock fibrils and no triblock fibrils. Such triblock structured fibrils can also be visualized with STORM and were found for fibrils consisting of α-synuclein [27]. This proves that our protein fibrils only grow from one end. This result is surprising, considering the highly symmetrical nature of our protein polymers. This behavior suggests a heterogeneous nucleation process in which nuclei, from which the fibrils grow, do not have identical ends. An inhomogeneous fibril nucleus is asymmetrical and is more likely to induce a specific direction for fibril growth.

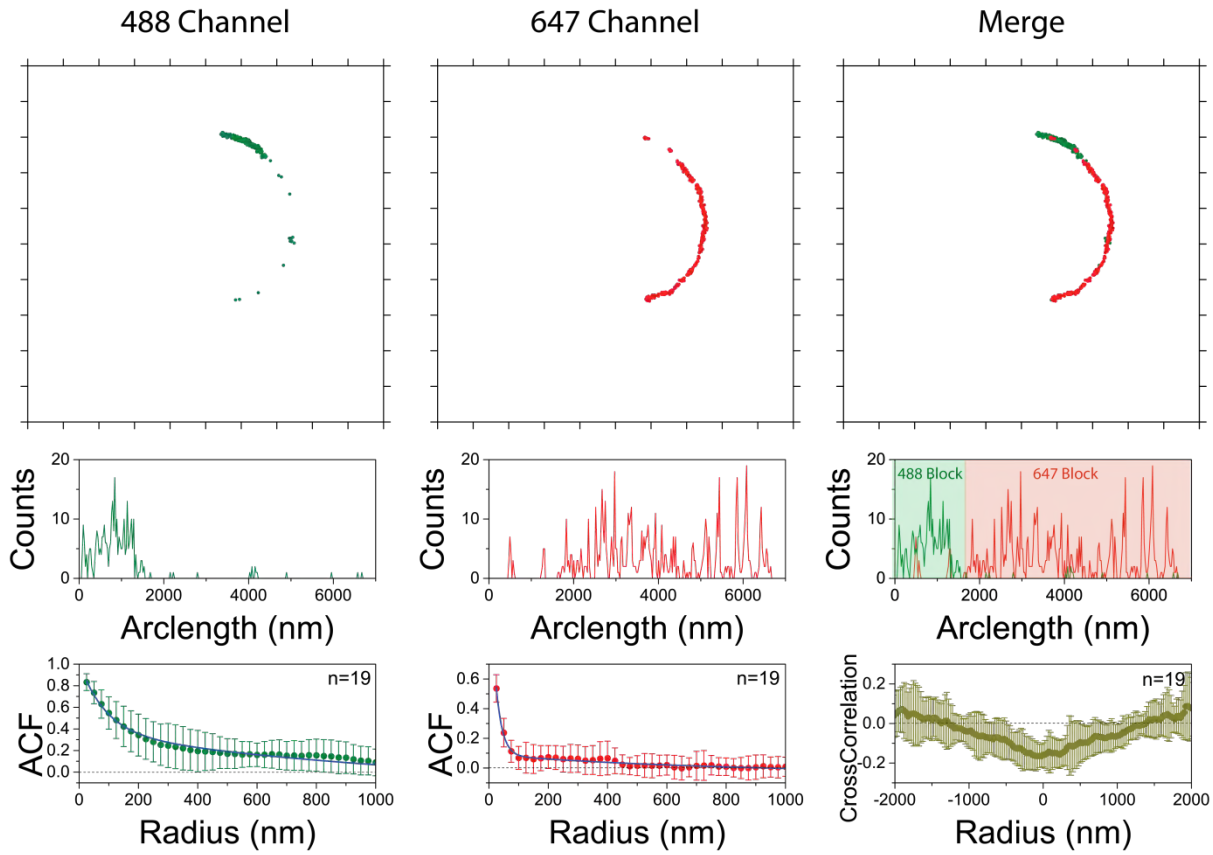

Figure 3.7: Analysis of STORM imaged bicolored self-assembled protein fibrils. The sample contained self-assembled red (647-labelled) fibrils (self-assembled for one week at pH 8.0 in 50mM phosphate buffer at 0.1 g/L of protein) to which molecularly dissolved green (488-labelled) protein polymers were added to a total concentration of 0.02 g/L. After 3 days the sample was imaged. Prior to imaging the sample was diluted 10x.

When analyzing the dimensions of each colored block in the diblock structured fibrils, we see that we have some control over size ratios of the different blocks. In Figure 3.8 we show that the ratio of concentrations of the differently labelled monomers has a clear effect on block length ratios. In both cases we create a buffered solution of red (647-labelled) fibrils, followed by the addition of green (488-labelled) molecularly dissolved proteins. When there is an excess of 647-labelled protein (ratio 5:1) we see the same ratio for the length of the two blocks. The relatively high concentration of red fibrils results predominantly in attachment of the green protein polymers to these red fibrils with only very limited nucleation of new, purely green fibrils. This is why the majority of the green labelled protein polymers ends up in diblock structured fibrils. When there is an equal amount of red labelled proteins (in fibrils) and green labelled proteins we do not observe a significant difference between block sizes in diblock structured fibrils, although any difference in size ratios could possibly be explained by the relatively high amount of newly nucleating purely green fibrils, resulting in a mixture of red-green diblock structured fibrils and purely green fibrils.

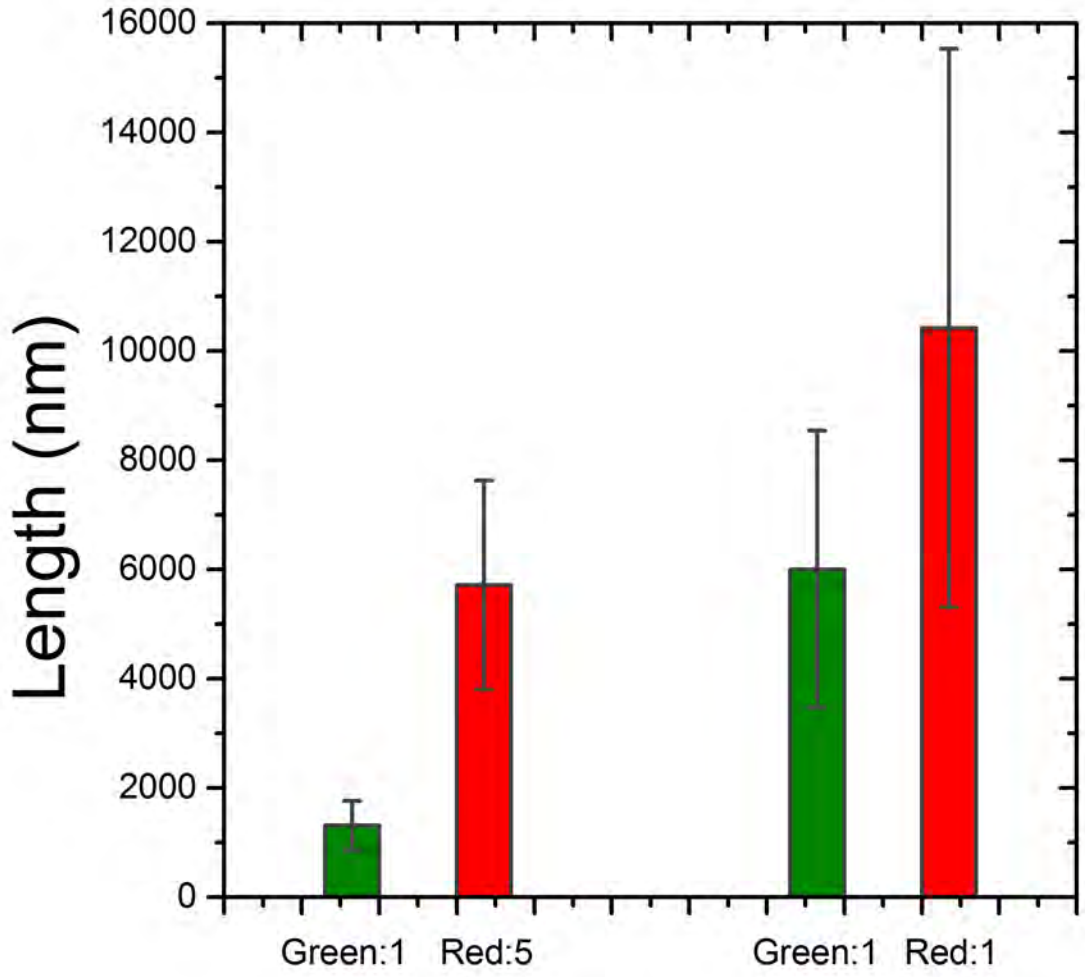

Figure 3.7: Size distribution of block structures in diblock colored fibrils (n = 20). Each sample contained 0.1 g/L of 647 (red) labelled protein polymer, self-assembled into fibrils (on week at pH 8.0, 50 mM phosphate buffer). Subsequently 488 (green) labelled protein polymers were added to 0.02 g/L (1:5 ratio) or 0.1 g/L (1:1 ratio) while the pH was kept constant. Samples were left to self-assemble for three days before imaging with STORM. Samples were diluted 10x prior to imaging.

CONCLUSION

We used stochastic optical reconstruction microscopy (STORM) and AFM to analyze growth and exchange dynamics of self-assembled protein fibrils. We demonstrate the power of STORM by analyzing these fibrils below the diffraction limit. The increased optical resolution compared to conventional fluorescence microscopy enabled us to probe exchange dynamics within fibrils on the molecular scale. We show the absence of molecular exchange dynamics in protein fibrils, providing valuable information on the stability of the fibril composition. We here explore a new regime, the one lacking exchange dynamics on the molecular scale, extending the pioneering work of some of us [33] on using STORM to probe exchange dynamics.

We also show that our self-assembled fibrils grow asymmetrically. That is, they always have only one living end. Considering the symmetric nature of the building blocks of these fibrils, this finding is very surprising. This asymmetric growth of protein fibrils, shown with STORM, and the continuous formation of new fibrils, shown with AFM, leads us to conclude that initial nucleation is heterogeneous. This knowledge provides new possibilities for controlling fibril dimensions: controlling the presence of the source of this heterogeneous nucleation gives control over the dimensions of the protein fibrils. This in turn will lead to an increased control over macroscopic properties of hydrogels based on these fibrils.

In our previous work, we described that $C_2S^H_{48}C_2$ protein polymers form dilute hydrogels under physiological conditions that are suitable for 2D cell cultures [37,40,41]. These fibrils however, do not form gels at extremely dilute conditions at which large pore sizes are present that have dimensions suitable for 3D cell cultures. To obtain these properties, we aim for higher order structures like bundled fibrils that will lead to longer stiffer protein fibers that form a gel at lower concentrations and with larger pores. The A-B diblock fibril structures we obtain in this study provide possibilities for controlled bundling of fibrils. By incorporating

appropriate chemical moieties in one block of the diblock fibril we can e.g., create diblock fibrils with one inert and one sticky block (e.g. opposite charges by choosing glutamic acids and arginines). In this way we can self-assemble A-B^+ and A-B^- fibrils separately in dilute solutions. Upon mixing both types of fibrils we can induce bundling of the fibrils and create a hydrogel. An advantage of this method is that the duration of the gelation is no longer dependent on the formation of fibrils from single protein molecules, but only depends on the time scale needed for fibrils to interact.

EXPERIMENTAL SECTION

Atomic Force Microscopy

AFM samples were prepared by first dissolving the protein polymer in a 10mM HCl solution. Subsequently the pH was adjusted by adding phosphate buffer stock solution to a final concentration of 50 mM at pH 8. At certain times after adjusting the pH, a drop of the solution was deposited on a 10 x 10 mm hydrophilic silicon wafer (Siltronic Corp.) with a thin oxide layer on top. The wafer was then rinsed with Milli-Q water and dried under a stream of nitrogen. The samples were analyzed using a Digital Instruments Nanoscope V in ScanAsyst mode and NP-10 silicon nitride tips (Bruker) with a nominal tip radius of 20 nm. The acquired images were analyzed using NanoScope Analysis 1.40.

STORM

Labelling

For STORM imaging we labelled two batches of the protein polymer with Alexa Fluor dyes (Life Technologies). Alexa Fluor 647 and Alexa Fluor 488 with NHS-ester were used to label the protein polymer at the N-terminus. Both labels are suitable for use in STORM [42] and the hydrophilic nature of Alexa Fluor labels minimizes the risk of interference with the self-assembling block of the protein polymer. The coupling reaction was performed overnight in phosphate buffer (50 mM) at pH 8.0. Afterwards the solution was run over a size exclusion column (PD-10 Desalting Column, GE Healthcare Life Sciences) to separate free label and exchange the solution for 10 mM HCl. Subsequently, the solution was filtered with centrifugal filters (Amicon Ultra, MWCO 3K, Merck Millipore) to determine the presence of any free label. Afterwards, protein concentration and labelling degree were determined spectrophotometrically.

Microscopy measurements

STORM measurements and analysis were based on previously described methods [33]. The samples containing separate red (647) labelled and green (488) labelled fibrils were prepared as follows: Stock solutions of each batch of labelled protein at pH 3 were prepared. From these solutions, a 0.1 g/L protein solution was prepared in 50mM phosphate buffer (pH 8). These solutions, in which the protein polymers self-assemble, were left for 3 days. Subsequently both solutions were mixed in a 1:1 ratio and left for 3 days. Afterwards, the solution was analyzed by means of STORM.

The samples containing the block structured fibrils were prepared as follows: From the stock solution of red (647) labelled protein, a 0.1 g/L protein solution was prepared in 50mM phosphate buffer (pH 8). This solution was left for 3 days. Subsequently, part of the stock solution of green (488) labelled protein was added, such that the ratio of 647:488 was either 1:1 or 5:1. The mixed solution was left for 3 days, before measuring with STORM.

APPENDIX

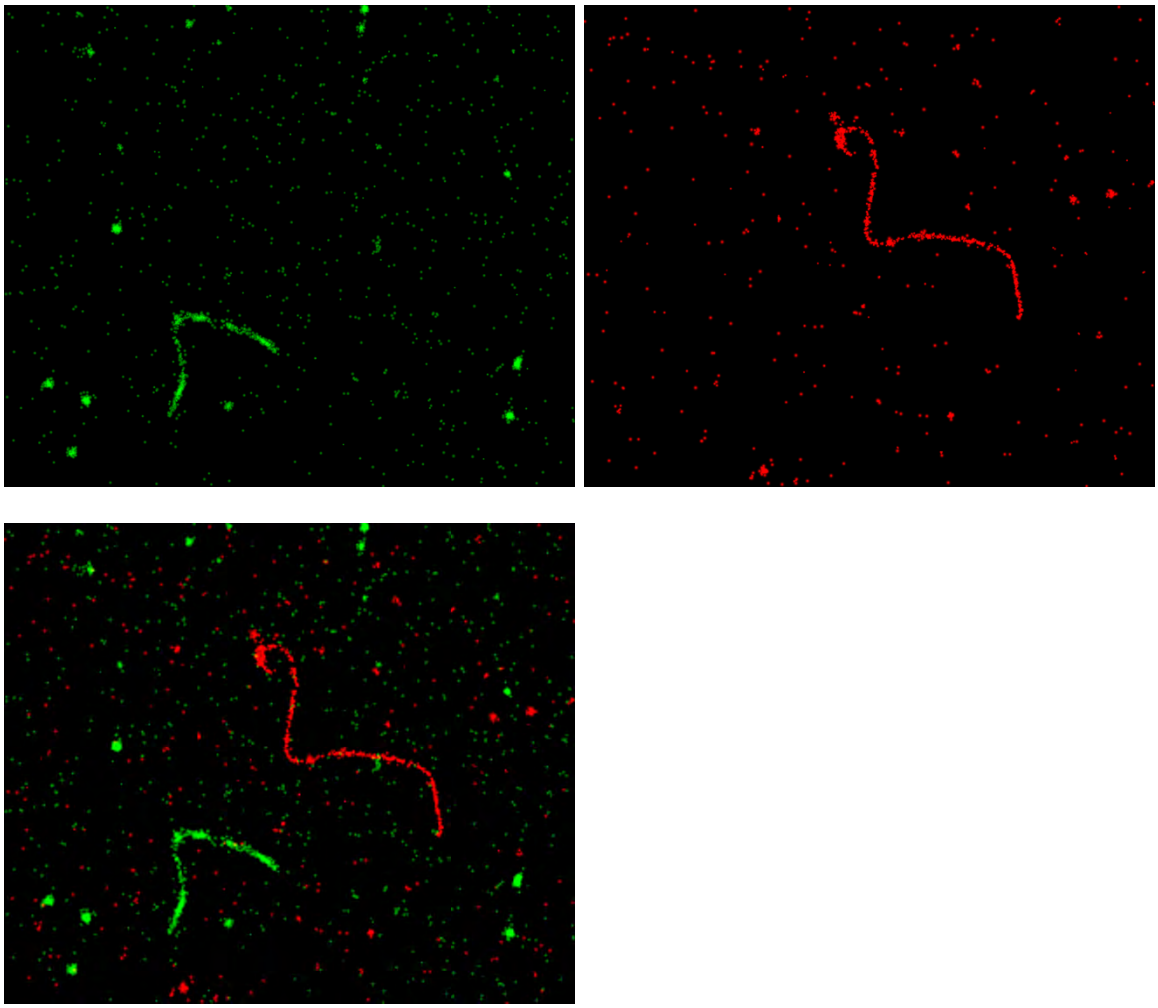

Figure A3.1: STORM images of separately created red and green labelled protein fibrils that were mixed subsequently. The images represent respectively the green (488) channel, the red (647) channel and the merged channel.

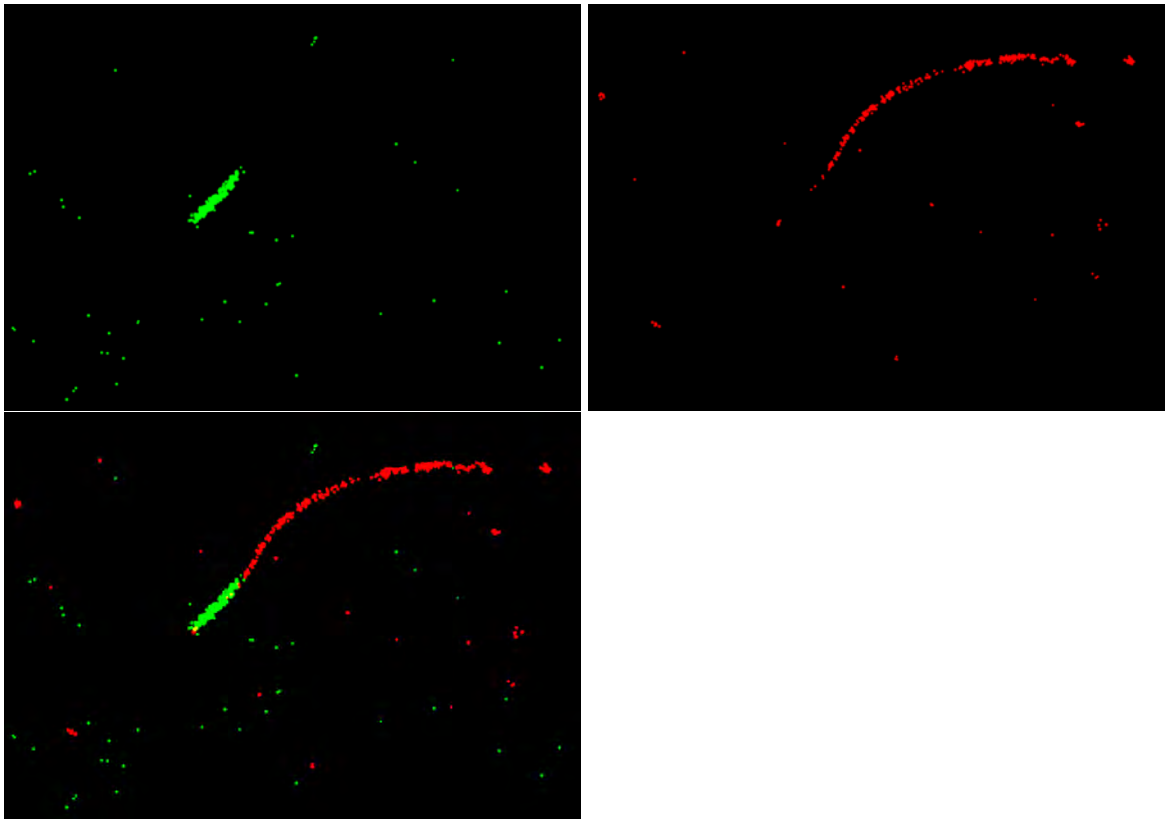

Figure A3.2: STORM images of diblock structured multi-colored fibril. The images represent respectively the green (488) channel, the red (647) channel and the merged channel.

REFERENCES

1. van Hest, J. C. M.; Tirrell, D. A. Protein-Based Materials, toward a New Level of Structural Control. *Chem Commun* **2001**, 1897-1904.
2. Li, M. Y.; Mondrinos, M. J.; Gandhi, M. R.; Ko, F. K.; Weiss, A. S.; Lelkes, P. I. Electrospun Protein Fibers as Matrices for Tissue Engineering. *Biomaterials* **2005**, 26, 5999-6008.
3. Daamen, W. F.; Veerkamp, J. H.; van Hest, J. C. M.; van Kuppevelt, T. H. Elastin as a Biomaterial for Tissue Engineering. *Biomaterials* **2007**, 28, 4378-4398.
4. Nettles, D. L.; Chilkoti, A.; Setton, L. A. Applications of Elastin-Like Polypeptides in Tissue Engineering. *Adv Drug Deliver Rev* **2010**, 62, 1479-1485.
5. Kundu, J.; Poole-Warren, L. A.; Martens, P.; Kundu, S. C. Silk Fibroin/Poly(Vinyl Alcohol) Photocrosslinked Hydrogels for Delivery of Macromolecular Drugs. *Acta Biomaterialia* **2012**, 8, 1720-1729.
6. Chilkoti, A.; Dreher, M. R.; Meyer, D. E. Design of Thermally Responsive, Recombinant Polypeptide Carriers for Targeted Drug Delivery. *Adv Drug Deliver Rev* **2002**, 54, 1093-1111.
7. Krejchi, M. T.; Atkins, E. D. T.; Waddon, A. J.; Fournier, M. J.; Mason, T. L.; Tirrell, D. A. Chemical Sequence Control of Beta-Sheet Assembly in Macromolecular Crystals of Periodic Polypeptides. *Science* **1994**, 265, 1427-1432.
8. Krejchi, M. T.; Atkins, E. D. T.; Fournier, M. J.; Mason, T. L.; Tirrell, D. A. Observation of a Silk-Like Crystal Structure in a Genetically Engineered Periodic Polypeptide. *J Macromol Sci Pure* **1996**, A33, 1389-1398.
9. Halbwirth, H.; Martens, S.; Wienand, U.; Forkmann, G.; Stich, K. Biochemical Formation of Anthocyanins in Silk Tissue of Zea Mays. *Plant Sci* **2003**, 164, 489-495.
10. Huang, J.; Foo, C. W. P.; Kaplan, D. L. Biosynthesis and Applications of Silk-Like and Collagen-Like Proteins. *Polym Rev* **2007**, 47, 29-62.
11. Werten, M. W. T.; Moers, A. P. H. A.; Vong, T.; Zuilhof, H.; van Hest, J. C. M.; de Wolff, F. A. Biosynthesis of an Amphiphilic Silk-Like Polymer. *Biomacromolecules* **2008**, 9, 1705-1711.
12. Martens, A. A.; Portale, G.; Werten, M. W. T.; de Vries, R. J.; Eggink, G.; Stuart, M. A. C.; de Wolf, F. A. Triblock Protein Copolymers Forming Supramolecular Nanotapes and Ph-Responsive Gels. *Macromolecules* **2009**, 42, 1002-1009.
13. Golinska, M. D.; Pham, T. T. H.; Werten, M. W. T.; de Wolf, F. A.; Stuart, M. A. C.; van der Gucht, J. Fibril Formation by Ph and Temperature Responsive Silk-Elastin Block Copolymers. *Biomacromolecules* **2013**, 14, 48-55.
14. Altman, G. H.; Diaz, F.; Jakuba, C.; Calabro, T.; Horan, R. L.; Chen, J. S.; Lu, H.; Richmond, J.; Kaplan, D. L. Silk-Based Biomaterials. *Biomaterials* **2003**, 24, 401-416.
15. Xia, X. X.; Wang, M.; Lin, Y. A.; Xu, Q. B.; Kaplan, D. L. Hydrophobic Drug-Triggered Self-Assembly of Nanoparticles from Silk-Elastin-Like Protein Polymers for Drug Delivery. *Biomacromolecules* **2014**, 15, 908-914.
16. Silva, C. I. F.; Skrzeszewska, P. J.; Golinska, M. D.; Werten, M. W. T.; Eggink, G.; de Wolf, F. A. Tuning of Collagen Triple-Helix Stability in Recombinant Telechelic Polymers. *Biomacromolecules* **2012**, 13, 1250-1258.
17. Skrzeszewska, P. J.; Jong, L. N.; de Wolf, F. A.; Stuart, M. A. C.; van der Gucht, J. Shape-Memory Effects in Biopolymer Networks with Collagen-Like Transient Nodes. *Biomacromolecules* **2011**, 12, 2285-2292.
18. Skrzeszewska, P. J.; de Wolf, F. A.; Werten, M. W. T.; Moers, A. P. H. A.; Stuart, M. A. C.; van der Gucht, J. Physical Gels of Telechelic Triblock Copolymers with Precisely Defined Junction Multiplicity. *Soft Matter* **2009**, 5, 2057-2062.

19. Schipperus, R.; Eggink, G.; de Wolf, F. A. Secretion of Elastin-Like Polypeptides with Different Transition Temperatures by Pichia Pastoris. *Biotechnol Progr* **2012**, 28, 242-247.
20. Meyer, D. E.; Trabbic-Carlson, K.; Chilkoti, A. Protein Purification by Fusion with an Environmentally Responsive Elastin-Like Polypeptide: Effect of Polypeptide Length on the Purification of Thioredoxin. *Biotechnol Progr* **2001**, 17, 720-728.
21. van Eldijk, M. B.; Wang, J. C. Y.; Minten, I. J.; Li, C. L.; Zlotnick, A.; Nolte, R. J. M.; Cornelissen, J. J. L. M.; van Hest, J. C. M. Designing Two Self-Assembly Mechanisms into One Viral Capsid Protein. *J Am Chem Soc* **2012**, 134, 18506-18509.
22. Li, L. Q.; Tong, Z. X.; Jia, X. Q.; Kiick, K. L. Resilin-Like Polypeptide Hydrogels Engineered for Versatile Biological Function. *Soft Matter* **2013**, 9, 665-673.
23. Charati, M. B.; Ifkovits, J. L.; Burdick, J. A.; Linhardt, J. G.; Kiick, K. L. Hydrophilic Elastomeric Biomaterials Based on Resilin-Like Polypeptides. *Soft Matter* **2009**, 5, 3412-3416.
24. Elvin, C. M.; Carr, A. G.; Huson, M. G.; Maxwell, J. M.; Pearson, R. D.; Vuocolo, T.; Liyou, N. E.; Wong, D. C. C.; Merritt, D. J.; Dixon, N. E. Synthesis and Properties of Crosslinked Recombinant Pro-Resilin. *Nature* **2005**, 437, 999-1002.
25. Geckil, H.; Xu, F.; Zhang, X. H.; Moon, S.; Demirci, U. Engineering Hydrogels as Extracellular Matrix Mimics. *Nanomedicine-Uk* **2010**, 5, 469-484.
26. Heilemann, M. Fluorescence Microscopy Beyond the Diffraction Limit. *J Biotechnol* **2010**, 149, 243-251.
27. Pinotsi, D.; Buell, A. K.; Galvagnion, C.; Dobson, C. M.; Schierle, G. S. K.; Kaminski, C. F. Direct Observation of Heterogeneous Amyloid Fibril Growth Kinetics Via Two-Color Super-Resolution Microscopy. *Nano Lett* **2014**, 14, 339-345.
28. Toomre, D.; Bewersdorf, J. A New Wave of Cellular Imaging. *Annu Rev Cell Dev Bi* **2010**, 26, 285-314.
29. Szymborska, A.; de Marco, A.; Daigle, N.; Cordes, V. C.; Briggs, J. A. G.; Ellenberg, J. Nuclear Pore Scaffold Structure Analyzed by Super-Resolution Microscopy and Particle Averaging. *Science* **2013**, 341, 655-658.
30. Doksani, Y.; Wu, J. Y.; de Lange, T.; Zhuang, X. W. Super-Resolution Fluorescence Imaging of Telomeres Reveals Trf2-Dependent T-Loop Formation. *Cell* **2013**, 155, 345-356.
31. Mennella, V.; Keszthelyi, B.; McDonald, K. L.; Chhun, B.; Kan, F.; Rogers, G. C.; Huang, B.; Agard, D. A. Subdiffraction-Resolution Fluorescence Microscopy Reveals a Domain of the Centrosome Critical for Pericentriolar Material Organization. *Nat Cell Biol* **2012**, 14, 1159-+.
32. Jones, S. A.; Shim, S. H.; He, J.; Zhuang, X. W. Fast, Three-Dimensional Super-Resolution Imaging of Live Cells. *Nat Methods* **2011**, 8, 499-U96.
33. Albertazzi, L.; van der Zwaag, D.; Leenders, C. M. A.; Fitzner, R.; van der Hofstad, R. W.; Meijer, E. W. Probing Exchange Pathways in One-Dimensional Aggregates with Super-Resolution Microscopy. *Science* **2014**, 344, 491-495.
34. Beun, L. H.; Beaudoux, X. J.; Kleijn, J. M.; de Wolf, F. A.; Stuart, M. A. C. Self-Assembly of Silk-Collagen-Like Triblock Copolymers Resembles a Supramolecular Living Polymerization. *Acs Nano* **2012**, 6, 133-140.
35. Schor, M.; Martens, A. A.; Dewolf, F. A.; Stuart, M. A. C.; Bolhuis, P. G. Prediction of Solvent Dependent Beta-Roll Formation of a Self-Assembling Silk-Like Protein Domain. *Soft Matter* **2009**, 5, 2658-2665.
36. Werten, M. W. T.; Wisselink, W. H.; van den Bosch, T. J. J.; de Bruin, E. C.; de Wolf, F. A. Secreted Production of a Custom-Designed, Highly Hydrophilic Gelatin in Pichia Pastoris. *Protein Eng* **2001**, 14, 447-454.

37. Golinska, M. D.; Wlodarczyk-Biegun, M. K.; Werten, M. W. T.; Stuart, M. A. C.; de Wolf, F. A.; de Vries, R. Dilute Self-Healing Hydrogels of Silk-Collagen-Like Block Copolypeptides at Neutral Ph. *Biomacromolecules* **2014**, 15, 699-706.
38. Martens, A. A.; van der Gucht, J.; Eggink, G.; de Wolf, F. A.; Stuart, M. A. C. Dilute Gels with Exceptional Rigidity from Self-Assembling Silk-Collagen-Like Block Copolymers. *Soft Matter* **2009**, 5, 4191-4197.
39. Valle, F.; Favre, M.; De Los Rios, P.; Rosa, A.; Dietler, G. Scaling Exponents and Probability Distributions of DNA End-to-End Distance. *Phys Rev Lett* **2005**, 95.
40. Beun, L. H.; Storm, I. M.; Werten, M. W.; de Wolf, F. A.; Cohen Stuart, M. A.; de Vries, R. From Micelles to Fibers: Balancing Self-Assembling and Random Coiling Domains in Ph-Responsive Silk-Collagen-Like Protein-Based Polymers. *Biomacromolecules* **2014**, 15, 3349-57.
41. Wlodarczyk-Biegun, M. K.; Werten, M. W.; de Wolf, F. A.; van den Beucken, J. J.; Leeuwenburgh, S. C.; Kamperman, M.; Cohen Stuart, M. A. Genetically Engineered Silk-Collagen-Like Copolymer for Biomedical Applications: Production, Characterization and Evaluation of Cellular Response. *Acta Biomaterialia* **2014**, 10, 3620-9.
42. Dempsey, G. T.; Vaughan, J. C.; Chen, K. H.; Bates, M.; Zhuang, X. W. Evaluation of Fluorophores for Optimal Performance in Localization-Based Super-Resolution Imaging. *Nat Methods* **2011**, 8, 1027-+.

Chapter 4

From Micelles to Fibers: Balancing Self-Assembling and Random Coil Domains in pH-Responsive Silk-Collagen-Like Protein-Based Polymers.

This chapter is published as: Beun, L. H.; Storm, I. M.; Werten, M. W. T.; de Wolf, F. A.; Cohen Stuart, M. A.; de Vries, R. *Biomacromolecules* **2014**, 15, 3349−3357

ABSTRACT

We study the self-assembly of genetically engineered protein-based triblock copolymers consisting of a central pH-responsive silk-like middle block (S^H_n, where S^H is a silk-like octapeptide, $(GA)_3GH$ and n is the number of repeats) flanked by hydrophilic random coil outer blocks (C_2). Our previous work has already shown that triblocks with very long midblocks (n=48) self-assemble into long, stiff protein filaments at pH values where the middle blocks are uncharged. Here we investigate the self-assembly behavior of the triblock copolymers for a range of midblock lengths, n = 8, 16, 24, 48. Upon charge neutralization of S^H_n by adjusting the pH, we find that $C_2S^H_8C_2$ and $C_2S^H_{16}C_2$ form spherical micelles, whereas both $C_2S^H_{24}C_2$ and $C_2S^H_{48}C_2$ form protein filaments with a characteristic beta-roll secondary structure of the silk mid-blocks. Hydrogels formed by $C_2S^H_{48}C_2$ are much stronger and form much faster than those formed by $C_2S^H_{24}C_2$. Enzymatic digestion of much of the hydrophilic outer blocks is used to show that with much of the hydrophilic outer blocks removed, all silk-midblocks are capable of self-assembling into stiff protein filaments. In that case, reduction of the steric repulsion by the hydrophilic outer blocks also leads to extensive fiber bundling. Our results highlight the opposing roles of the hydrophilic outer blocks and central silk-like midblocks in driving protein filament formation. They provide crucial information for future designs of triblock protein-based polymers that form stiff filaments with controlled bundling, which could mimic properties of collagen in the extracellular matrix.

INTRODUCTION

Designed recombinant protein-based polymers are a promising class of new polymer materials with potential applications in fields such as tissue engineering, drug- and gene delivery or self-healing biomaterials [1-8]. A major advantage of recombinant protein-based polymers over polymers produced using synthetic chemistry is that the route of genetic engineering provides in principle a virtually perfect control over size, amino acid sequence and stereochemistry of the polymers. As a consequence, the final degree of control over the relevant physicochemical properties of materials made of these polymers is superior to that of any established chemical polymerization method. Being based on amino acids, a vast array of naturally occurring peptide sequences or domains can be used as inspiration for new designs. Domains that have been extensively explored in recent years include those with sequences inspired by, or based on structural proteins known for their superior stimulus-responsive, mechanical, biocompatible and structural properties. These include natural elastin [9-15], collagen [16-19], silk [9, 19-24] and resilin [25-27].

A key challenge in biomaterials is to mimic the extracellular matrix, in order to make materials that can act as scaffolds for cell- and tissue growth. Stiff collagen-like fibers are thought to be an important element in such materials. We have previously designed pH-responsive recombinant protein-based polymers that self-assemble into stiff fibrils. The polymers have a symmetric triblock structure and are composed of a silk-like mid-block flanked on both sides by hydrophilic random coiling outer blocks.

The proteins in this study have a triblock conformation, with a silk-like middle block and random coil hydrophilic outer blocks. The silk-like middle block consists of a number of repeats of the octapeptide GAGAGAGX (S^X). This amino acid sequence is inspired by natural silk produced by the silk worm *Bombyx Mori* [23] and is known to trigger self-assembly into a filamentous structure that most likely is a stack of so-called beta-rolls [19, 20, 28]. Charges on the

residue X prevent the self-assembly, and by choosing amino acids with basic or acidic side chains, self-assembly of the protein filaments can be controlled by pH. The random coil hydrophilic outer blocks are essential, since without them, the protein filaments aggregate and precipitate [29]. Hence, their role is to provide colloidal stability by exposing a hydrophilic polymer brush on the outside of the filaments [30]. The block is rich in hydrophilic amino acids glutamine, asparagine and serine and has a sequence that has similarities to natural collagen (GXY triplets). The basic repeating unit for this protein-based polymer is a 99 amino acid long "C"-block [19, 30]. The exact sequence can be found in the supporting information (Fig. S4.1)

In previous studies, we have characterized protein filaments and gels formed by $C_2S^X_{48}C_2$ protein-based triblock copolymers, where C_2 is a dimer of the "C" block, and S^X_{48} is a 48-fold repetition of the silk-like octapeptide S^X. pH-responsive residues in our previous studies have been glutamic acid (X=E), histidine (X=H) or lysine (X=K) [19, 20, 31].

For use of these and other protein filaments in applications, one ideally should have full and independent control over the relevant material properties such as gelling time after a pH adjustment, control of gel rheology independent from polymer concentration, etc. This, in turn, requires full control over the properties of the protein filaments: growth kinetics, length- and rigidity, and lateral association into fiber bundles. A key variable in controlling the self-assembly of our triblock copolymers into filaments obviously is the relative size of the various blocks. Therefore, we here study the role of the balance of self-assembling and random coil domains for pH-responsive silk-collagen-like protein-based polymers.

We focus on the effect of changing the size of the central silk-like domain. As the X residue we choose histidine, since this results in protein filament formation at physiological pH [32] , which is most relevant for biomedical applications. A series of four protein-based polymers $C_2S^H_nC_2$ was constructed, produced and characterized with a number *n* of octapeptide repeats

of n = 8, 16, 24 and 48. As we will show, the silk-like blocks S^{H}_{n} with n = 8, 16, 24 and 48 all have a tendency to form protein filaments, but the driving force for doing so increases with the number of repeats n. Filament formation is opposed by the C_2 sideblocks, and below a certain critical number of repeats n of the silk block, $C_2S^{H}_{n}C_2$ polymers start forming micelles rather than filaments. Our study provides insights into the driving forces of filament formation of protein-based polymers that are crucial for future protein-based polymer designs with improved independent control over filament growth, lateral association of protein filaments and the resulting hydrogel properties.

RESULTS AND DISCUSSION

Protein characterization

The four proteins described in this study include 3 new constructs and one described previously [32]. The molecular weight (MW) of each newly constructed protein was measured with MALDI-TOF MS and compared to the theoretical mass predicted from the amino acid composition. As shown in Table 3.1, experimentally determined masses match those expected theoretically within the experimental uncertainty. Additionally, Dynamic Light Scattering (DLS) was used to determine the size of the proteins when fully charged at pH 2. Hydrodynamic sizes of the four proteins $C_2S^H_nC_2$ with n = 8, 16, 24 and 48 in solution at pH 2 are shown in Table 4.1, and are typical for molecularly dissolved non-globular proteins of these molar masses.

Table 4.1: Characterization of protein-polymers described in this study. Theoretical and measured (MALDI-TOF MS) mass, and hydrodynamic radius (Rh) as measured by DLS at pH 2 (10mM HCl).

Protein	Theoretical MW (Da)	Measured MW (Da)	Rh at pH 2 (nm)
$C_2S^H_8C_2$	42992	42952	4.9 ± 0.2
$C_2S^H_{16}C_2$	47621	47617	5.6 ± 0.6
$C_2S^H_{24}C_2$	52249	52242	6.2 ± 0.2
$C_2S^H_{48}C_2$	66135	66076 [32]	6.8 ± 0.6

Protein polymers are secreted in the medium by the production organism, *Pichia pastoris*, and simple ammonium sulfate precipitation suffices to obtain highly pure protein polymers. SDS-PAGE gels for the newly constructed proteins $C_2S^H_8C_2$, $C_2S^H_{16}C_2$ and $C_2S^H_{24}C_2$ after purification using ammonium sulfate precipitation are shown in Figure 4.1.

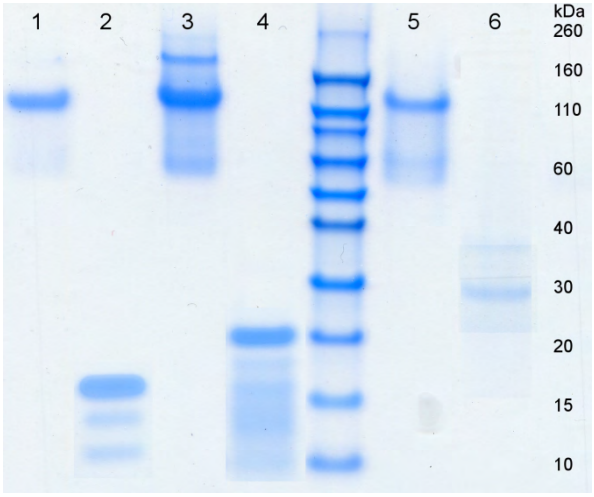

Figure 4.1: SDS-PAGE gel of purified and trypsin treated protein-polymers. Lane 1: $C_2S^H{}_8C_2$; lane 2: $C_2S^H{}_8C_2$ after trypsin digestion; lane 3: $C_2S^H{}_{16}C_2$; lane 4: $C_2S^H{}_{16}C_2$ after trypsin digestion; lane 5: $C_2S^H{}_{24}C_2$; lane 6: $C_2S^H{}_{24}C_2$ after trypsin digestion.

For each of the three proteins, there was a clear main band corresponding to the protein polymer. Note that the migration of the protein-based polymers is anomalously slow due to the poor SDS-binding capacity of the hydrophilic C_2-blocks, as has been described before. [19, 30]. This leads to an apparent mass of approximately 120 kDa. The band that is visible for all proteins migrating to an apparent mass of 60 kDa is similar to the band found in purified $C_2S^H{}_{48}C_2$. This band represents an SDS-PAGE artifact, as N-terminal sequencing combined with MALDI-TOF showed it was the intact protein [33]. We attribute the band at 200 kDa to multimers of the intact protein. The high purity of the protein samples is also confirmed with MALDI-TOF (Fig S4.2). Figure 4.1 also shows SDS-PAGE of purified proteins treated with trypsin to remove most of the outer blocks. These digested protein-polymers are also used in our physical studies and will be discussed in detail later on.

AFM

First we study the self-assembly of the protein-polymers after a pH shift from pH 2 to pH 8 using Atomic Force Microscopy (AFM) imaging. As is shown by the AFM images in Figure 3.2(a,b), after prolonged incubation at pH 8 (72h) the proteins with the longest silk-like mid-blocks, $C_2S^H_{48}C_2$ and $C_2S^H_{24}C_2$, form long, stiff filaments. For both proteins, the filaments have a height of approximately 2 nm, and lengths up to many micrometers. We did not find significant differences in the final filament lengths for the two proteins. The average width of the $C_2S^H_{24}C_2$ is 7 nm smaller than that of the $C_2S^H_{48}C_2$ filaments, which is close to half of the expected width of the folded S_{48} blocks [19, 28]. In contrast, the proteins with the shorter silk-like midblocks, $C_2S^H_{16}C_2$ and $C_2S^H_8C_2$, did not form filaments after a pH shift from pH 2 to pH 8, after prolonged incubation. Instead, these proteins appear to form micelles, as suggested by the pancake-like structures found with AFM and shown in Figure 4.2(c,d).

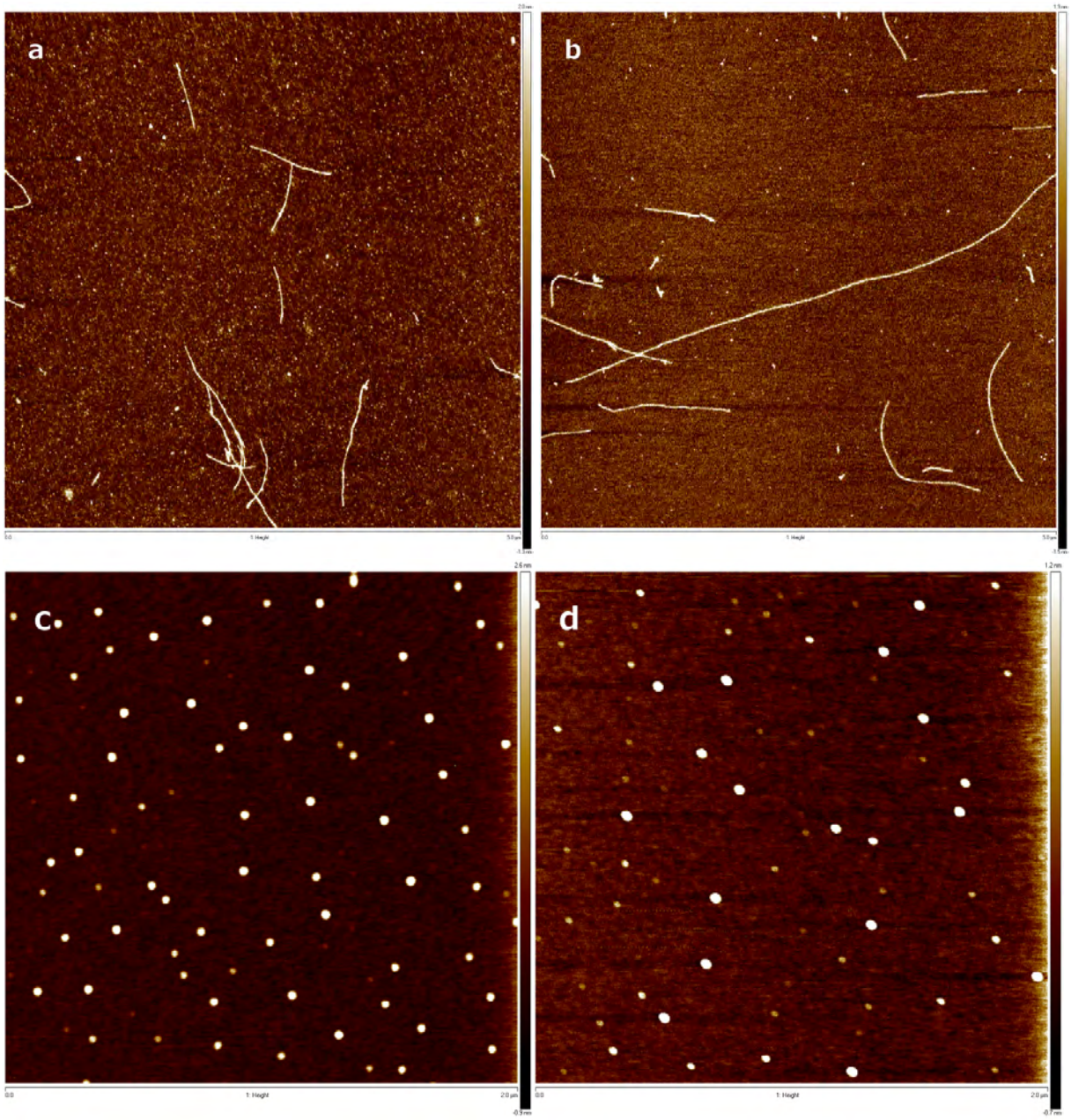

Figure 4.2: AFM images of self-assembled protein-polymers (1g/L), adsorbed to silica 72h after a pH quench from pH 2 to pH 8 (50 mM phosphate buffer). (a) $C_2S^H_{48}C_2$,(b) $C_2S^H_{24}C_2$, (c) $C_2S^H_{16}C_2$ (d) $C_2S^H_8C_2$. Images are 5x5 µm (a, b) or 2x2 µm (c, d).

DLS

Dynamic light scattering confirms the appearance of micelles at pH 8 in samples of $C_2S^H_{16}C_2$ and $C_2S^H_8C_2$. While at pH 2 both proteins are present as single molecules with R_h =

5.6 nm and 4.9 nm, at pH 8 they assemble into micelles with hydrodynamic radii more than doubled: 12.6 nm and 11.2 nm respectively.

When the pH of a solution containing micelles or fibers was lowered well below the pK_a of histidine by the addition of an excess HCl, we observed an immediate drop in scattered intensity and observed molecularly dissolved protein polymers. This shows that the self-assembly of all four protein polymers is fully reversible.

Circular Dichroism

The very different self-assembled structures of the proteins with the longest silk-like midblocks versus those with the shorter ones raises the question whether their secondary structure is also different. In order to assess changes in secondary structure after the pH shift from pH 2 to pH 8, we have performed circular dichroism (CD) spectroscopy of all proteins, both in their fully charged, monomeric form at pH 2, and in their neutralized and self-assembled form at pH 8.

Figure 4.3 shows that at pH 2 all proteins have nearly identical spectra. These spectra clearly have the signature of a random coil and are very similar to that of a pure C_4 block, for which it was previously shown that it behaves as a random coil over a wide range of solution conditions [30]. The similarity of the spectra over the entire series of triblocks leads us to conclude that at pH 2, both the hydrophilic outer blocks and the silk-like middle blocks have a random coil conformation.

Figure 4.3 also shows the CD spectra for the proteins at pH 8. The micelle-forming proteins with the shortest silk-like middle blocks only show a minor spectral shift as compared to the spectra at pH 2. The spectrum at pH 8 still mostly resembles that of a random coil. Note however, that this could still simply be a consequence of the relatively small contributions of the rather short silk-like middle-blocks to the total spectra. In contrast, the spectra of the

filament forming proteins with the longer silk-like midblocks at pH 8 show a very clear spectral shift as compared to pH 2. For this case, it is clear that a significant change of secondary structure occurs upon adjusting the pH.

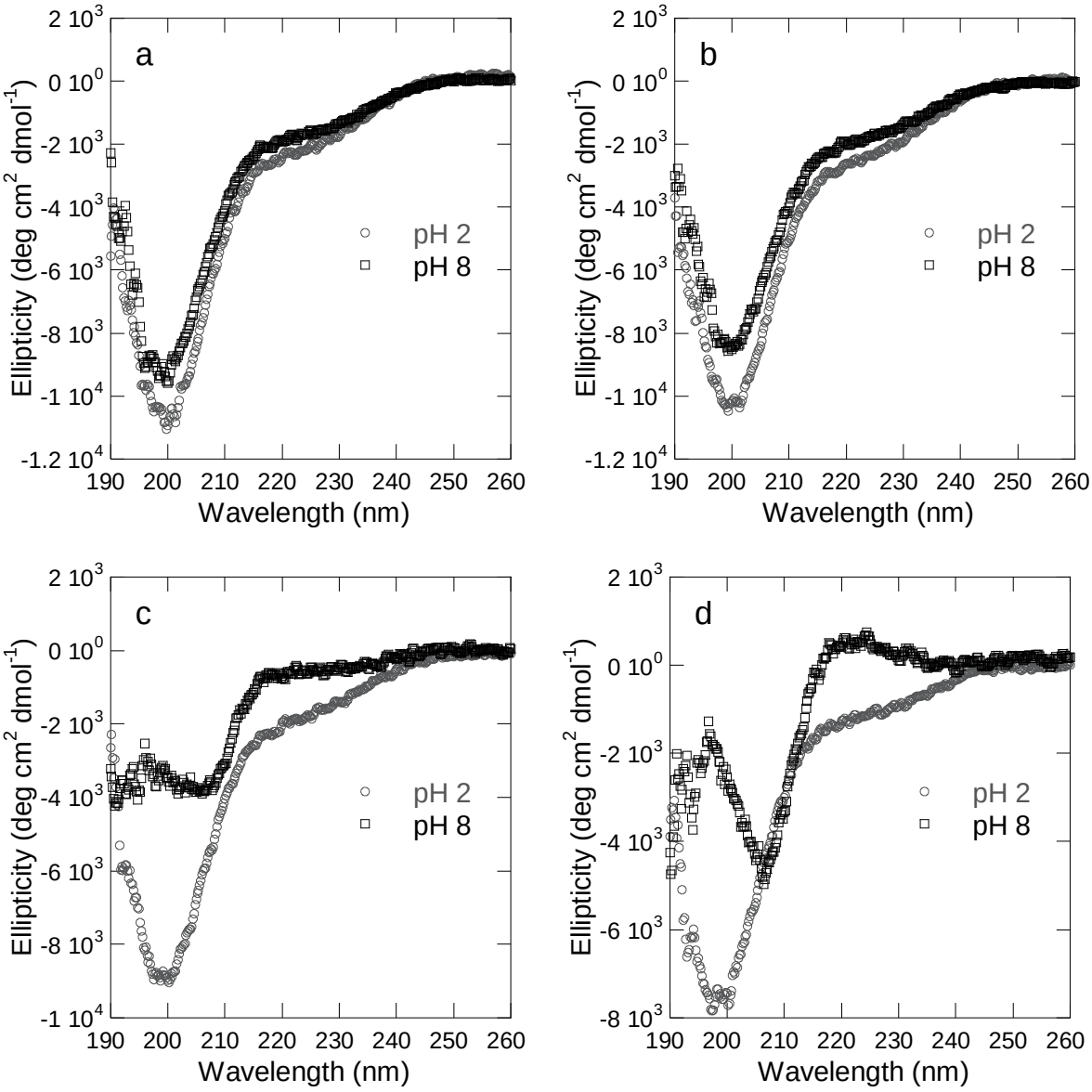

Figure 4.3: Molar ellipticity per amino acid of protein-polymer solutions of $C_2S^H{}_8C_2$ (a), $C_2S^H{}_{16}C_2$ (b), $C_2S^H{}_{24}C_2$ (c) and $C_2S^H{}_{48}C_2$ (d) in 10 mM HCl (pH 2) and 50 mM phosphate buffer (pH 8). Samples at pH 8 were measured 96 hours after adjusting the pH from 2 to 8.

In order to isolate the contribution of the silk-like midblocks to the total CD spectra, we have also acquired the spectra of a pure C_4 polymer, that should be identical to the combined spectrum of the two C_2 outer-blocks. Difference spectra pertaining to the isolated silk-like midblocks obtained by subtracting the spectra of the outer blocks are shown, for all four proteins, in Figure 4.4. For each protein, the mass fraction of the outer blocks was determined and the spectrum of the corresponding concentration of C_2-blocks was subtracted from the spectrum of the whole protein. It is clear that the absence of a change in secondary structure for the two proteins with the shortest silk-like midblocks is real, and is not caused by the signal of the outer blocks overwhelming that of the silk-like midblocks: for this case, the difference spectrum still has the signature characteristic of a random coil. Difference spectra for the S^H_{24} and S^H_{48} mid-blocks at pH 8 are also very similar to each other, but have a distinctly different CD spectrum suggesting that both have a secondary structure that is very different from a random coil. Molecular Dynamics simulations have indicated that the neutralized and folded silk-like block S^E_{48} obtains a beta-roll structure in solution [28]. This structure consists of two interconnected parallel beta-sheets and is consistent with fiber dimensions found with AFM and SAXS [19]. The CD spectra at pH 8 of $C_2S^H_{24}C_2$ and $C_2S^H_{48}C_2$ are very similar to that of neutralized $C_2S^E_{48}C_2$ [19], leading us to conclude the same beta-roll structure is present in the folded $C_2S^H_{24}C_2$ and $C_2S^H_{48}C_2$.

Moreover, from the fact that after extensive incubation at pH 8 the ellipticities per amino acid estimated for the S^H_{24} and S^H_{48} mid-blocks are very nearly equal in magnitude, we conclude that most likely, in both cases virtually all protein molecules self-assemble into filaments.

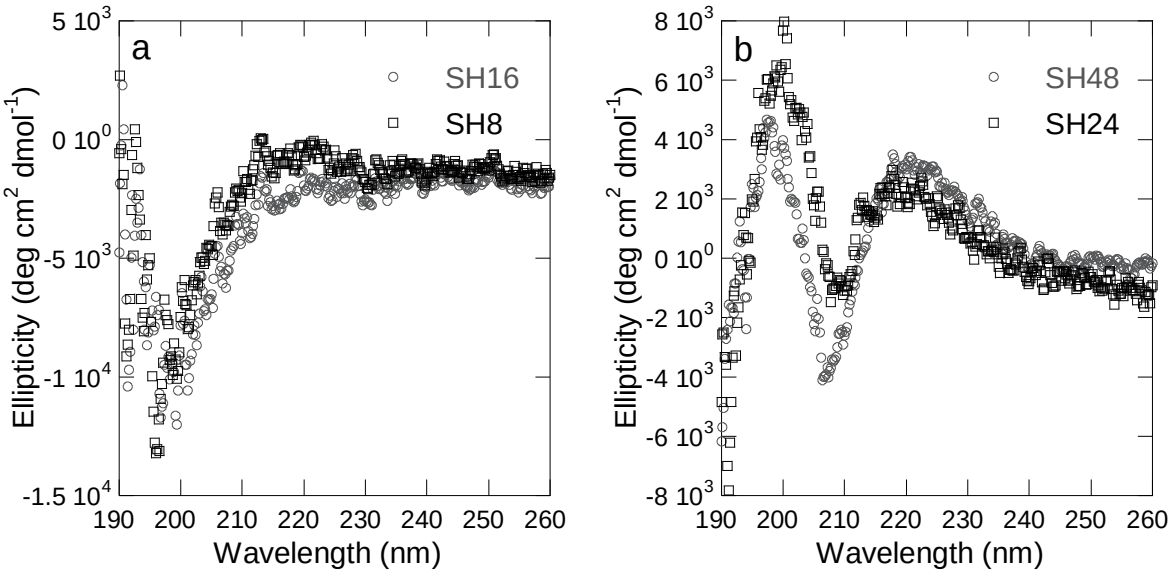

Figure 4.4: Molar ellipticity per amino acid of the isolated S^H_8 and S^H_{16} (a) and S^H_{24} and S^H_{48} (b) after subtraction of the signal of the C_2 sidechains from the signal of the triblock protein-polymers. All samples contained a total of 0.25 g/L of protein and were measured at pH 8 (50 mM phosphate buffer) 96 hours after a pH adjustment from pH2.

Time Resolved AFM

For the two proteins that self-assemble into filaments ($C_2S^H_{48}C_2$ and $C_2S^H_{24}C_2$), we have also elucidated the kinetics of filament formation using time resolved AFM imaging. This was achieved by taking aliquots after different times of incubation at pH 8, after the pH adjustment from acidic pH. Immediately after taking the aliquot, it was deposited on a silica wafer, to quench the filament growth. For each aliquot, the length of a fair number of filaments (50-90) was determined and used to estimate the average filament length and its standard deviation. Results of this analysis are shown in Figure 4.5.

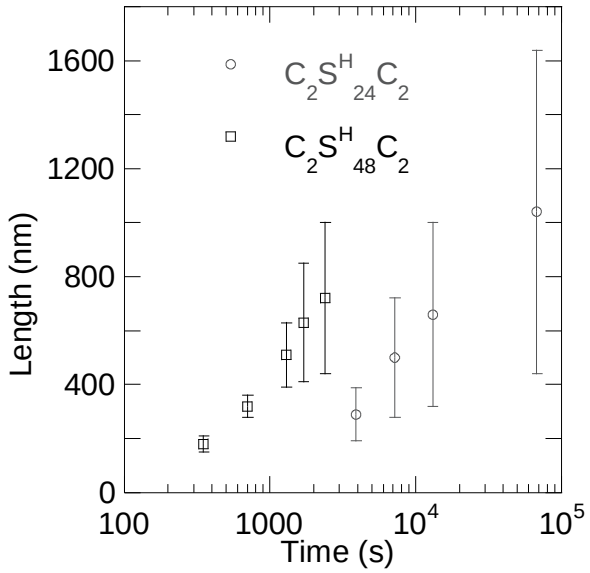

Figure 4.5: Average fiber length (n = 50-90) as a function of the time after shift from pH2 to pH8 (50 mM phosphate buffer) for 1 g/L solutions of $C_2S^H_{24}C_2$ and $C_2S^H_{48}C_2$, as measured by AFM. Error bars represent standard deviations.

Clearly, the average length of the $C_2S^H_{48}C_2$ filaments increases at a much higher rate than the average length of the $C_2S^H_{24}C_2$ filaments. For both proteins, the size distribution of the filaments quite dramatically broadens with incubation time. This must mean that there is continuous nucleation of filaments, with existing fibers elongating by the attachment of additional proteins, and new filaments being formed at the same time. Such a continuous nucleation is very different from the self-assembly of proteins of an inverted silk-collagen triblocks $S^E_{24}C_2C_2S^E_{24}$ that we have studied before. For that polymer, we observed fast nucleation immediately after the pH induced charge neutralization, followed by elongation of existing fibers without the formation of many new ones [20]. Such a mechanism obviously leads to a much narrower size distribution than the continuous nucleation mechanism that we observe for $C_2S^H_{48}C_2$ and $C_2S^H_{24}C_2$. The inverted sequence of $S^E_{24}C_2C_2S^E_{24}$ results in an extra complicating factor for nucleation, namely the meeting of the two ends of one molecule. This

can slow down homogeneous nucleation of new fibers severely. We anticipate that the occurrence of heterogeneous nucleation (possibly initiated by a small fraction of irreversibly folded protein, partially degraded protein or impurities that bind protein) leads to a fast nucleation step, followed by elongation of growing fibers. During this elongation, homogeneous nucleation is almost non-existing. $C_2S^H_{48}C_2$ and $C_2S^H_{24}C_2$ do not require this extra step during homogeneous nucleation and can therefore combine a quick heterogeneous nucleation with a continuous homogeneous one.

Time Resolved CD

While Time Resolved AFM is a powerful tool to obtain kinetic data on the growth of individual protein filaments, it does not provide information on the total conversion of protein monomers into filaments. To obtain such data, we have used time resolved CD. As the spectrum of this type of proteins only changes when they assemble into filaments [20], one can use the magnitude of this spectral shift as a measure for the total fraction of proteins that have self-assembled. At a wavelength of 198 nm, where the change in ellipticity (θ) between pH 2 and pH 8 is the largest, we have followed the change in ellipticity over time, for both $C_2S^H_{48}C_2$ and $C_2S^H_{24}C_2$. The fraction *f* of unfolded (and thus molecularly dissolved) proteins at time *t* is estimated from:

$$f = 1 - \frac{\theta(t) - \theta(0)}{\theta(\infty) - \theta(0)} \quad (1)$$

The result of the analysis of the time-resolved CD experiment for the fraction *f* of unfolded protein as a function of incubation time is shown in figure 4.6 for both $C_2S^H_{48}C_2$ and $C_2S^H_{24}C_2$.

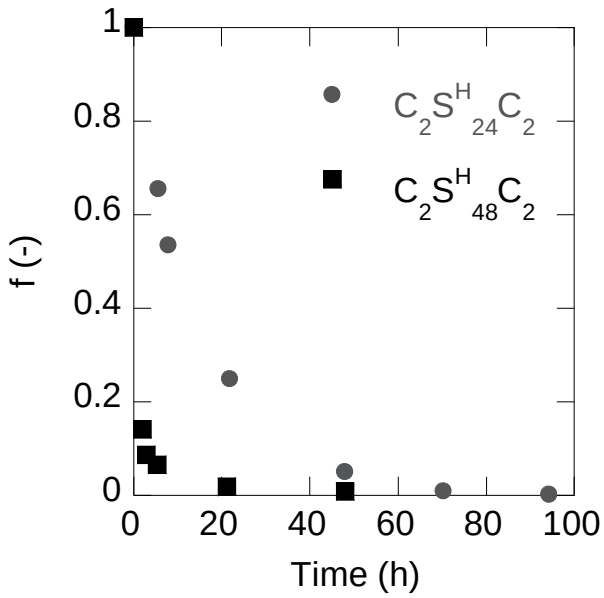

Figure 4.6: Fraction f of unfolded protein of $C_2S^H_{24}C_2$ and $C_2S^H_{48}C_2$ in time after incubation in 50 mM phosphate buffer (pH 8). Both solutions contained 1 g/L of protein.

The CD-data fully confirm the conclusion from the AFM data that under the same conditions (pH and weight concentration), the self-assembly of $C_2S^H_{48}C_2$ into filaments is significantly faster than that of $C_2S^H_{24}C_2$, This must mean that the folding of the silk-like block is not the rate determining step. A large silk-like block would take longer to fold. The fact that $C_2S^H_{48}C_2$ has twice the hydrophobic surface area compared to $C_2S^H_{24}C_2$, must be a key factor in the docking of a new protein onto a growing end of an existing fiber. Next we consider implications of the differences in filament formation and filament properties for gels that form when letting the proteins self-assemble into filaments at much higher concentrations.

Rheology

$C_2S^H_{48}C_2$ is already known to form hydrogels at neutral or higher pH [32], at weight concentrations exceeding 10 g/L. Here we have shown that the $C_2S^H_{24}C_2$ protein also self-assembles into protein filaments, and that after prolonged incubation, essentially all protein is incorporated in protein filaments. Next, we follow the gelation of 25 g/L solutions of both proteins by on-line rheometry, as a function of the incubation time at pH 8, for a time period of up to 2 days. Figure 4.7 shows the development of the storage modulus of both solutions in time. There are two distinct differences between the curves for the two proteins. First, gelation of $C_2S^H_{24}C_2$ is very much slower than that of $C_2S^H_{48}C_2$. The graph shows a lag time of several hours before the storage modulus starts increasing, while $C_2S^H_{48}C_2$ starts gelling virtually instantaneously. This observation is in line with our findings with Time Resolved AFM of much slower filament growth rates. Apparently, filaments of $C_2S^H_{24}C_2$ grow so slowly that it takes a significant time to reach the overlap concentration, while this transition point is reached much faster for the case of $C_2S^H_{48}C_2$. Second, the limiting value of the storage modulus (after 48 h of incubation time at pH 8) differs by almost an order of magnitude. Since it appears that all protein is eventually incorporated into protein filaments, at identical weight concentrations, we anticipate that the total length of protein filament should be roughly equal, and the difference observed must be due to differences in either the length or structural organization of the fibers in the network structure. For dilute samples we have observed that final filament lengths are comparable for the two proteins. Assuming that this also holds for more concentrated samples, a possible cause could be a difference in filament-filament interactions, that leads to a different structural organization of the fibers in the network structure. The $C_2S^H_{48}C_2$ fibers have twice the exposed histidine rich (hydrogen bonding and aromatic character) surface area as compared to $C_2S^H_{24}C_2$ fibers, and this might leads to a stronger attractive force between fibers. The difference in size of the tightly packed

silk-like domain in the protein filaments may result in a difference in stiffness of the filaments. This might contribute to the difference in gel properties as well. If these hypotheses are true, a further increase of the silk-like domain, or a decrease of the random coil domain (facilitating contact between the silk-like domains of neighboring filaments) should lead to stronger hydrogels, at even lower concentrations than those we observe here for $C_2S^H_{48}C_2$.

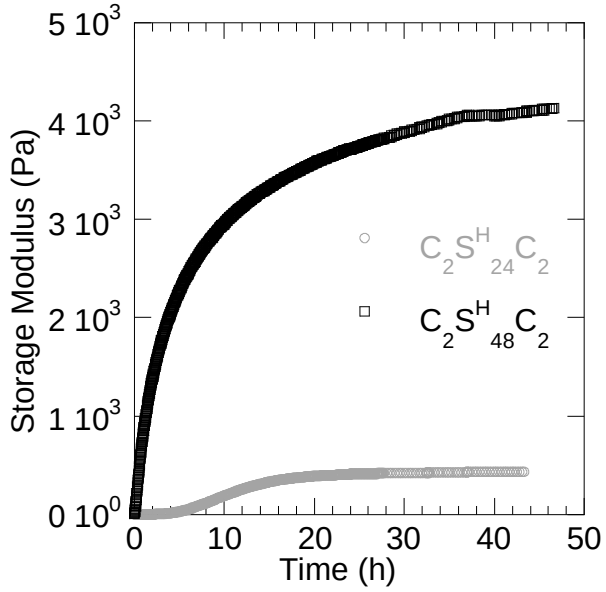

Figure 4.7: Storage modulus in time of 25 g/L solutions of $C_2S^H_{24}C_2$ and $C_2S^H_{48}C_2$ directly after adjusting the pH to 8 in 50 mM phosphate buffer at 298 K.

Enzymatic digestion of the C_2-blocks

So far, our analysis of the series of triblocks has shown that decreasing the ratio of the self-assembling silk-like block to the random coiling blocks by reducing the length of the former, leads to a transition from fibers to micelles at pH 8. This raises the question whether the tendency of the triblocks to self-assemble into filaments is completely lost below a certain length of the silk-like mid-blocks, or that below this critical length, filament growth is simply opposed too much by the random coiling outer blocks. In order to distinguish between these cases, we have used enzymatic degradation by trypsin of the C_2-blocks for the three smallest

triblocks. Trypsin typically cleaves at sites immediately following a lysine or arginine, except when this amino acid is followed by proline.[34] The C_2-block has a total of 8 putative cleavage sites, while the silk-like blocks have none. Hence, we expect the size of the C_2-block can be reduced down to 42 amino acids on the N-terminus and 23 amino acids on the C-terminus using trypsin digestion. The enzyme works optimally at pH 8, corresponding to the conditions that the proteins self-assemble into either micelles or protein filaments. The presence of a clear main band in the SDS-PAGE gels in Figure 4.1 of digested $C_2S^H_8C_2$, $C_2S^H_{16}C_2$, and $C_2S^H_{24}C_2$, with highly increased mobilities compared to the intact protein polymers, confirms that indeed much of the hydrophilic C_2-blocks was removed by the enzyme. Note that the C-fragments after digestion are smaller than 4 kDa and are therefore not visible on the gel. After extensive trypsin digestion, AFM imaging was used to check for changes in the self-assembled structures. Selected images are shown in Figure 4.8. For $C_2S^H_8C_2$, we find very few micellar structures, plus some short filaments. For $C_2S^H_{16}C_2$, there is a very clear transition from micelle formation to filament formation upon removal of much of the outer block by trypsin digestion. We also find that the filaments formed by trypsin-treated triblocks have a notable tendency to bundle. Finally, for $C_2S^H_{24}C_2$, we find that trypsin digestion leads to very strong filament bundling. Returning to the question posed at the beginning of this paragraph, it is now clear that even the shorter silk-like midblocks do have an intrinsic tendency to fold and stack into filaments, but that filament-formation can apparently be halted by the hydrophilic random coil outer blocks, if these are sufficiently long. It is also clear that the precise length of the outer blocks not only determines whether micelles will be formed or filaments, but that it also determines the likelihood of the silk-like mid-blocks of neighboring filaments coming into contact, and leading to lateral filament-filament association and bundling, which is crucial in determining the final mechanical properties of hydrogels formed by our triblock protein-based polymers.

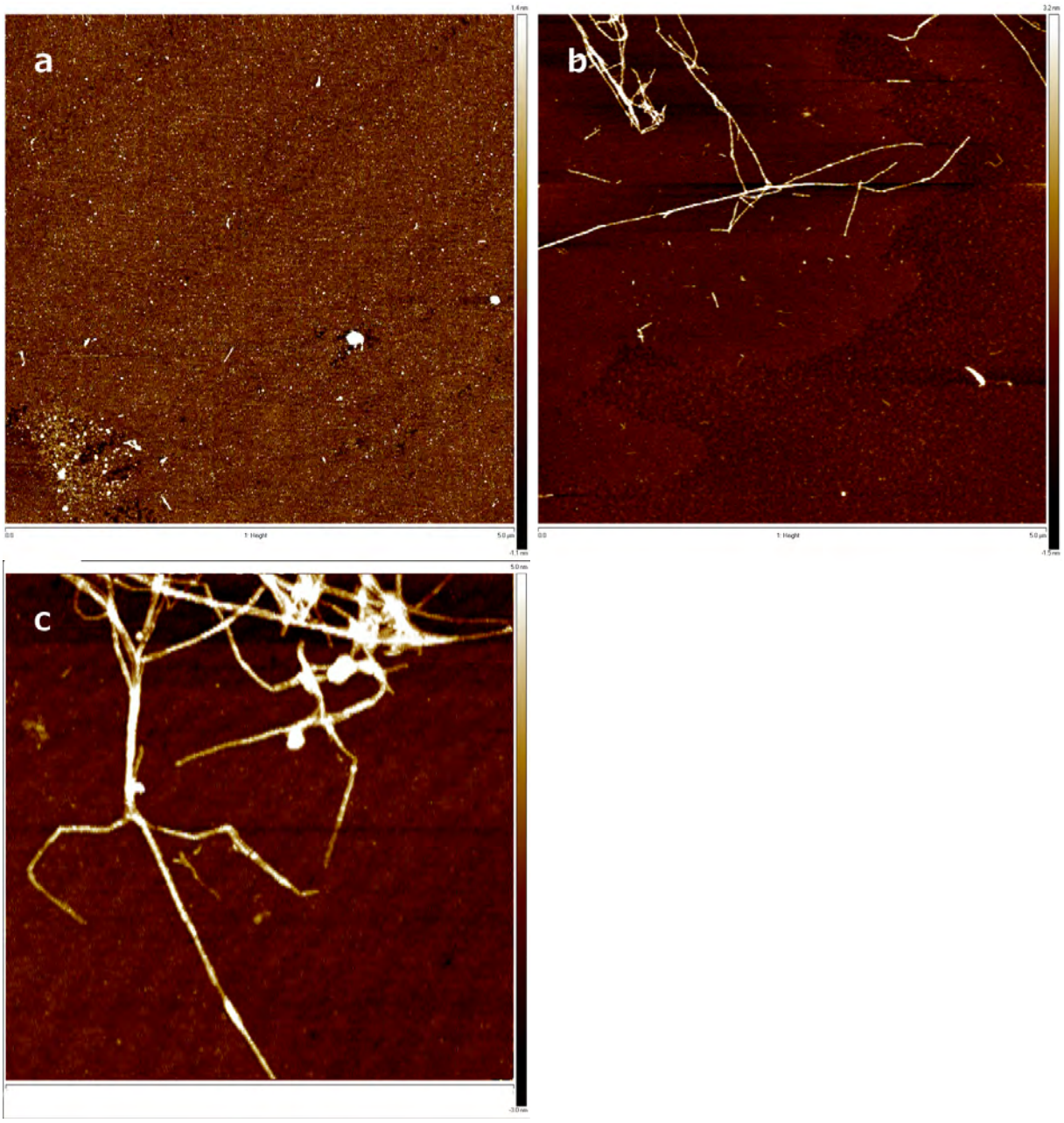

Figure 4.8: Effect of trypsin digestion on fibril formation and fiber bundling. AFM pictures of $C_2S^H{}_8C_2$ (a), $C_2S^H{}_{16}C_2$ (b) and $C_2S^H{}_{24}C_2$ (c) adsorbed on silica after digestion by trypsin. All samples contained 1 g/L protein and 0.02 g/L trypsin. Samples were analyzed after 72 h of incubation at pH 8 (50 mM phosphate buffer) at 310 K. Image size is 5 x 5 µm (a and b) or 2 x 2 µm (c).

CONCLUSIONS

We have constructed a series of recombinant triblock protein polymers that consist of a hydrophilic inert random coiling block and a pH-responsive silk-like block. The number of octapeptide repeats in the silk-like midblock was varied over a broad range: 8, 16, 24 and 48. All proteins show pH-responsive self-assembly behavior. In each case there was a transition from molecularly dissolved charged proteins at pH 2 to self-assembled structures at pH 8. We observed a transition from spherical micelles ($C_2S^H_8C_2$ and $C_2S^H_{16}C_2$) to fiber formation ($C_2S^H_{24}C_2$ and $C_2S^H_{48}C_2$). The longest silk-like block yields the strongest and fastest forming hydrogels. Enzymatic digestion of the random coil block triggered the micelle forming proteins into forming fibers. It also leads to more sticky fibers than the ones formed by intact $C_2S^H_{24}C_2$ and $C_2S^H_{48}C_2$.

In our previous work, we have described fiber-forming triblock protein-polymers with the structure $C_2S^X_{48}C_2$ that form dilute hydrogels, for some residues X (notably histidine) at physiological conditions (pH, temperature, ionic strength). [20, 31, 32]. Although the current dimensions of the two different domains are suitable for making hydrogels, they may not be ideal when aiming for strong hydrogels at extremely dilute concentrations, or for hydrogels with large pore sizes. Bundling of protein filaments can lead to both gelation at very low concentrations [35] and to large pore sizes that may be desirable in applications such as tissue culture. This leads us to believe that a further increase of the silk-like block or a decrease of the hydrophilic random coil block could give controlled bundling of the protein filaments, leading to extremely long and stiff fiber bundles, more faithfully mimicking the structure of collagen bundles in the extracellular matrix. Such control over bundling would very much broaden the range of moduli and pore sizes that can be acquired using our fiber based gels.

The micelles formed by $C_2S^H_8C_2$ and $C_2S^H_{16}C_2$ might be worthwhile candidates for nanodelivery vehicles that release their contents in acidic environments such as the stomach.

For example, this could be useful in taste-masking. It would also be interesting to aim for a much more precise control of the pH dependence of the self-assembly, in view of delivery to tumor cells exploiting the somewhat more acidic extracellular environment of tumor cells (6.5-6.9 compared to 7.2-7.4 around healthy cells) [36].

Finally, our work highlights how the familiar concept of the control of block-copolymer self-assembly by tuning block lengths, translates to the case of protein-based polymers, with blocks that not merely self-assemble, but have well defined folds into specific secondary structures. Specifically, our results point to the possibility to design self-assembling triblock protein-polymers with not only controlled fibril growth, but also controlled bundling into fibers.

EXPERIMENTAL SECTION

Construction of recombinant strains and protein biosynthesis.

The cloning of the triblock $C_2S^H_{48}C_2$ has been described by us previously [32, 37]. The DNA fragment encoding the midblock in this protein consists of 24 repeats of a $[(GAGAGAGH]_2$-encoding *Bsa*I/*Ban*I fragment. The DNA fragments encoding the shorter mid blocks studied here, S^H_n (n=8, 16, and 24), were constructed in the same manner. These fragments consist of 4, 8, and 12 repeats of the *Bsa*I/*Ban*I fragment, respectively, and were released from their vector by digestion with *Acc*I/*Ban*I. Vector pMTL23-C_2 [32] was opened with *Acc*I/*Bsa*I, after which the S^H_n fragments were inserted. The resulting plasmids were openened with *Acc*I/*Bsa*I, after which the second C_2-encoding DNA fragment was inserted. This fragment had been obtained by digestion of pMTL23-C_2 [32] with *Acc*I/*Ban*I. The final $C_2S^H_nC_2$-encoding genes were cloned into expression vector pPIC9 (Invitrogen) via *Eco*RI/*Not*I. Transformation of *P. pastoris* and protein production in bioreactors were as before [38].

Purification

The purification of the three smallest proteins ($C_2S^H_8C_2$, $C_2S^H_{16}C_2$, $C_2S^H_{24}C_2$) was performed by first selectively precipitating the protein polymers from cell-free fermentation broth in a similar way as for $C_2S^H_{48}C_2$ [32]. This was done by adding ammonium sulphate up to 45% saturation. After an incubation time of 30 minutes at room temperature the solution was centrifuged (16000 x g, 40 minutes, 4°C). The protein polymer pellet was resuspended in 60% of the original volume of 50 mM formic acid. The precipitation step with ammonium sulphate (45% saturation) was repeated once. After the centrifugation step the protein polymers were resuspended in 100 mL 50 mM formic acid and extensively dialysed against 10 mM formic acid at 4°C. Finally the proteins were freeze dried for storage.

MALDI-TOF

Matrix-assisted laser desorption/ionization (MALDI) mass spectrometry was performed using an ultrafleXtreme mass spectrometer (Bruker). Samples were prepared by the dried droplet method on a 600 μm AnchorChip target (Bruker), using 5 mg/ml 2,5-dihydroxyacetophenone, 1.5 mg/ml diammonium hydrogen citrate, 25% (v/v) ethanol and 1% (v/v) trifluoroacetic acid as matrix. Spectra were derived from ten 500-shot (1,000 Hz) acquisitions taken at non-overlapping locations across the sample. Measurements were made in the positive linear mode, with ion source 1, 25.0 kV; ion source 2, 23.3 kV; lens, 6.5 kV; pulsed ion extraction, 680 ns. Protein Calibration Standard II (Bruker) was used for external calibration.

SDS-PAGE

Electrophoresis (SDS-PAGE) was performed using the NuPAGE Novex system with 10% Bis-Tris gels, MES-SDS running buffer, and Novex Sharp Protein Standard prestained molecular mass markers. Gels were stained with Coomassie SimplyBlue SafeStain (all Invitrogen).

Dynamic Light Scattering (DLS)

DLS measurements were performed using a Zetasizer NanoZS (Malvern Instruments, UK), equipped with a He-Ne laser (4 mW), operating at a wavelength of 633 nm. Each measurement was performed at an angle of 173° and a temperature of 25 °C. Measurements at pH 2 were performed by dissolving protein in 10 mM HCl at a concentration of 1 g/L. Solutions were filtrated (200 nm, Millipore). Measurements at pH 8 were performed by diluting the former solutions a factor 2, using filtrated 100 mM phosphate buffer (pH 8). Reported hydrodynamic radii are z-averaged values determined by DTS Software, version

5.10. Reversibility was examined by adding an excess of 1M filtered HCl to solutions containing protein micelles or fibers.

Atomic Force Microscopy

AFM samples were made by applying a drop of protein solution on a 10 × 10 mm hydrophilic silicon wafer (Siltronic Corp.) bearing a thin oxide layer, rinsing the wafer with milli-Q water to remove any nonadsorbed material, and drying it under a stream of nitrogen. The samples were analyzed using a Digital Instruments Nanoscope V in ScanAsyst mode and NP-10 silicon nitride tips with a spring constant of 0.350 N/m and a 10 nm tip radius (Bruker, CA, USA). Images were processed using NanoScope Analysis 1.40. All samples contained 1 g/L of protein and a 50 mM phosphate buffer (pH 8).

Circular Dichroism

CD measurements were performed on a Jasco J-715 spectropolarimeter at 298 K. The spectra were recorded between 190 and 260 nm with a resolution of 0.2 nm and a scanning speed of 1 nm/s. Each spectrum was an average of 20 measurements. A Quartz cuvette with a path length of 0.5 mm was used. Protein concentration was 0.25 g/L and the solvent was 10 mM HCl (pH 2) or 50 mM phosphate buffer (pH 8). For the kinetic study 1 g/L solutions in 50 mM phosphate buffer (pH 8) were used, which were diluted 4 times with the same buffer prior to measuring. Ellipticity was measured at a wavelength of 198 nm.

Rheology

Rheological measurements were performed on an Anton Paar MCR 301 rheometer with Couette CC10/TI geometry. Cup and bob radii were 5.420 mm and 5.002 mm respectively. A solvent trap was used to prevent evaporation. Samples containing 25 g/L of protein were

adjusted to pH 8 in a 50 mM phosphate buffer. Immediately after adjusting the pH the storage modulus was measured using oscillatory deformation (f = 1 Hz and γ = 0.1%) until a plateau value was reached. Temperature was controlled by a Peltier element at 298 K during measurements.

Enzymatic digestion

Trypsin from bovine pancreas (Sigma-Aldrich) was used to digest the C_2-block of $C_2S^H{}_8C_2$, $C_2S^H{}_{16}C_2$ and $C_2S^H{}_{24}C_2$. Samples contained 1 g/L of protein and 0.02 g/L of trypsin. After mixing protein and enzyme, we adjusted the pH to 8 in 50 mM phosphate buffer. Samples were incubated for 72 hours at 310 K before measuring them with AFM and SDS-PAGE.

APPENDIX

YVEFGLGAGAPGEPGNPGSPGNQGQPGNKGSPGNPGQPGNEGQPGQPGQNGQPGEP

GSNGPQGSQGNPGKNGQPGSPGSQGSPGNQGSPGQPGNPGQPGEQGKPGNQGPAGE

PGNPGSPGNQGQPGNKGSPGNPGQPGNEGQPGQPGQNGQPGEPGSNGPQGSQGNPG

KNGQPGSPGSQGSPGNQGSPGQPGNPGQPGEQGKPGNQGPAGE$(GAGAGAGH)_n$GAG

APGEPGNPGSPGNQGQPGNKGSPGNPGQPGNEGQPGQPGQNGQPGEPGSNGPQGSQ

GNPGKNGQPGSPGSQGSPGNQGSPGQPGNPGQPGEQGKPGNQGPAGEPGNPGSPGN

QGQPGNKGSPGNPGQPGNEGQPGQPGQNGQPGEPGSNGPQGSQGNPGKNGQPGSPG

SQGSPGNQGSPGQPGNPGQPGEQGKPGNQGPAGEGA

Figure A4.1: Amino acid sequence of protein polymers (n = 8, 16, 24 or 48) used in this study.

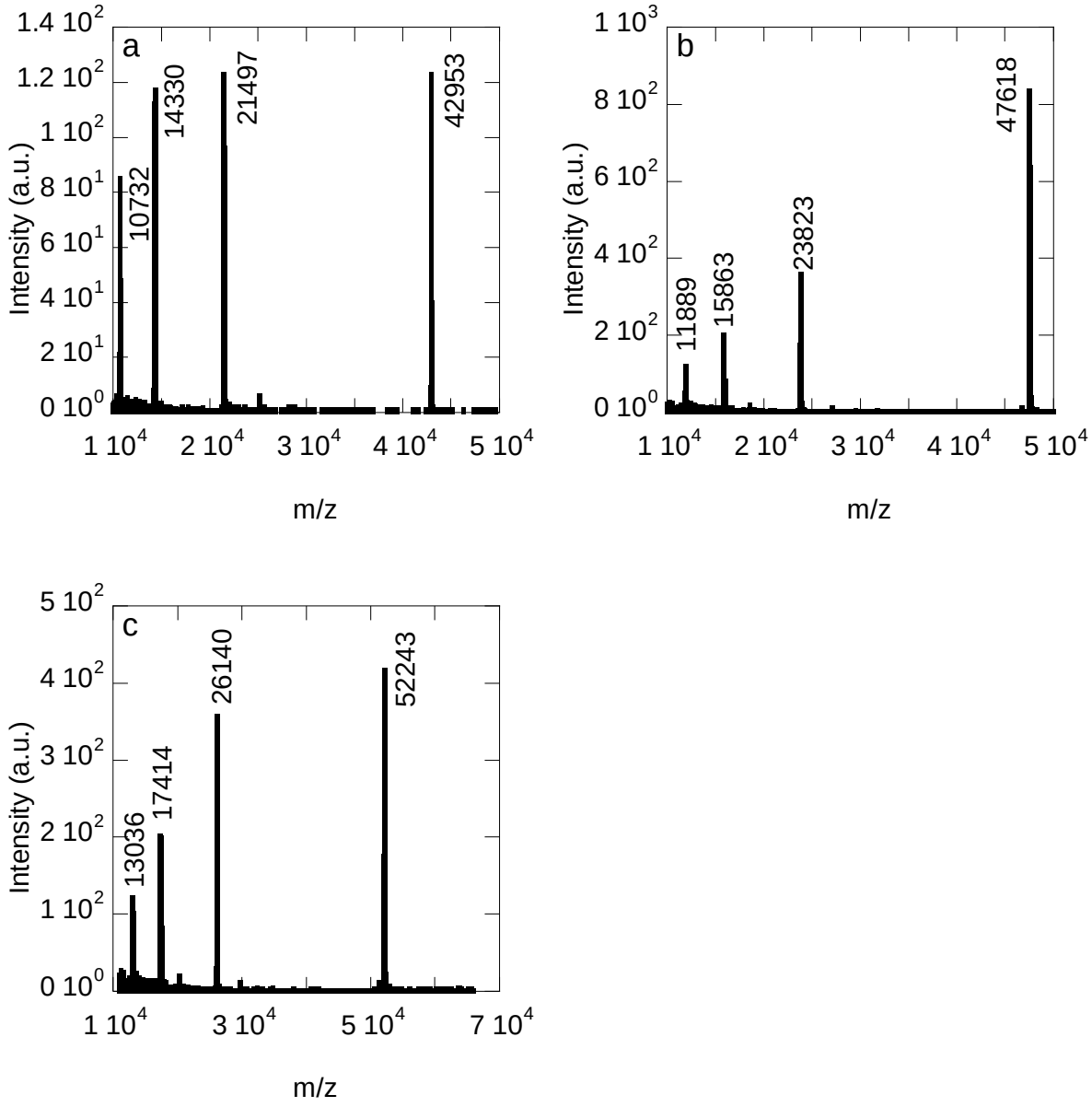

Figure A4.2: MALDI-TOF spectra of $C_2S^H{}_8C_2$ (a), $C_2S^H{}_{16}C_2$ (b) and $C_2S^H{}_{24}C_2$ (c). Each spectrum shows four peaks corresponding to the $(M + H)^+$, $(M + 2H)^{2+}$, $(M + 3H)^{3+}$ and $(M + 4H)^{4+}$.

REFERENCES

1. Huang, J.; Foo, C. W. P.; Kaplan, D. L., Biosynthesis and applications of silk-like and collagen-like proteins. *Polym Rev* **2007,** 47, (1), 29-62.
2. Meyer, D. E.; Trabbic-Carlson, K.; Chilkoti, A., Protein purification by fusion with an environmentally responsive elastin-like polypeptide: Effect of polypeptide length on the purification of thioredoxin. *Biotechnol Progr* **2001,** 17, (4), 720-728.
3. Li, M. Y.; Mondrinos, M. J.; Gandhi, M. R.; Ko, F. K.; Weiss, A. S.; Lelkes, P. I., Electrospun protein fibers as matrices for tissue engineering. *Biomaterials* **2005,** 26, (30), 5999-6008.
4. Daamen, W. F.; Veerkamp, J. H.; van Hest, J. C. M.; van Kuppevelt, T. H., Elastin as a biomaterial for tissue engineering. *Biomaterials* **2007,** 28, (30), 4378-4398.
5. Nettles, D. L.; Chilkoti, A.; Setton, L. A., Applications of elastin-like polypeptides in tissue engineering. *Adv Drug Deliver Rev* **2010,** 62, (15), 1479-1485.
6. Hernandez-Garcia, A.; Werten, M. W. T.; Stuart, M. C.; de Wolf, F. A.; de Vries, R., Coating of Single DNA Molecules by Genetically Engineered Protein Diblock Copolymers. *Small* **2012,** 8, (22), 3491-3501.
7. Chilkoti, A.; Dreher, M. R.; Meyer, D. E., Design of thermally responsive, recombinant polypeptide carriers for targeted drug delivery. *Adv Drug Deliver Rev* **2002,** 54, (8), 1093-1111.
8. van Hest, J. C. M.; Tirrell, D. A., Protein-based materials, toward a new level of structural control. *Chem Commun* **2001**, (19), 1897-1904.
9. Golinska, M. D.; Pham, T. T. H.; Werten, M. W. T.; de Wolf, F. A.; Stuart, M. A. C.; van der Gucht, J., Fibril Formation by pH and Temperature Responsive Silk-Elastin Block Copolymers. *Biomacromolecules* **2013,** 14, (1), 48-55.
10. Meyer, D. E.; Chilkoti, A., Genetically encoded synthesis of protein-based polymers with precisely specified molecular weight and sequence by recursive directional ligation: Examples from the elastin-like polypeptide system. *Biomacromolecules* **2002,** 3, (2), 357-367.
11. Koria, P.; Yagi, H.; Kitagawa, Y.; Megeed, Z.; Nahmias, Y.; Sheridan, R.; Yarmush, M. L., Self-assembling elastin-like peptides growth factor chimeric nanoparticles for the treatment of chronic wounds. *P Natl Acad Sci USA* **2011,** 108, (3), 1034-1039.
12. Anumolu, R.; Gustafson, J. A.; Magda, J. J.; Cappello, J.; Ghandehari, H.; Pease, L. F., Fabrication of Highly Uniform Nanoparticles from Recombinant Silk-Elastin-like Protein Polymers for Therapeutic Agent Delivery. *Acs Nano* **2011,** 5, (7), 5374-5382.
13. van Eldijk, M. B.; Wang, J. C. Y.; Minten, I. J.; Li, C. L.; Zlotnick, A.; Nolte, R. J. M.; Cornelissen, J. J. L. M.; van Hest, J. C. M., Designing Two Self-Assembly Mechanisms into One Viral Capsid Protein. *J Am Chem Soc* **2012,** 134, (45), 18506-18509.
14. Schipperus, R.; Teeuwen, R. L. M.; Werten, M. W. T.; Eggink, G.; de Wolf, F. A., Secreted production of an elastin-like polypeptide by Pichia pastoris. *Appl Microbiol Biot* **2009,** 85, (2), 293-301.
15. Schipperus, R.; Eggink, G.; de Wolf, F. A., Secretion of elastin-like polypeptides with different transition temperatures by Pichia pastoris. *Biotechnol Progr* **2012,** 28, (1), 242-247.
16. Silva, C. I. F.; Skrzeszewska, P. J.; Golinska, M. D.; Werten, M. W. T.; Eggink, G.; de Wolf, F. A., Tuning of Collagen Triple-Helix Stability in Recombinant Telechelic Polymers. *Biomacromolecules* **2012,** 13, (5), 1250-1258.
17. Skrzeszewska, P. J.; Jong, L. N.; de Wolf, F. A.; Stuart, M. A. C.; van der Gucht, J., Shape-Memory Effects in Biopolymer Networks with Collagen-Like Transient Nodes. *Biomacromolecules* **2011,** 12, (6), 2285-2292.

18. Skrzeszewska, P. J.; de Wolf, F. A.; Werten, M. W. T.; Moers, A. P. H. A.; Stuart, M. A. C.; van der Gucht, J., Physical gels of telechelic triblock copolymers with precisely defined junction multiplicity. *Soft Matter* **2009,** 5, (10), 2057-2062.
19. Martens, A. A.; Portale, G.; Werten, M. W. T.; de Vries, R. J.; Eggink, G.; Stuart, M. A. C.; de Wolf, F. A., Triblock Protein Copolymers Forming Supramolecular Nanotapes and pH-Responsive Gels. *Macromolecules* **2009,** 42, (4), 1002-1009.
20. Beun, L. H.; Beaudoux, X. J.; Kleijn, J. M.; de Wolf, F. A.; Stuart, M. A. C., Self-Assembly of Silk-Collagen-like Triblock Copolymers Resembles a Supramolecular Living Polymerization. *Acs Nano* **2012,** 6, (1), 133-140.
21. Smeenk, J. M.; Otten, M. B. J.; Thies, J.; Tirrell, D. A.; Stunnenberg, H. G.; van Hest, J. C. M., Controlled assembly of macromolecular beta-sheet fibrils. *Angewandte Chemie-International Edition* **2005,** 44, (13), 1968-1971.
22. Krejchi, M. T.; Atkins, E. D. T.; Fournier, M. J.; Mason, T. L.; Tirrell, D. A., Observation of a silk-like crystal structure in a genetically engineered periodic polypeptide. *J Macromol Sci Pure* **1996,** A33, (10), 1389-1398.
23. Krejchi, M. T.; Cooper, S. J.; Deguchi, Y.; Atkins, E. D. T.; Fournier, M. J.; Mason, T. L.; Tirrell, D. A., Crystal structures of chain-folded antiparallel beta-sheet assemblies from sequence-designed periodic polypeptides. *Macromolecules* **1997,** 30, (17), 5012-5024.
24. Krejchi, M. T.; Atkins, E. D. T.; Waddon, A. J.; Fournier, M. J.; Mason, T. L.; Tirrell, D. A., Chemical Sequence Control of Beta-Sheet Assembly in Macromolecular Crystals of Periodic Polypeptides. *Science* **1994,** 265, (5177), 1427-1432.
25. Li, L. Q.; Tong, Z. X.; Jia, X. Q.; Kiick, K. L., Resilin-like polypeptide hydrogels engineered for versatile biological function. *Soft Matter* **2013,** 9, (3), 665-673.
26. Elvin, C. M.; Carr, A. G.; Huson, M. G.; Maxwell, J. M.; Pearson, R. D.; Vuocolo, T.; Liyou, N. E.; Wong, D. C. C.; Merritt, D. J.; Dixon, N. E., Synthesis and properties of crosslinked recombinant pro-resilin. *Nature* **2005,** 437, (7061), 999-1002.
27. Charati, M. B.; Ifkovits, J. L.; Burdick, J. A.; Linhardt, J. G.; Kiick, K. L., Hydrophilic elastomeric biomaterials based on resilin-like polypeptides. *Soft Matter* **2009,** 5, (18), 3412-3416.
28. Schor, M.; Martens, A. A.; Dewolf, F. A.; Stuart, M. A. C.; Bolhuis, P. G., Prediction of solvent dependent beta-roll formation of a self-assembling silk-like protein domain. *Soft Matter* **2009,** 5, (13), 2658-2665.
29. Werten, M. W. T.; Moers, A. P. H. A.; Vong, T.; Zuilhof, H.; van Hest, J. C. M.; de Wolff, F. A., Biosynthesis of an amphiphilic silk-like polymer. *Biomacromolecules* **2008,** 9, (7), 1705-1711.
30. Werten, M. W. T.; Wisselink, W. H.; van den Bosch, T. J. J.; de Bruin, E. C.; de Wolf, F. A., Secreted production of a custom-designed, highly hydrophilic gelatin in Pichia pastoris. *Protein Eng* **2001,** 14, (6), 447-454.
31. Martens, A. A.; van der Gucht, J.; Eggink, G.; de Wolf, F. A.; Stuart, M. A. C., Dilute gels with exceptional rigidity from self-assembling silk-collagen-like block copolymers. *Soft Matter* **2009,** 5, (21), 4191-4197.
32. Golinska, M. D.; Wlodarczyk-Biegun, M. K.; Werten, M. W. T.; Stuart, M. A. C.; de Wolf, F. A.; de Vries, R., Dilute Self-Healing Hydrogels of Silk-Collagen-Like Block Copolypeptides at Neutral pH. *Biomacromolecules* **2014,** 15, (3), 699-706.
33. Wlodarczyk-Biegun, M. K.; Werten, M. W.; de Wolf, F. A.; van den Beucken, J. J.; Leeuwenburgh, S. C.; Kamperman, M.; Cohen Stuart, M. A., Genetically engineered silk-collagen-like copolymer for biomedical applications: Production, characterization and evaluation of cellular response. *Acta Biomaterialia* **2014,** 10, (8), 3620-9.
34. ExPASy Bioinformatics Resource Portal Peptide Cutter. http://web.expasy.org/peptide_cutter/ ((accessed 22 august 2013)),

35. Kouwer, P. H. J.; Koepf, M.; Le Sage, V. A. A.; Jaspers, M.; van Buul, A. M.; Eksteen-Akeroyd, Z. H.; Woltinge, T.; Schwartz, E.; Kitto, H. J.; Hoogenboom, R.; Picken, S. J.; Nolte, R. J. M.; Mendes, E.; Rowan, A. E., Responsive biomimetic networks from polyisocyanopeptide hydrogels. *Nature* **2013,** 493, (7434), 651-655.
36. Estrella, V.; Chen, T. A.; Lloyd, M.; Wojtkowiak, J.; Cornnell, H. H.; Ibrahim-Hashim, A.; Bailey, K.; Balagurunathan, Y.; Rothberg, J. M.; Sloane, B. F.; Johnson, J.; Gatenby, R. A.; Gillies, R. J., Acidity Generated by the Tumor Microenvironment Drives Local Invasion. *Cancer Res* **2013,** 73, (5), 1524-1535.
37. Yan, Y.; Martens, A. A.; Besseling, N. A. M.; de Wolf, F. A.; de Keizer, A.; Drechsler, M.; Stuart, M. A. C., Nanoribbons self-assembled from triblock peptide polymers and coordination polymers. *Angew Chem Int Edit* **2008,** 47, (22), 4192-4195.
38. Werten, M. W. T.; Van den Bosch, T. J.; Wind, R. D.; Mooibroek, H.; De Wolf, F. A., High-yield secretion of recombinant gelatins by Pichia pastoris. *Yeast* **1999,** 15, (11), 1087-1096.

Chapter 5

Changing Fibril-Fibril Interaction in Self-Assembled Silk-Like Protein Polymers Leads to a Change in Gel Type.

ABSTRACT

We designed and produced two new protein diblock polymers that consist of a silk-like pH-responsive self-assembling block (S^{H}_{48}) and a hydrophilic random coil block (C_1 or C_2). Both proteins self-assemble into fibrils at similar rates and with similar structures at pH 8. Fibrils of $C_2S^{H}_{48}$ show predominantly repulsive interaction due to the nature and size of the C-block. Fibrils of $C_1S^{H}_{48}$ have a more exposed hydrophobic silk-like core and balance attractive interaction of this silk-like core with the repulsive interaction of the random coil blocks. These fibrils start to bundle together into higher order structures. Hydrogels of both protein polymers behave quite differently from each other. Gels from $C_2S^{H}_{48}$ have a scaling of modulus with concentration that is consistent with a non-cross-linked network of semiflexible polymers. Gels from $C_1S^{H}_{48}$ show much stronger scaling behavior, which is consistent with cross-linked networks. The latter gels are stronger and more porous than those of $C_2S^{H}_{48}$. Our work shows that a simple change in molecular design leads to different fibril-fibril interactions. This is an important step in designing protein polymers that can form higher order fibrous protein structures that can mimic the Extracellular Matrix.

INTRODUCTION

Mimicking the Extracellular Matrix (ECM) is one of the key challenges in the design of biomaterials for tissue engineering. The ECM is a complex matrix with many components, with proteins, polysaccharides and proteoglycans as the most abundant ones. The structural integrity of the ECM is mainly due to the presence of proteins (collagen, actin, laminin, fibronectin) that self-assemble into supramolecular fibrous structures, which form porous networks [1, 2]. The key properties of the ECM are structural and anchoring support for cells, while transport of nutrients, waste products and signaling molecules should be facilitated as well [3, 4].

Hydrogels are promising candidates as mimics for the extracellular matrix (ECM) [4-7]. Although hydrogels can be constructed from a plethora of synthetic, natural, or hybrid polymers, naturally derived materials are thought to be more suitable for biomedical applications because their chemical and structural nature resembles the components of the ECM the closest. In particular, the hierarchical structures formed by collagen, the most abundant protein in the ECM, provide an inspiration for newly constructed biomaterials. Collagen molecules assemble into triple helical fibrils that can bundle into long, thick fibers. Intuitively, when designing biomaterials that mimic the ECM, one would be inclined to also think of protein-based structures. A well-controlled system of protein fibrils that bundle into well-defined fiber structures can be the key in designing an ECM mimic.

Using protein-based building blocks has a major advantage over the use of any other polymer, namely that one can use the route of genetic engineering for production. The sophisticated cellular machinery which produces proteins from the well-defined DNA template in principle yields a nearly perfectly monodisperse population of proteins, with exact control over size, amino acid sequence and stereochemistry. This unmatched control in protein polymerization can lead to a superior control over the physico-chemical properties,

compared to what is possible with any chemically synthesized polymer. In addition, any newly designed protein can include natural peptide or protein sequences that are known to have desirable structural or stimulus-responsive (pH, temperature, ionic strength, etc.) properties [8]. Such domains include natural silk [9-14], collagen [15-17], elastin [18-21], resilin [22-24], etc.

We have previously designed protein polymers that combine the self-assembling capacity of natural silk, with a hydrophilic random coiling block [25-28]. The silk-inspired domain consists of repeats of an octapeptide, GAGAGAGH (S^H), that is pH-responsive. The alkaline nature of histidine (pKa ~ 6) gives it a charge at low pH, while at neutral or higher pH the block becomes neutral and folds into a highly structured betaroll formation and stack into fibrils. The silk-like block is flanked by random coil hydrophilic domains (C) [29, 30] that are necessary for colloidal stability of the fibrils as without them the neutralized silk-blocks aggregate and precipitate. The basic unit of this random coiling block is a 99 amino acid long sequence of predominantly hydrophilic amino acids that can be included as multimers (C_2, C_4, etc.).

A protein polymer we reported on previously consists of 48 repeats of the silk-like octapeptide, flanked on both sided by a dimer of the random coil block, called $C_2S^H_{48}C_2$. At concentrations above 10 g/L this protein polymer self-assembles into fibrils at physiological conditions and forms weak hydrogels [31] that are suitable for 2D cell cultures [32]. Individual fibrils grow up to several microns in size, while their persistence length is of the same magnitude. In order to obtain stiffer gels from similar building blocks, one might think of making bundles of these individual fibrils, in a controlled way. Controlled bundling of these individual fibrils could lead to much longer and stiffer structures. This in turn can lead to much more dilute, yet rigid hydrogels [33]. In previous work we used (partial) enzymatic digestion of the C-blocks to enhance fibril-fibril attraction and obtain higher order structures [34]. This work showed that a decrease in size of the repulsive C-blocks indeed leads to extensive fibril bundling into fibrous structures. This decrease in size of the hydrophilic

repulsive domain should lead to a more exposed hydrophobic silk-like core. This, in turn, leads to stronger hydrophobic interaction between individual fibrils. This attractive force then leads to bundling into fibrous structures. Based on these results, we designed two new proteins in which we changed the size of the random coil C-block in a precise way. The two newly constructed protein polymers are both diblocks with the same silk-like domain S^{H}_{48} but with only one N-terminal hydrophilic random coil domain that is present as a dimer in $C_2S^{H}_{48}$ or as a monomer in $C_1S^{H}_{48}$. The complete amino acid sequence of each protein polymer is provided in Figure A5.1.

Here we present a detailed characterization of the self-assembling behavior of the two newly constructed proteins. We use Atomic Force Microscopy and Circular Dichroism to study the size and structure of individual self-assembled fibrils and compare them to $C_2S^{H}_{48}C_2$. Next, we report on the rheological properties of the fiber based hydrogels formed by $C_1S^{H}_{48}$ and $C_2S^{H}_{48}$. We observe a clear change in gel type and properties as a result of varying the size of the random coil block. Finally we characterize gel structure and pore size dimensions to assess the suitability of these hydrogels as scaffolds for 3D cell cultures.

We demonstrate the role of changing the relative sizes of the self-assembling pH-responsive hydrophilic/hydrophobic domain and the repulsive hydrophilic random coil domain in diblock structured protein polymers. A simple change in the molecular design gives us control over protein fibril-fibril interaction. This interaction can lead to extensive bundling into fibrous structures. Control over this association into higher order structures is a key element in constructing ECM mimics.

RESULTS AND DISCUSSION

Protein Characterization

The two newly constructed protein polymers were purified and then analyzed using MALDI-TOF MS and SDS-PAGE. Purified samples of the two protein polymers were measured using MALDI-TOF and the determined masses were compared to their theoretical masses, as we present in Table 5.1.

Table 5.1: Theoretical and measured masses of the two newly constructed protein polymers used in this study.

Protein	Theoretical Mass (Da)	Measured Mass (Da)
$C_1S^H_{48}$	38282	38282
$C_2S^H_{48}$	47390	47375

The measured masses we present in Table 5.1 are well inside the experimental uncertainty of several tens of Da. The full MALDI-TOF spectra (Figure A5.2) show that both purified samples are highly pure. The protein polymers are secreted by the organism *Pichia pastoris* during a batch fermentation and a simple ammonium sulfate precipitation suffices to obtain highly pure samples as is visible in Figure 5.1.

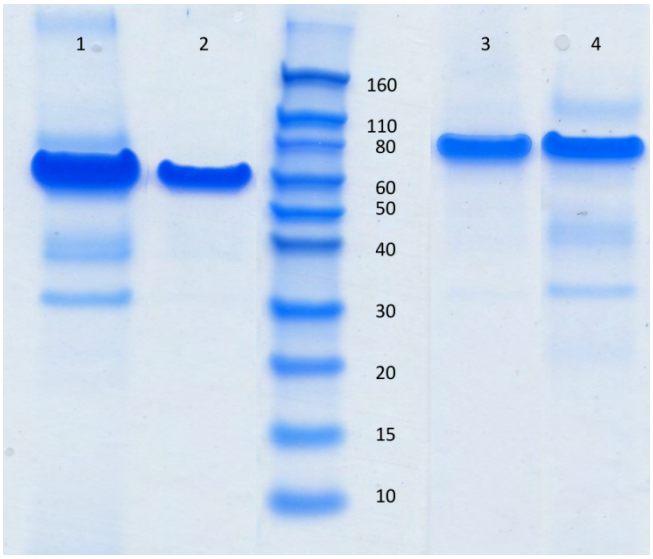

Figure 5.1: SDS-PAGE gel of newly produced protein polymers. Lane 1: Cell free broth of $C_1S^H_{48}$ fermentation; lane 2: purified $C_1S^H_{48}$; lane 3: purified $C_2S^H_{48}$; lane 4: cell free broth of $C_2S^H_{48}$ fermentation. Marker with masses in kDa included (middle lane). Band intensities are not quantitative as purification involved precipitation and redissolution.

The gel we present in Figure 5.1 shows that a single band is present after purification for both protein polymers. As we see time and again, protein polymers that include the random coil C-block give an overestimated apparent mass on SDS-PAGE gels [25, 28, 34]. This behavior is due to the poor SDS-binding and non-globular nature of this C-block, leading to a low mobility. $C_2S^H_{48}C_2$ with a mass of 66 kDa gives an apparent mass of 160 kDa with SDS-PAGE. Consistently, we observe here that a smaller sized C-block comes with a smaller overestimation of the apparent mass shown by SDS-PAGE: $C_2S^H_{48}$ has an apparent mass of 80 kDa, more than 30 kDa higher than the real mass, whereas $C_1S^H_{48}$ has an apparent mass of 60 kDa, which is an overestimation of only 20 kDa.

AFM

Both newly constructed protein polymers can self-assemble into fibers at pH 8. This behavior is similar to that of $C_2S^H_{48}C_2$ [25, 28]. We observe fibrils with lengths up to several microns, as is shown in Figure 5.2. The fibrils that are formed by $C_1S^H_{48}$ show stronger fibril-fibril interaction as they start to bundle together, while we hardly observe this behavior with the fibrils formed by $C_2S^H_{48}$. This means that in $C_2S^H_{48}$ fibril-fibril interaction is still dominated by the repulsive C-blocks, while in $C_1S^H_{48}$ the attraction of the hydrophobic silk-like blocks begins to balance the repulsion of the smaller C-blocks. This shift in fibril-fibril interaction can have an important effect on the properties of fiber-based gels that this type of protein polymer can form.

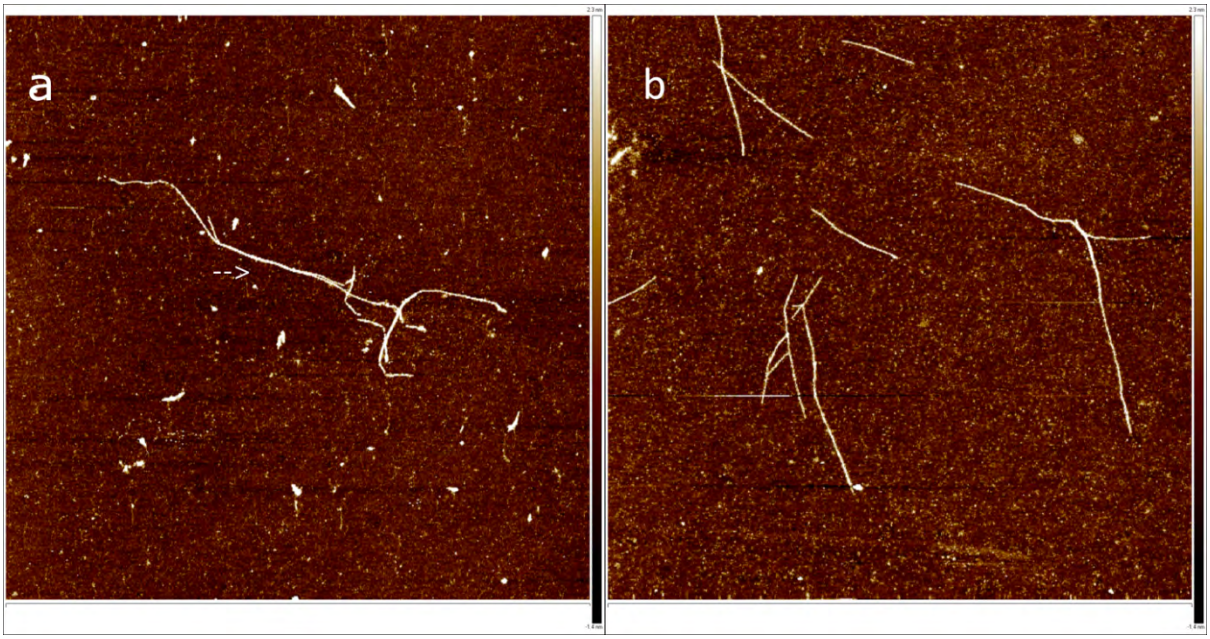

Figure 5.2: AFM images of self-assembled protein-polymers $C_1S^H_{48}$ (a) and $C_2S^H_{48}$ (b), adsorbed on silica 72h after a pH shift from pH 2 to pH 8 (50 mM phosphate buffer). Image size represents 5 x 5 µm. The arrow in figure a points at two laterally associated fibrils.

Surprisingly, the rate at which self-assembling fibrils grow is independent of the size of the random coil block. Figure 5.3 shows an initial growth (length vs time) that is nearly linear with a steadily increasing width of the size distribution for both newly constructed proteins as

well as for $C_2S^H_{48}C_2$. Apparently, the rate of self-assembly is determined by the size of the silk-like block [34] rather than by the size of the repulsive C-block. The docking and folding of the silk-like block is the rate determining step in self-assembly of these molecules. This implies that increasing the size of the silk-like block is the easiest way to speed up self-assembly and decrease the gelation time. An additional advantage of a larger silk-like domain is a possibly increased stiffness of the fibrils, because of the increased size of the compact folded silk-like core. Such an increase in fibril stiffness can enhance gel rigidity.

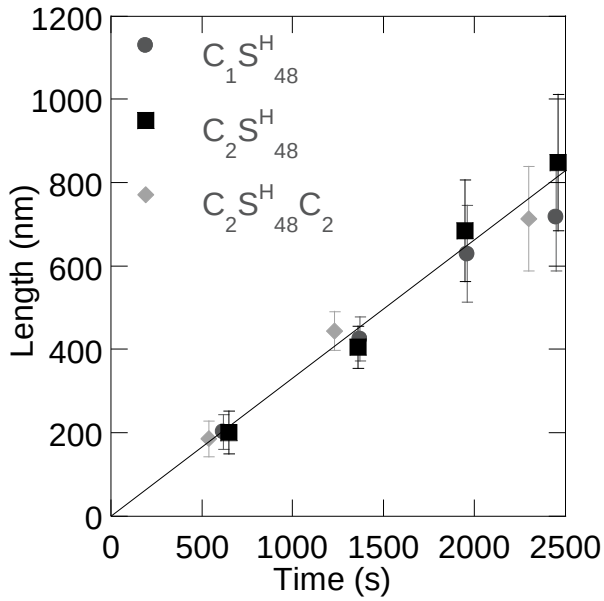

Figure 5.3: Evolution of average fibril length (n = 50-70) in time for three types of protein after incubation at pH 8 (50 mM phosphate buffer) as analyzed with AFM. Each sample contained 7.6 µM of protein. Error bars represent standard deviations.

Circular Dichroism

We performed circular dichroism (CD) measurements to compare the structure of molecularly dissolved $C_1S^H_{48}$ and $C_2S^H_{48}$ at pH 2 and self-assembled protein fibrils at pH 8 and present the data in Figure 5.4. For $C_2S^H_{48}C_2$ we reported earlier a random coil structure in its charged state at low pH [34]. In the self-assembled state at neutral or higher pH the folding of the silk-like block leads to a spectral shift towards that of a betaroll structure [25, 27, 35]. It

appears that at pH 2, not surprisingly, both $C_1S^H_{48}$ and $C_2S^H_{48}$ have spectral signatures that resemble that of $C_2S^H_{48}C_2$. At this pH, the C-block and the silk-like block both have a random coil structure [34]. After incubating solutions containing 0.25 g/L of protein at pH 8 for 96 hours we measured the spectrum again. The spectral shift that we observe is qualitatively very similar for both protein polymers and resembles that of $C_2S^H_{48}C_2$. The change in ellipticity is the largest for $C_1S^H_{48}$. This is due to the fact that a larger fraction of this molecule consists of the silk-like block, and it is this block that changes its secondary structure during self-assembly. Based on these spectra we attribute the same secondary structure to $C_1S^H_{48}$ and $C_2S^H_{48}$, as we did to $C_2S^H_{48}C_2$, namely the betaroll structure of the silk-like block at pH 8, while the C-block remains a random coil.

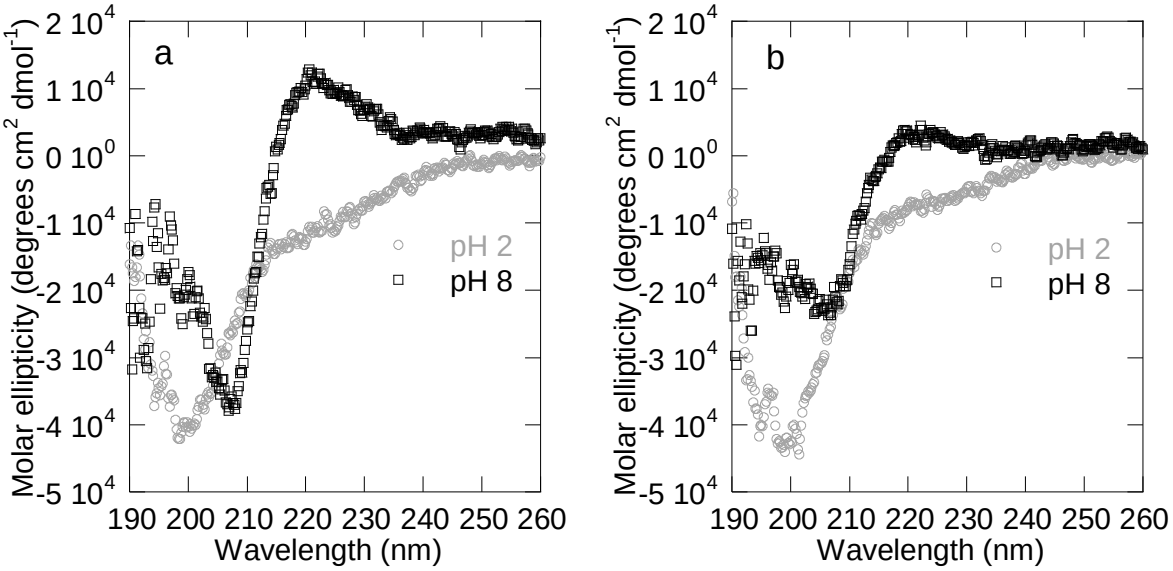

Figure 5.4: Molar ellipticity per amino acid of 0.25 g/L protein-polymer solutions of $C_1S^H_{48}$ (a) and $C_2S^H_{48}$ (b) in 10 mM HCl (pH 2) and 50 mM phosphate buffer (pH 8). Samples at pH 8 have been measured 96 hours after adjusting the pH from pH 2 to pH 8.

Rheology

Our two newly constructed protein polymers, just like $C_2S^H_{48}C_2$, self-assemble into fibrils at pH 8. We expect these protein polymers to form fiber-based hydrogels under similar conditions as $C_2S^H_{48}C_2$. Gel properties of $C_2S^H_{48}C_2$ have already been reported [28]. This protein polymer forms weak hydrogels at concentrations above 10 g/L at neutral or basic pH. We here report the gelation behavior of $C_1S^H_{48}$ and $C_2S^H_{48}$ at pH 8 over time. We monitored the storage modulus at different weight concentrations over a time period up to 48 hours and present these data in Figures 5.5 and 5.6.

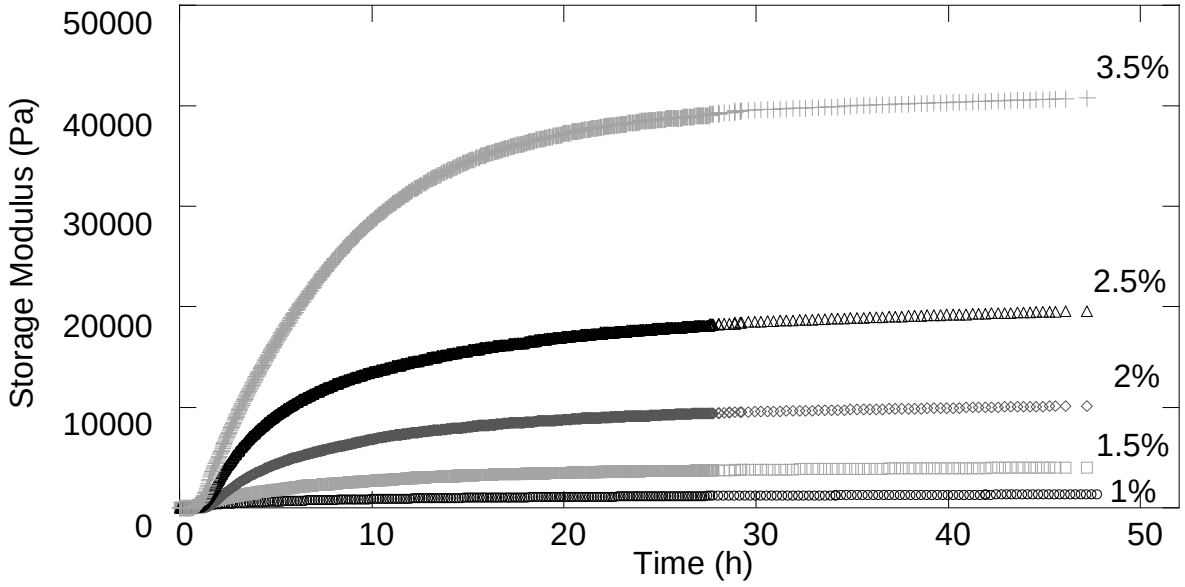

Figure 5.5: Storage moduli of $C_1S^H_{48}$ gels at pH 8 (50mM phosphate buffer) in time for different weight concentrations.

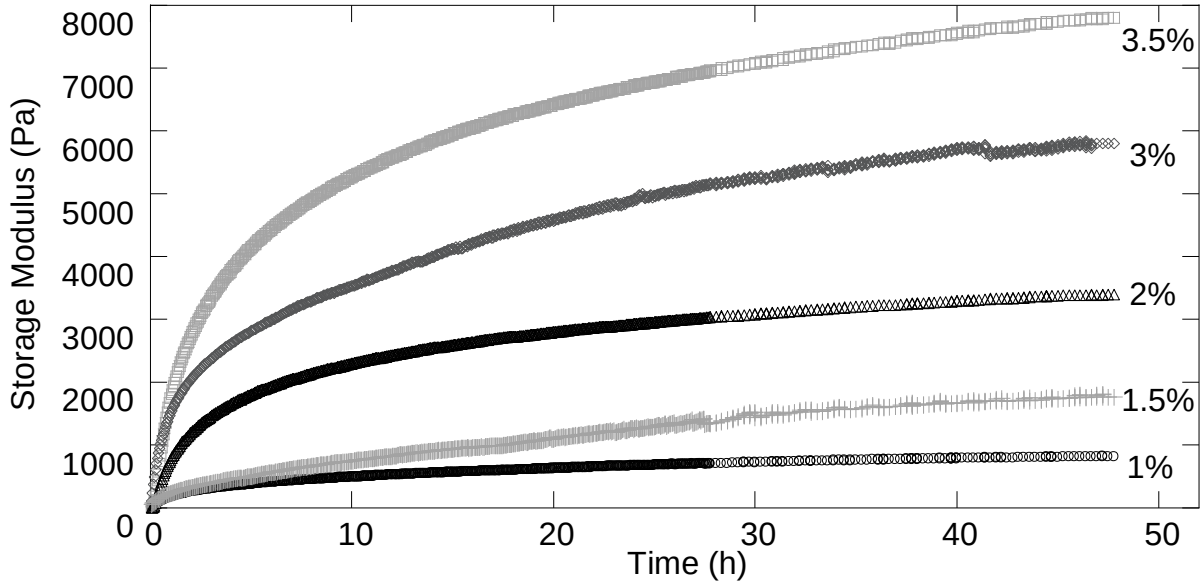

Figure 5.6: Storage moduli of $C_2S^H_{48}$ gels at pH 8 (50mM phosphate buffer) in time for different weight concentrations.

In Figures 5.5 and 5.6 we observe a rather similar gelation behavior for our two protein polymers. The main difference is that $C_1S^H_{48}$ has a short lag time before the storage modulus starts to increase, while $C_2S^H_{48}$ starts gelling instantly. Both gels show a steady increase of their storage moduli during the first few hours followed by a gradual leveling-off. Gels formed by $C_1S^H_{48}$ reach a plateau modulus after 24 hours, while the gels formed by $C_2S^H_{48}$ continue to stiffen for another 24 hours. We attribute this to the difference in interaction among the self-assembled protein fibrils. The weaker fibril-fibril interaction in $C_2S^H_{48}$ gels makes structural rearrangement of fibrils more feasible compared to $C_1S^H_{48}$ gels.

We do observe a major difference in gel rigidity for the two different protein gels. The range of moduli we can obtain with $C_1S^H_{48}$ is much wider than with $C_2S^H_{48}$. We present the dependence of the storage modulus after 48 hours as a function of concentration for both protein gels in Figure 5.7.

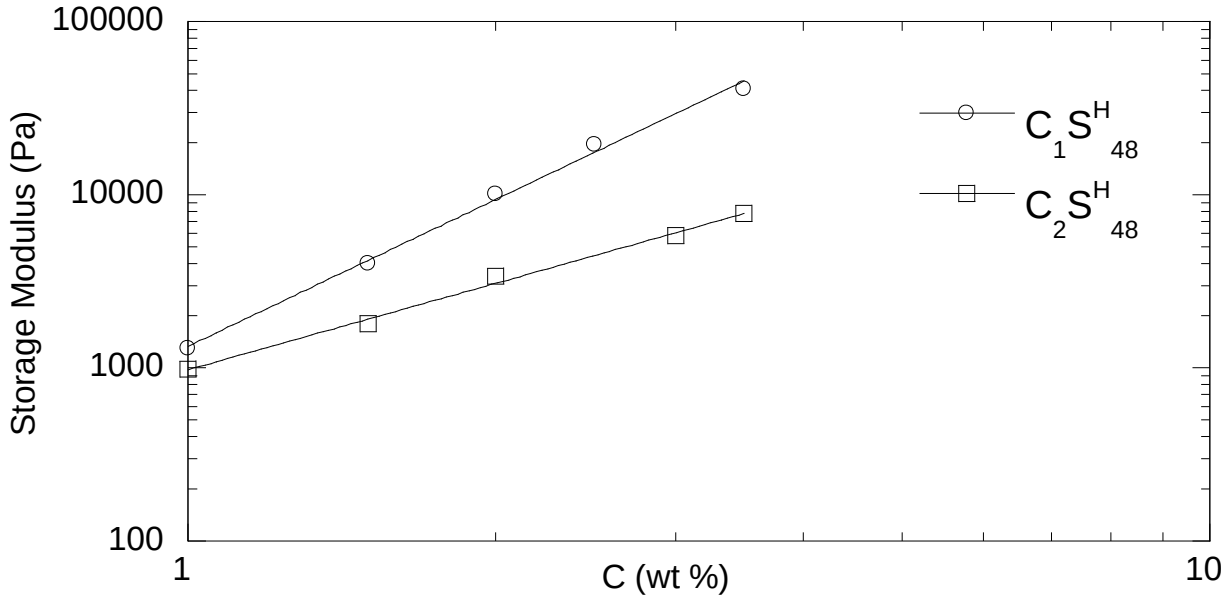

Figure 5.7: Storage modulus as a function of concentration for gels of $C_1S^H_{48}$ and $C_2S^H_{48}$. The lines represent power law fits with an exponent of 2.81 ($C_1S^H_{48}$) and 1.66 ($C_2S^H_{48}$).

Both types of gels show a power law dependency of storage modulus on concentration. The scaling exponent we find for $C_1S^H_{48}$ gels (2.8) is much higher than the one we find for $C_2S^H_{48}$ gels (1.7). The value for $C_2S^H_{48}$ is close to that of $C_2S^H_{48}C_2$ (1.5) [28] and non-cross-linked actin networks (1.4) [36], revealing a fiber-based gel with very few or weak physical cross-links. In this range of concentrations $C_2S^H_{48}$ attains moduli that are roughly a factor 2 higher than those for $C_2S^H_{48}C_{2,}$ which is consistent with the ratio in molar concentrations (corresponding to the total length of fibril), which is a factor 1.4 ($1.4^{1.66} = 2$).

The scaling exponent of $C_1S^H_{48}$ resembles that of natural collagen gels (2.8) [37] and cross-linked actin gels (2.5) [38]. This resemblance indicates that $C_1S^H_{48}$ gels act as networks of (physically) cross-linked fibers. This behavior is very consistent with the image that AFM measurements provide of strongly interacting self-assembled fibrils that can bundle together and form physical crosslinks.

The strength of the hydrogels of $C_1S^H_{48}$ and $C_2S^H_{48}$ was tested by performing a strain sweep after gelation for 48 hours at pH 8 and 298 K. From Figure 5.8 we see that all gels show strain

hardening, which is a typical feature for gels of semiflexible fibers [26, 39]. Both gels become more brittle as the concentration increases, as was reported for $C_2S^H_{48}C_2$ before [28], and which is similar to cross-linked actin gels [38].

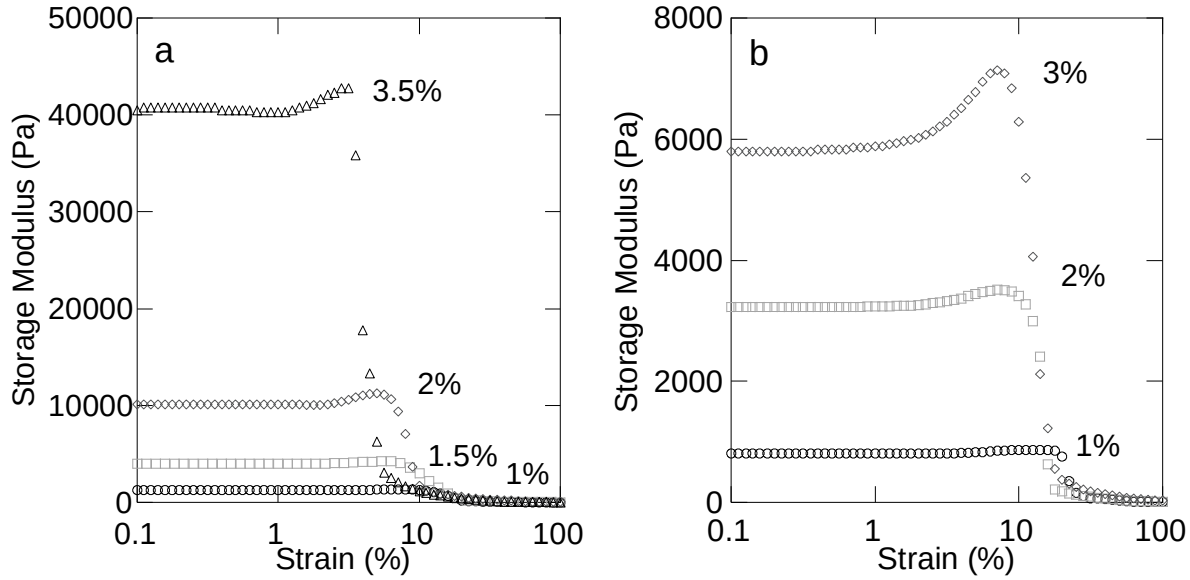

Figure 5.8: Strain sweep after 48 hours of gelation for $C_1S^H_{48}$ (a) and $C_2S^H_{48}$ (b) for different weight concentrations at 1 Hz and 298 K.

We observe that the high stiffness of $C_1S^H_{48}$ comes at a price. These gels break at small deformations, as compared to gels formed by $C_2S^H_{48}$ and $C_2S^H_{48}C_2$. In Figure 5.9 we take a closer look at the relation between stiffness of the gels and their response to strain.

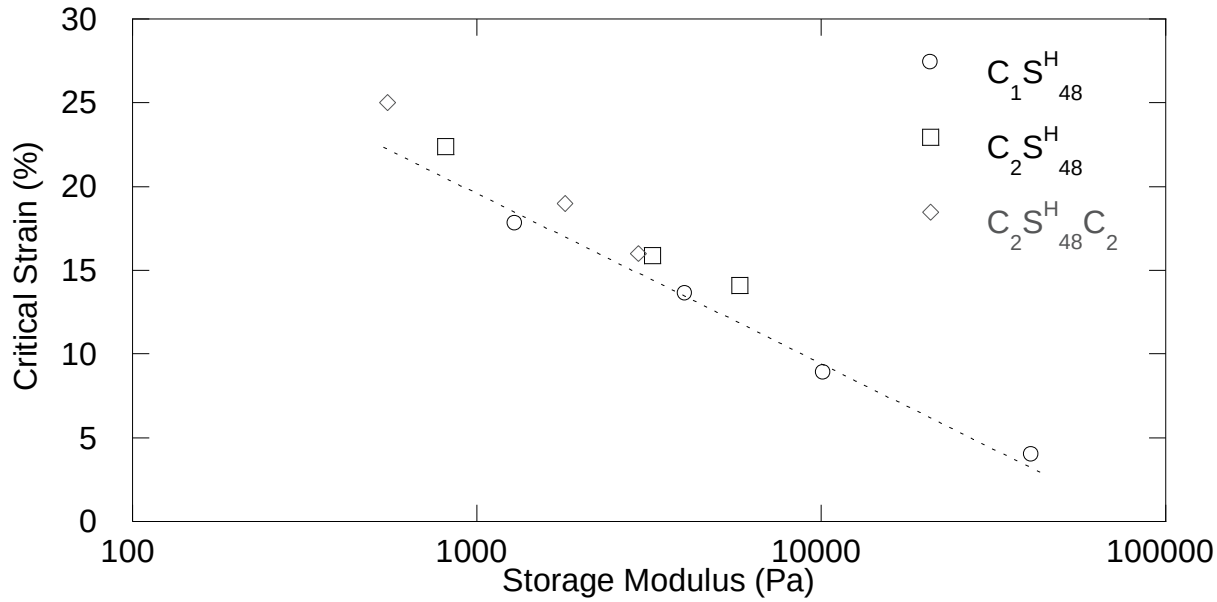

Figure 5.9: Critical strain at which gels break as a function of storage modulus at low strain (linear regime) for three types of protein gels. The dashed line represents a logarithmic fit with exponent 9.5.

We report the critical strain as a function of storage modulus for three types of gels in Figure 5.9. We define the critical strain as the relative deformation at which the storage modulus drops below 50% of the value at low strain (0.1%). All fiber based gels have a logarithmic dependence of critical strain on the storage modulus. $C_2S^H{}_{48}$ and $C_2S^H{}_{48}C_2$ behave nearly identically, while $C_1S^H{}_{48}$ turns out to be slightly more brittle. This difference is another proof that $C_1S^H{}_{48}$ forms a different type of hydrogel than $C_2S^H{}_{48}$ and $C_2S^H{}_{48}C_2$ do.

Pore Size Distribution

In order to make hydrogels that are suitable for 3D cell cultures, the structure of the gel has to be very porous. Ideally the pore size of the gel is similar to the size of human cells in order to provide not only support, but also accessibility. The size of human cells is typically in the range of tens of microns. We estimated pore sizes of our hydrogels by determining the diffusion of fluorescently labelled dextran particles into the gels. Hydrogels of the three protein polymers at different concentrations were covered with solutions of FITC-labelled dextran of different sizes (20 kDa – 2 MDa)[40]. After 2 weeks of incubation, the concentration of dextran in the top layer was determined spectrophotometrically. The concentration of dextran in the gel phase was determined by calculating the depletion of dextran in the liquid top layer. We acquired the dextran partition coefficient by calculating the ratio of the dextran concentration in the gel and in the liquid phase according to:

Partition coefficient = C_{gel} / C_{liquid} (1)

We present the partition coefficient for differently sized particles in our three protein gels at varying concentrations in Figure 5.10.

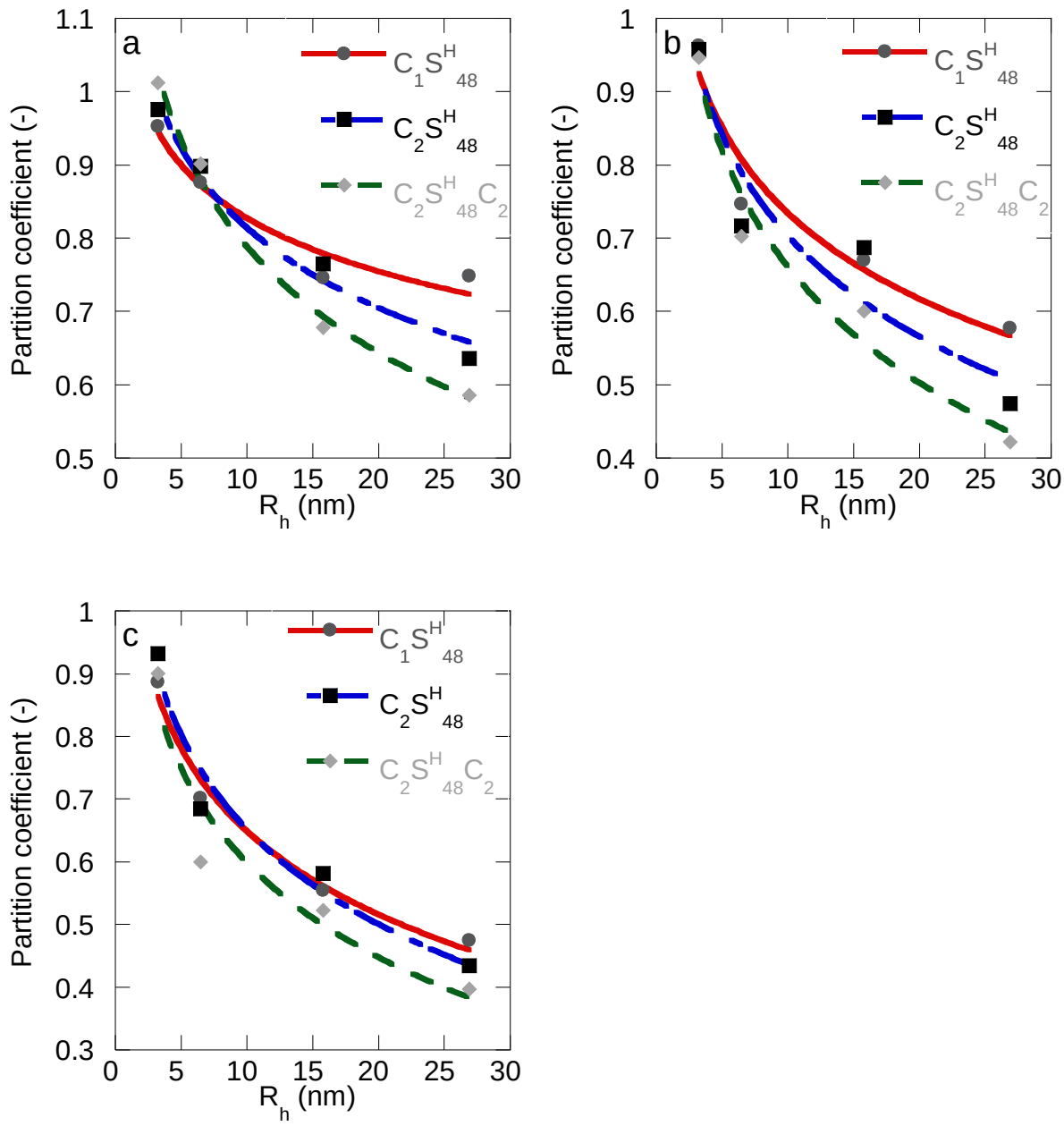

Figure 5.10: Partition coefficients of FITC-labelled dextran particles (R_h 3.2 – 28 nm) in gels of $C_1S^H_{48}$, $C_2S^H_{48}$ and $C_2S^H_{48}C_2$ at pH 8.0 (50 mM phosphate buffer) at different protein weight concentrations: 1% (a), 2% (b) and 3% (c).

Figure 5.10 clearly shows that all gels are fully permeable to dextran particles with a diameter of 6.5 nm. It also shows that a diameter of 13 nm already prevents the dextran particles from completely penetrating the gel. The largest dextran particles with a diameter of 57 nm can only penetrate 40-75% of the gel, depending on gel type and concentration. We

conclude that the pore sizes of all examined gels exceed 6.5 nm, but a significant part of the pores does not exceed 57 nm in diameter. The three different types of protein polymers all show similar partition coefficients at identical weight concentrations. When looking at molar concentrations, the $C_1S^H_{48}$ and $C_2S^H_{48}$ gels are obviously more concentrated than the $C_2S^H_{48}C_2$ gels, with a factor of 1.73 and 1.40 respectively. If we look at particle diffusion at similar gel rigidity, we see that $C_1S^H_{48}$ has a more open structure, because it requires a lower protein concentration to obtain the same modulus than gels from $C_2S^H_{48}$ and $C_2S^H_{48}C_2$. This means that there is a tendency to form more open gel structure with decreasing C-block size. The pore sizes of all tested gels are, however, still too small for 3D cell cultures.

CONCLUSIONS

We constructed two new protein polymers, $C_1S^H_{48}$ and $C_2S^H_{48}$. These two protein polymers were designed to self-assemble into fibrils with partly exposed hydrophobic silk-like cores that can trigger fibril-fibril association. Both form fibrils at the same rate and of the same basic structure as our reference protein polymer $C_2S^H_{48}C_2$. However, we also find that changing the size of the repulsive random coil domain leads to a different type of gel. In $C_2S^H_{48}$, the fibril-fibril interaction is still predominantly repulsive, as it is for $C_2S^H_{48}C_2$. In contrast, for $C_1S^H_{48}$, an attractive interaction shows up, leading to fibril bundling, and a different scaling of gel modulus with concentration. The dominant repulsive fibril-fibril interaction for $C_2S^H_{48}$ leads to a fiber-based gel with few or weak physical crosslinks, while fibrils formed by $C_1S^H_{48}$ are attractive and start bundling. These fibers form much stronger hydrogels that behave as physically cross-linked networks. With our relatively simple change in the protein design we have entered a new regime in which self-assembled fibrils start to strongly interact and bundle together. This new regime opens the possibility for creating highly porous, yet rigid, biocompatible hydrogels that are suitable for 3D cell cultures.

We can further explore this regime by designing protein polymers with even smaller C-blocks. The fact that the size of the C-block does not have any measurable effect on the rate of self-assembly, has an important practical benefit. If this behavior extends to pure silk-like blocks (S^H_{48}), mixing this block with any $C_nS^H_{48}$ protein yields mixed self-assembled fibrils with a C-block density that depends on the concentration ratio of the two proteins. This way, one would only need one cycle of designing and producing/purifying a new protein polymer. With this one new protein polymer S^H_{48}, combined with $C_1S^H_{48}$, we can then cover the entire regime of C-block densities that should include the transition from precipitation to maximum fibril bundling.

EXPERIMENTAL SECTION

Construction of recombinant strains and polymer biosynthesis

A derivative of the previously described vector pMTL23-aII [28] was prepared via gene synthesis (GenScript, Piscataway, NJ) in which no *Ban*I and *Bsa*I sites are present except those originating from the aII adapter. The vector pMTL23ΔBB-aII so obtained was digested with *Dra*III and dephosphorylated. Vectors pMTL23-P and pMTL23-P2 [30] contain the genes referred to here as C_1 and C_2, respectively. These genes encode the ~9 kDa hydrophilic random coil protein C_1, and its ~18 kDa tandem repeat C_2. Vector pMTL23-P was digested with *Dra*III/*Van*91I and the released insert was ligated into the digested pMTL23ΔBB-aII plasmid, which resulted in pMTL23ΔBB-aII-C. Vector pMTL23ΔBB-aII-C_2 was constructed in the same manner using pMTL23-P_2. Gene S^H_{24} [28] encodes 24 repeats of the silk-like sequence $(Gly\text{-}Ala)_3$-Gly-His. The gene was released from vector pMTL23-S^H_{24} via *Acc*I/*Ban*I and reinserted into the same vector digested with *Acc*I/*Bsa*I to yield pMTL23-S^H_{48}. The S^H_{48} insert was then released via *Bsa*I/*Xho*I, and ligated into plasmids pMTL23ΔBB-aII-C_1 and pMTL23ΔBB-aII-C_2 previously digested with *Ban*I/*Xho*I. This resulted in vectors pMTL23ΔBB-aII-C_1-S^H_{48} and pMTL23ΔBB-aII-C_2-S^H_{48}, respectively. The final $C_1S^H_{48}$- and $C_2S^H_{48}$-encoding genes were cloned into expression vector pPIC9 (Invitrogen) via *Eco*RI/*Not*I. Transformation of *Pichia pastoris*, protein production in bioreactors, and polymer purification were as before for $C_2S^H_{48}C_2$ [28].

Purification

The purification of $C_1S^H_{48}$ and $C_2S^H_{48}$ was performed in a similar way as for $C_2S^H_{48}C_2$ [28]. The proteins were selectively precipitated by adding ammonium sulphate to the cell-free fermentation broth. We added ammonium sulphate to 50% saturation and subsequently centrifuged at 8000 g at 4°C for 30 minutes. The precipitate was resuspended in 50 mM

formic acid in 50% of its original volume. Precipitation in 50% ammonium sulphate was repeated once. After a second centrifugation the precipitate was resuspended in 50 mM formic acid in 50 % of the original volume and extensively dialyzed against 10 mM formic acid at 4°C. The dialyzed samples were freeze dried for storage.

MALDI-TOF

MALDI-TOF was performed using an ultrafleXtreme mass spectrometer (Bruker). Samples were prepared by the dried droplet method on a 600 µm AnchorChip target (Bruker), using 5 mg/ml 2,5-dihydroxyacetophenone, 1.5 mg/ml diammonium hydrogen citrate, 25% (v/v) ethanol and 1% (v/v) trifluoroacetic acid as matrix. Spectra were derived from ten 500-shot (1,000 Hz) acquisitions taken at non-overlapping locations across the sample. Measurements were made in the positive linear mode, with ion source 1, 25.0 kV; ion source 2, 23.3 kV; lens, 6.5 kV; pulsed ion extraction, 680 ns. Protein Calibration Standard II (Bruker) was used for external calibration.

SDS-PAGE

Electrophoresis (SDS-PAGE) was performed using the NuPAGE Novex system with 10% Bis-Tris gels, MES-SDS running buffer, and Novex Sharp Protein Standard prestained molecular mass markers. Gels were stained with Coomassie SimplyBlue SafeStain (all Invitrogen).

AFM

AFM samples were made by applying a drop of protein solution on a 10 × 10 mm hydrophilic silicon wafer (Siltronic Corp.) bearing a thin oxide layer, rinsing the wafer with milli-Q water to remove any nonadsorbed material, and drying it under a stream of nitrogen. The samples were analyzed using a Digital Instruments Nanoscope V in ScanAsyst mode and NP-10 silicon nitride tips with a spring constant of 0.350 N/m and a 10 nm tip radius (Bruker, CA, USA). Images were processed using NanoScope Analysis 1.40.

Circular Dichroism

CD measurements were performed on a Jasco J-715 spectropolarimeter at 298 K. The spectra were recorded between 190 and 260 nm with a resolution of 0.2 nm and a scanning speed of 1 nm/s. Each spectrum was an average of 20 measurements. A Quartz cuvette with a path length of 0.5 mm was used. Protein concentration was 0.25 g/L and the solvent was 10 mM HCl (pH 2) or 50mM phosphate buffer (pH 8).

Rheology

Rheological measurements were performed on an Anton Paar MCR 301 rheometer with Couette CC10/TI geometry. Cup and bob radii were 5.420 mm and 5.002 mm respectively. A solvent trap was used to prevent evaporation. Samples containing 10-35 g/L of protein were adjusted to pH 8 in a 50 mM phosphate buffer. Immediately after adjusting the pH the storage modulus was measured using oscillatory deformation ($f = 1$ Hz and $\gamma = 0.1\%$) for 48 hours. After 48 h we performed a strain sweep (0.1% - 100% deformation) at 1 Hz. The temperature was controlled by a Peltier element at 298 K during all measurements.

Pore Size Distribution Measurements

We prepared 1 mL gels of $C_1S^H_{48}$, $C_2S^H_{48}$ and $C_2S^H_{48}C_2$ at different weight concentrations (1%, 2% and 3%) at pH 8 (50mM phosphate buffer). After 72 hours of gelation we deposited 1 mL solutions of FITC-labeled dextran particles of different sizes (20kDa, 70kDa, 500kDa and 2MDa, Sigma-Aldrich) on top of the gels. Absorbance at 488 nm was determined specrophotometrically for all FITC-dextran solutions beforehand. After incubating for 2 weeks, part of the FITC-dextran solution on top of the gels was removed and the absorbance was measured again. All gels had a homogeneous yellow color from FITC after two weeks, indicating that equilibrium was reached. We calculated depletion of FITC-dextran from the solution and thus penetration of FITC-dextran particles into the gel phase.

APPENDIX

YVEFGLGAGAPGEPGNPGSPGNQGQPGNKGSPGNPGQPGNEGQPGQPGQNGQPGE
PGSNGPQGSQGNPGKNGQPGSPGSQGSPGNQGSPGQPGNPGQPGEQGKPGNQGPAG
EGAGAGAGHGAGAGAGHGAGAGAGHGAGAGAGHGAGAGAGHGAGAGAGHGAG
AGAGHGAGAGAGHGAGAGAGHGAGAGAGHGAGAGAGHGAGAGAGHGAGAGAG
HGAGAGAGHGAGAGAGHGAGAGAGHGAGAGAGHGAGAGAGHGAGAGAGHGAG
AGAGHGAGAGAGHGAGAGAGHGAGAGAGHGAGAGAGHGAGAGAGHGAGAGAG
HGAGAGAGHGAGAGAGHGAGAGAGHGAGAGAGHGAGAGAGHGAGAGAGHGAG
AGAGHGAGAGAGHGAGAGAGHGAGAGAGHGAGAGAGHGAGAGAGHGAGAGAG
HGAGAGAGHGAGAGAGHGAGAGAGHGAGAGAGHGAGAGAGHGAGAGAGHGAG
AGAGHGAGAGAGHGAGAGAGHGA

YVEFGLGAGAPGEPGNPGSPGNQGQPGNKGSPGNPGQPGNEGQPGQPGQNGQPGE
PGSNGPQGSQGNPGKNGQPGSPGSQGSPGNQGSPGQPGNPGQPGEQGKPGNQGPAG
EPGNPGSPGNQGQPGNKGSPGNPGQPGNEGQPGQPGQNGQPGEPGSNGPQGSQGNP
GKNGQPGSPGSQGSPGNQGSPGQPGNPGQPGEQGKPGNQGPAGEGAGAGAGHGAG
AGAGHGAGAGAGHGAGAGAGHGAGAGAGHGAGAGAGHGAGAGAGHGAGAGAG
HGAGAGAGHGAGAGAGHGAGAGAGHGAGAGAGHGAGAGAGHGAGAGAGHGAG
AGAGHGAGAGAGHGAGAGAGHGAGAGAGHGAGAGAGHGAGAGAGHGAGAGAG
HGAGAGAGHGAGAGAGHGAGAGAGHGAGAGAGHGAGAGAGHGAGAGAGHGAG
AGAGHGAGAGAGHGAGAGAGHGAGAGAGHGAGAGAGHGAGAGAGHGAGAGAG
HGAGAGAGHGAGAGAGHGAGAGAGHGAGAGAGHGAGAGAGHGAGAGAGHGAG
AGAGHGAGAGAGHGAGAGAGHGAGAGAGHGAGAGAGHGAGAGAGHGAGAGAG
HGAGAGAGHGA

Figure A5.1: Amino acid sequence of $C_1S^H_{48}$ (top) and $C_2S^H_{48}$ (bottom).

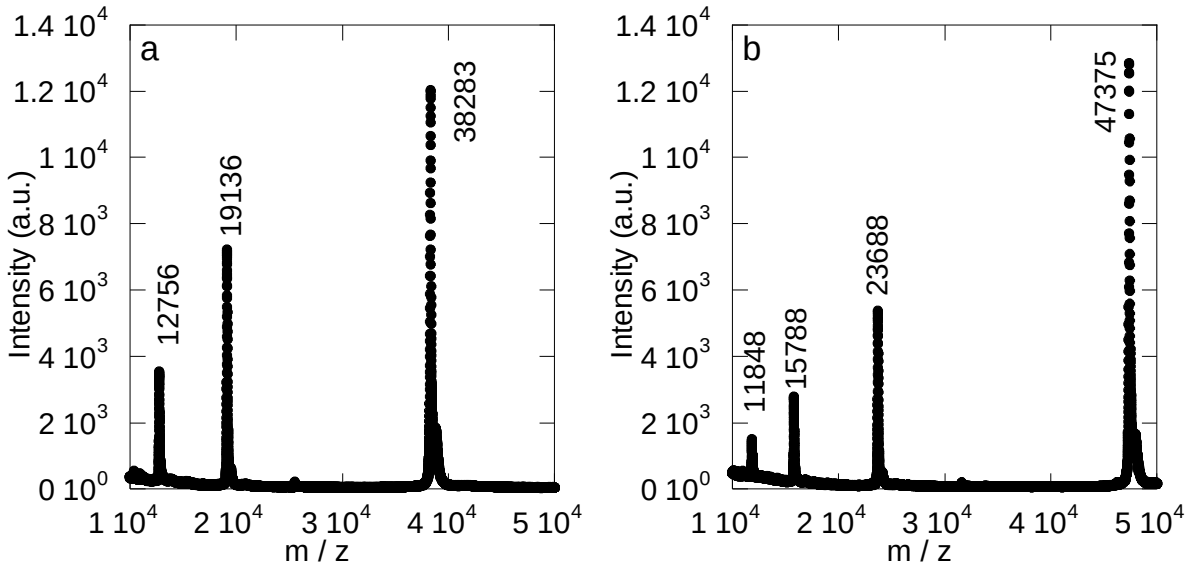

Figure A5.2: MALDI-TOF spectra of $C_1S^H_{48}$ (a) and $C_2S^H_{48}$ (b). The peaks correspond from right to left the $(M + H)^+$, $(M + 2H)^{2+}$, $(M + 3H)^{3+}$ and (only in b) $(M + 4H)^+$.

REFERENCES

1. Baker, E. L.; Bonnecaze, R. T.; Zamao, M. H., Extracellular Matrix Stiffness and Architecture Govern Intracellular Rheology in Cancer. *Biophys J* **2009**, 97, 1013-1021.
2. Forgacs, G.; Newman, S. A.; Hinner, B.; Maier, C. W.; Sackmann, E., Assembly of collagen matrices as a phase transition revealed by structural and rheologic studies. *Biophys J* **2003**, 84, 1272-1280.
3. Tibbitt, M. W.; Anseth, K. S., Hydrogels as Extracellular Matrix Mimics for 3D Cell Culture. *Biotechnol Bioeng* **2009**, 103, 655-663.
4. Geckil, H.; Xu, F.; Zhang, X. H.; Moon, S.; Demirci, U., Engineering hydrogels as extracellular matrix mimics. *Nanomedicine-Uk* **2010**, 5, 469-484.
5. Skardal, A.; Smith, L.; Bharadwaj, S.; Atala, A.; Soker, S.; Zhang, Y. Y., Tissue specific synthetic ECM hydrogels for 3-D in vitro maintenance of hepatocyte function. *Biomaterials* **2012**, 33, 4565-4575.
6. Mintz, B. R.; Cooper, J. A., Jr., Hybrid hyaluronic acid hydrogel/poly(varepsilon-caprolactone) scaffold provides mechanically favorable platform for cartilage tissue engineering studies. *Journal of biomedical materials research. Part A* **2014**, 102, 2918-26.
7. Schulte, V. A.; Hahn, K.; Dhanasingh, A.; Heffels, K. H.; Groll, J., Hydrogel-fibre composites with independent control over cell adhesion to gel and fibres as an integral approach towards a biomimetic artificial ECM. *Biofabrication* **2014**, 6.
8. van Hest, J. C. M.; Tirrell, D. A., Protein-based materials, toward a new level of structural control. *Chem Commun* **2001**, 1897-1904.
9. Omenetto, F. G.; Kaplan, D. L., New Opportunities for an Ancient Material. *Science* **2010**, 329, 528-531.
10. Krejchi, M. T.; Atkins, E. D. T.; Waddon, A. J.; Fournier, M. J.; Mason, T. L.; Tirrell, D. A., Chemical Sequence Control of Beta-Sheet Assembly in Macromolecular Crystals of Periodic Polypeptides. *Science* **1994**, 265, 1427-1432.
11. Krejchi, M. T.; Atkins, E. D. T.; Fournier, M. J.; Mason, T. L.; Tirrell, D. A., Observation of a silk-like crystal structure in a genetically engineered periodic polypeptide. *J Macromol Sci Pure* **1996**, A33, 1389-1398.
12. Smeenk, J. M.; Otten, M. B. J.; Thies, J.; Tirrell, D. A.; Stunnenberg, H. G.; van Hest, J. C. M., Controlled assembly of macromolecular beta-sheet fibrils. *Angew Chem Int Edit* **2005**, 44, 1968-1971.
13. Huang, J.; Foo, C. W. P.; Kaplan, D. L., Biosynthesis and applications of silk-like and collagen-like proteins. *Polym Rev* **2007**, 47, 29-62.
14. Altman, G. H.; Diaz, F.; Jakuba, C.; Calabro, T.; Horan, R. L.; Chen, J. S.; Lu, H.; Richmond, J.; Kaplan, D. L., Silk-based biomaterials. *Biomaterials* **2003**, 24, 401-416.
15. Skrzeszewska, P. J.; de Wolf, F. A.; Werten, M. W. T.; Moers, A. P. H. A.; Stuart, M. A. C.; van der Gucht, J., Physical gels of telechelic triblock copolymers with precisely defined junction multiplicity. *Soft Matter* **2009**, 5, 2057-2062.
16. Werten, M. W. T.; Teles, H.; Moers, A. P. H. A.; Wolbert, E. J. H.; Sprakel, J.; Eggink, G.; de Wolf, F. A., Precision Gels from Collagen-Inspired Triblock Copolymers. *Biomacromolecules* **2009**, 10, 1106-1113.
17. Silva, C. I. F.; Skrzeszewska, P. J.; Golinska, M. D.; Werten, M. W. T.; Eggink, G.; de Wolf, F. A., Tuning of Collagen Triple-Helix Stability in Recombinant Telechelic Polymers. *Biomacromolecules* **2012**, 13, 1250-1258.
18. Daamen, W. F.; Veerkamp, J. H.; van Hest, J. C. M.; van Kuppevelt, T. H., Elastin as a biomaterial for tissue engineering. *Biomaterials* **2007**, 28, 4378-4398.

19. Anumolu, R.; Gustafson, J. A.; Magda, J. J.; Cappello, J.; Ghandehari, H.; Pease, L. F., Fabrication of Highly Uniform Nanoparticles from Recombinant Silk-Elastin-like Protein Polymers for Therapeutic Agent Delivery. *Acs Nano* **2011**, 5, 5374-5382.
20. Koria, P.; Yagi, H.; Kitagawa, Y.; Megeed, Z.; Nahmias, Y.; Sheridan, R.; Yarmush, M. L., Self-assembling elastin-like peptides growth factor chimeric nanoparticles for the treatment of chronic wounds. *P Natl Acad Sci USA* **2011**, 108, 1034-1039.
21. Schipperus, R.; Eggink, G.; de Wolf, F. A., Secretion of elastin-like polypeptides with different transition temperatures by Pichia pastoris. *Biotechnol Progr* **2012**, 28, 242-247.
22. Elvin, C. M.; Carr, A. G.; Huson, M. G.; Maxwell, J. M.; Pearson, R. D.; Vuocolo, T.; Liyou, N. E.; Wong, D. C. C.; Merritt, D. J.; Dixon, N. E., Synthesis and properties of crosslinked recombinant pro-resilin. *Nature* **2005**, 437, 999-1002.
23. Charati, M. B.; Ifkovits, J. L.; Burdick, J. A.; Linhardt, J. G.; Kiick, K. L., Hydrophilic elastomeric biomaterials based on resilin-like polypeptides. *Soft Matter* **2009**, 5, 3412-3416.
24. Lyons, R. E.; Lesieur, E.; Kim, M.; Wong, D. C. C.; Huson, M. G.; Nairn, K. M.; Brownlee, A. G.; Pearson, R. D.; Elvin, C. M., Design and facile production of recombinant resilin-like polypeptides: gene construction and a rapid protein purification method. *Protein Eng Des Sel* **2007**, 20, 25-32.
25. Martens, A. A.; Portale, G.; Werten, M. W. T.; de Vries, R. J.; Eggink, G.; Stuart, M. A. C.; de Wolf, F. A., Triblock Protein Copolymers Forming Supramolecular Nanotapes and pH-Responsive Gels. ***Macromolecules*** 2009, 42, 1002-1009.
26. Martens, A. A.; van der Gucht, J.; Eggink, G.; de Wolf, F. A.; Stuart, M. A. C., Dilute gels with exceptional rigidity from self-assembling silk-collagen-like block copolymers. *Soft Matter* **2009**, 5, 4191-4197.
27. Beun, L. H.; Beaudoux, X. J.; Kleijn, J. M.; de Wolf, F. A.; Stuart, M. A. C., Self-Assembly of Silk-Collagen-like Triblock Copolymers Resembles a Supramolecular Living Polymerization. *Acs Nano* **2012**, 6, 133-140.
28. Golinska, M. D.; Wlodarczyk-Biegun, M. K.; Werten, M. W. T.; Stuart, M. A. C.; de Wolf, F. A.; de Vries, R., Dilute Self-Healing Hydrogels of Silk-Collagen-Like Block Copolypeptides at Neutral pH. *Biomacromolecules* **2014**, 15, 699-706.
29. Werten, M. W. T.; Van den Bosch, T. J.; Wind, R. D.; Mooibroek, H.; De Wolf, F. A., High-yield secretion of recombinant gelatins by Pichia pastoris. *Yeast* **1999**, 15, 1087-1096.
30. Werten, M. W. T.; Wisselink, W. H.; van den Bosch, T. J. J.; de Bruin, E. C.; de Wolf, F. A., Secreted production of a custom-designed, highly hydrophilic gelatin in Pichia pastoris. *Protein Eng* **2001**, 14, 447-454.
31. Golinska, M. D.; Pham, T. T. H.; Werten, M. W. T.; de Wolf, F. A.; Stuart, M. A. C.; van der Gucht, J., Fibril Formation by pH and Temperature Responsive Silk-Elastin Block Copolymers. *Biomacromolecules* **2013**, 14, 48-55.
32. Wlodarczyk-Biegun, M. K.; Werten, M. W.; de Wolf, F. A.; van den Beucken, J. J.; Leeuwenburgh, S. C.; Kamperman, M.; Cohen Stuart, M. A., Genetically engineered silk-collagen-like copolymer for biomedical applications: Production, characterization and evaluation of cellular response. *Acta Biomaterialia* **2014**, 10, 3620-9.
33. Kouwer, P. H. J.; Koepf, M.; Le Sage, V. A. A.; Jaspers, M.; van Buul, A. M.; Eksteen-Akeroyd, Z. H.; Woltinge, T.; Schwartz, E.; Kitto, H. J.; Hoogenboom, R.; Picken, S. J.; Nolte, R. J. M.; Mendes, E.; Rowan, A. E., Responsive biomimetic networks from polyisocyanopeptide hydrogels. *Nature* **2013**, 493, 651-655.
34. Beun, L. H.; Storm, I. M.; Werten, M. W.; de Wolf, F. A.; Cohen Stuart, M. A.; de Vries, R., From Micelles to Fibers: Balancing Self-Assembling and Random Coiling Domains in pH-Responsive Silk-Collagen-Like Protein-Based Polymers. *Biomacromolecules* **2014**, 15, 3349-57.

35. Schor, M.; Martens, A. A.; Dewolf, F. A.; Stuart, M. A. C.; Bolhuis, P. G., Prediction of solvent dependent beta-roll formation of a self-assembling silk-like protein domain. *Soft Matter* **2009**, 5, 2658-2665.
36. Hinner, B.; Tempel, M.; Sackmann, E.; Kroy, K.; Frey, E., Entanglement, elasticity, and viscous relaxation of actin solutions. *Phys Rev Lett* **1998**, 81, 2614-2617.
37. Yang, Y. L.; Leone, L. M.; Kaufman, L. J., Elastic Moduli of Collagen Gels Can Be Predicted from Two-Dimensional Confocal Microscopy. *Biophys J* 2009, 97, 2051-2060.
38. Gardel, M. L.; Shin, J. H.; MacKintosh, F. C.; Mahadevan, L.; Matsudaira, P.; Weitz, D. A., Elastic Behavior of cross-linked and bundled actin networks. *Science* **2004**, 304, 1301-1305.
39. Mackintosh, F. C.; Kas, J.; Janmey, P. A., Elasticity of Semiflexible Biopolymer Networks. *Phys Rev Lett* **1995**, 75, 4425-4428.
40. Armstrong, J. K.; Wenby, R. B.; Meiselman, H. J.; Fisher, T. C., The hydrodynamic radii of macromolecules and their effect on red blood cell aggregation. *Biophys J* **2004**, 87, 4259-4270.

Chapter 6

Summary

In this thesis we present the design and characterization of bio-inspired hybrid protein polymers. All polymers are composed of two distinct types of building blocks. The first type is a silk-inspired block that is pH-responsive and can fold and self-assemble into highly ordered structures. The basic structure of this building block is an octapeptide (GAGAGAGX), denoted S^X. We include multiple repeats n of this octapeptide (S^X_n) in our protein polymers. The amino acid X is always an acidic or basic one. This way, the pH of the solvent determines the charge of this amino acid; in the charged state the silk-like blocks repel each other and the proteins are molecularly dissolved. When charge neutralized, the silk-like blocks become hydrophobic and can fold and stack. The second building block is very hydrophilic and acts as a random coil under a wide range of aqueous solvent conditions. The basic structure of this block is a 99 amino acids long sequence of mostly hydrophilic amino acids, that we included either as a single block or as multimers, denoted C_n. The combination of these two blocks in one molecule leads to a pH-responsive protein polymer that switches from hydrophilic to amphiphilic due to solvent pH. The amphiphilic nature of the neutralized protein polymer leads to microscopic phase separation.

All protein polymers were designed by genetic engineering and produced by genetically modified *Pichia pastoris* in a batch fermentation. A simple ammonium sulfate precipitation was sufficient for all types of proteins to acquire highly pure samples.

The types of hybrid protein polymers we produced and characterized differ in three aspects. Firstly, we designed different silk-like blocks in which the amino acid X had three varieties. We included the acidic amino acid glutamic acid (E) with a pKa ~ 4, to obtain a block that is charged at high pH values and neutral under acidic conditions. We also designed this silk-like block with basic amino acids lysine (K) or histidine (H). These blocks are positively charged under acidic conditions, while being neutral at higher pH. Lysine with a pKa ~ 10 remains charged under slightly alkaline conditions, and is only neutralized at rather extreme pH

values. The pKa of histidine (~ 6) means this is the only pH-responsive amino acid that's almost completely neutral under physiological conditions (a pH of 7.4). This makes histidine the most interesting residue from a biomedical point of view.

The second variety in design is the relative sizes of the two blocks. For any amphiphile, the relative sizes of the two blocks determine the structure that is formed upon self-assembly. The size of the silk-like block was chosen to be 8, 16, 24 or 48 repeats of the octapeptide S^X_N. The random coil block was included as monomer C_1, dimer C_2 or tetramer C_4.

Our third variation in molecular design is the order of the two building blocks. We constructed two diblock structured protein polymers: $C_1S^H_{48}$ and $C_2S^H_{48}$. All other protein polymers had a triblock structure. We constructed $C_2S^X_NC_2$ protein polymers, where the self-assembling silk-like domain was the central block, and $S^X_{24}C_4S^X_{24}$ protein polymers, with telechelic end blocks. All types of protein polymers that we studied are presented in Table 6.1.

Table 6.1: Overview of different protein polymers studied in this thesis.

Telechelic (Ch. 2)	Varying Silk-Like Block (Ch. 3 & 4)	Varying Random Coil Block (Ch. 5)
$S^E_{24}C_4S^E_{24}$	$C_2S^H_8C_2$	$C_1S^H_{48}$
$S^H_{24}C_4S^H_{24}$	$C_2S^H_{16}C_2$	$C_2S^H_{48}$
$S^K_{24}C_4S^K_{24}$	$C_2S^H_{24}C_2$	$C_2S^H_{48}C_2$
	$C_2S^H_{48}C_2$	

In **chapter 2** we report on the self-assembly behavior of triblock structured telechelic protein polymers $S^X_{24}C_4S^X_{24}$. We analyzed the pH-dependent self-assembly into fibrillar structures of three different protein polymers. These proteins only differ in the amino acid X

in the silk-like block. We found that all proteins self-assemble into fibrils under solvent conditions at which the amino acid X is uncharged. This self-assembly is completely reversible; changing the solvent pH to a value at which the amino acid X is fully charged, leads to immediate disassembly of the fibrils. The secondary structures of the fibrils are comparable, and are a combination of a random coil corona and a crystalline folded and self-assembled core. The self-assembly process is a pseudo-first order one. Initial fast (heterogeneous) nucleation is followed by elongation of existing fibrils, without the formation of new fibrils. These kinetics lead to monodisperse samples of fibrils. Existing fibrils have at least one living end: addition of new proteins in solution leads to further growth of these fibrils.

In **chapter 3** we use super resolution fluorescence microscopy and atomic force microscopy to analyze the self-assembly mechanism of the protein polymer $C_2S^H_{48}C_2$. Surprisingly, we found that self-assembly of these fibrils is an asymmetric process. The fibrils grow in only one direction with one living end, although the protein polymer that is the building block of these fibrils is highly symmetric. We therefore conclude that nucleation is a heterogeneous process. We observed that once a protein molecule is part of a fibril, it is kinetically trapped. In a timeframe of 3 days, we don't observe exchange of protein molecules inside fibrils, with proteins in solution. The interactions of uncharged folded protein polymers inside a fibril are simply too strong to overcome to be released into solution. We also report that self-assembly of these fibrils is a process that involves continuous nucleation; elongation of existing fibrils is accompanied by the genesis of new ones. This leads to samples that contain fibrils with a wide variety of sizes, quite different from the populations found for the protein polymers with the inverted block sequence that we presented in chapter 2.

In **chapter 4 and 5** we present our findings on several protein polymers in which we varied the relative sizes of the silk-like block and of the random coil blocks. In **chapter 4** we present

the characterization of protein polymers that have differently sized silk-like domains. We studied 4 protein polymers with the general structure $C_2S^H_nC_2$; the series consisted of n = 8, 16, 24 or 48. The two smallest protein polymers form micelles when charge neutralized (pH 8). The two largest protein polymers form fibrils under these conditions. At low pH, when the silk-like block is highly charged, this block behaves as (extended) random coil, according to circular dichroism measurements. This behavior is consistent for all block sizes that we studied. In the self-assembled state, there is a distinct difference in secondary structure of the micelles and the fibrils. The silk-like core of the micelles has a secondary structure that differs only slightly from the structure in the charged state. It merely acts as a collapsed coil. The secondary structures of the fibril forming protein polymers are very different in neutralized state. Their structures are mutually nearly identical, similar to that of a betaroll.

We observed that the size of the silk-like block has a strong effect on the kinetics of self-assembly. The largest protein polymer $C_2S^H_{48}C_2$ self-assembles into fibrils at a rate that is over a decade faster than the protein polymer with the smaller silk-like block $C_2S^H_{24}C_2$. Both fibril forming protein polymers can form hydrogels. There is however a great difference in rigidity of the gels at similar concentrations. The gel that consists of fibrils of $C_2S^H_{48}C_2$ is a decade stiffer than the one consisting of $C_2S^H_{24}C_2$. This stronger fibril-fibril interaction due to the more exposed silk-like core of $C_2S^H_{48}C_2$ clearly has a strong effect on macroscopic gel properties. We used partial enzymatic degradation of the random coil block to determine the influence of decreasing the hydrophilic block on self-assembly behavior. Both micelle forming protein polymers are able to form fibrils after up to 80% of the random coil blocks has been cleaved off. This shows the intrinsic capacity of the silk-like block to form fibrils even at a size as small as 64 amino acids. The fibrils of $C_2S^H_{24}C_2$ show an increase in interaction after partial cleavage of the random coil block. Individual fibrils start to associate

laterally. This is a strong indication that fibrils with smaller random coil blocks can form more rigid hydrogels, based on their increased core-core interaction.

Based on these findings, we designed two new protein polymers with smaller random coil blocks: $C_1S^H_{48}$ and $C_2S^H_{48}$. With these protein polymers we systematically probe the role of a more exposed silk-like core in gel properties, presented in **chapter 5**. Both proteins self-assemble into fibrils when neutralized. Fibrils of $C_1S^H_{48}$ differ from those of $C_2S^H_{48}$ and $C_2S^H_{48}C_2$ as they start to laterally associate. Surprisingly, the rates at which self-assembling fibrils are formed, are identical for these protein polymers, and also equal to the rate of $C_2S^H_{48}C_2$. Apparently, for these sizes of the blocks, the size of the silk-like block is what determines the rate of self-assembly. These two protein polymers attain secondary structures that are very similar to that of $C_2S^H_{48}C_2$. When looking at macroscopic properties of hydrogels formed by these protein polymers, we do observe a very clear difference. Both $C_2S^H_{48}C_2$ and $C_2S^H_{48}$ form fibril based hydrogels that act as gels with very few (weak) crosslinks. These two gels show similar scaling behavior of modulus with concentration (exponents of 1.52 and 1.66). The attractive interaction of fibrils of $C_1S^H_{48}$ leads to a different type of gel. The modulus of this hydrogel scales strongly with concentration (exponent of 2.8), typical for a (physically) cross-linked gel. The latter gels can have much greater moduli than gels of $C_2S^H_{48}C_2$ and $C_2S^H_{48}$, but are also slightly more brittle. The porosity of the gels (an important parameter for biomedical applications) increases when decreasing the size of the random coil domain. However, for this series of protein polymers, the porosity is in the order of 10-100 nm, which makes these gels not suitable for using them to grow 3D cell cultures.

Chapter 7

General Discussion

SCIENTIFIC RESULTS

The development of recombinant proteins including the silk-like GA-rich domain was pioneered by the groups of Tirrell and Ferrari [1-4]. This work was extended by other researchers, who included this domain in multi-block structured molecules. The groups of Kaplan [5-8] and Van Hest [9-12] have been active in exploring the use of this domain in new materials. Martens et al. engineered amphiphilic protein polymers that consist of the silk-like domain $(GAGAGAGX)_n$ that is pH-responsive and can induce self-assembly, combined with a hydrophilic random coil domain [13, 14]. These protein polymers can self-assemble into fibrils with a ribbon-like structure. The core of these fibrils consists of the folded and highly structured silk-like domain, while on both sides the random coil domain forms a repulsive polymer brush. These structures can form physical hydrogels, which due to their protein-based structure are believed to be biocompatible and suitable for use in tissue engineering.

In this thesis we extend the work of Martens et al. by studying the self-assembly behavior of protein polymers that combine a silk-like domain $(GAGAGAGX)_n$ with a random coil domain C_m. Although our work extends the knowledge on self-assembly behavior of these amphiphilic protein polymers on the molecular scale, as well as the effect of molecular design on macroscopic behavior, there are still several questions that remain to be answered. Here we will address some of these questions, before discussing the promises and challenges of protein polymers, such as the ones we developed.

The structure of the silk-like core in the folded state has been studied extensively for the protein polymer $C_2S^E_{48}C_2$. A combination of Circular Dichroism (CD), Small Angle X-ray Scattering (SAXS)[14] and Molecular Modelling (MD)[15-18] has led to conclude that the structure of the folded and stacked silk-like core, consisting of the octapeptide repeat GAGAGAGE, is that of a betaroll. This structure consists of two beta-sheets that are internally parallel oriented. The orientation of these two beta-sheets towards each other is anti-parallel. At each

turn in the betaroll, there is a polar amino acid, in this case glutamic acid (E). As a consequence, self-assembled fibrils have an array of exposed glutamic acid side chains. Attractive fibril-fibril interaction is therefore mostly due to the interaction of these side chains. The structure of the silk-like block S^{H}_{n}, containing histidine (H) as the pH-responsive amino acid, has only been studied by CD and AFM. CD shows that the structure of the self-assembled silk-like core of GAGAGAGH-containing protein polymers resembles that of the core of self-assembled $C_2S^{E}_{48}C_2$, but is not exactly the same. As a consequence, we do not have detailed information about the way the side chain of histidine is exposed to the solvent in a self-assembled fibril. Acquiring these details may be very beneficial for a better control on fibril-fibril interaction of S^{H}_{n} containing self-assembled protein polymers. This knowledge can be extended by performing SAXS-measurements and doing MD simulations.

The exact mechanism of nucleation of fibrils of our silk-inspired protein polymers remains one of the open questions in our research. The heterogeneity of fibril nucleation implies that sample impurities might have an important effect on nucleation, and, as a consequence, final fibril dimensions. It could prove very useful to study nucleation behavior as a function of extent of purification. If extensive purification can lead to an increased ratio protein:nuclei, this will result in an increase in length of individual fibrils. This could be beneficial for gel properties, leading to lower gelling concentrations and more open hydrogels. An interesting experiment to expand our knowledge on fibril growth would be to break up existing fibrils in a controlled way into at least two pieces. This way, the part of the fibril that contains the living end of the intact fibril, now contains an identical end on the other side. Possibly, this broken up fibril will grow from both directions. Experimentally, two-colored STORM microscopy would be an excellent tool to check this hypothesis. Should this experiment lead to the observation of fibrils growing in two directions, this would be additional proof that fibril nucleation is a heterogeneous process.

We found that self-assembly of $C_2S^H_{48}C_2$ is an asymmetrical process; fibrils only grow from one end (chapter 3). This is surprising, considering the symmetrical nature of the protein polymer itself. However, the symmetry of the protein polymer depends on the amount of coarse graining. When considering the protein polymer as A-B-A triblock, it is indeed perfectly symmetrical. On a more detailed level however, the symmetry becomes less and less. The amino acid orders in the N-terminal and in the C-terminal C-blocks are not mirrored, so on this detailed level the symmetry is broken. The same holds for the silk-like block. It is therefore not unlikely that stacking of the protein polymers inside a self-assembled fibril has a favorable orientation. Possibly, all N-terminal C-blocks are aligned on one side of the fibril, while all C-terminal C-blocks are aligned on the opposite side. Checking this assumption should be fairly straight-forward by means of Förster Resonance Energy Transfer (FRET) microscopy. Upon covalently attaching the FRET-donor on the N-terminus and the FRET-acceptor on the C-terminus (or vice versa), one should obtain a self-assembled mixture of these two populations that should yield fluorescent fibrils in the case of non-favorable orientation of the silk-like blocks (N-terminal and C-terminal C-blocks are present on both sides of the fibril). Should there, however, be a uniform orientation of the silk-like blocks, resulting in homogeneous sides of the fibrils, FRET microscopy would hardly visualize any fibrils.

The orientation of the protein polymer inside a self-assembled fibril has no important implication for the triblock structured $C_2S^H_{48}C_2$. Both options would, after all, result in a fibril with a silk-like core and a random coil polymer brush on each side, with matching amino acid composition and density. For asymmetrically sized protein polymers, such as $C_1S^H_{48}$ and $C_2S^H_{48}$, both options would result in rather different fibrils. A uniform orientation of the N-terminus at one side of the fibril would result in asymmetrical fibrils with an exposed silk-like block on one side and the polymer brush of the random coil C-block on the other side. A

random orientation of the silk-like block would result in symmetrical fibrils, with a purely stochastic distribution of C-blocks on each side of the fibril, with matching densities. The former structure likely induces some bending of the fibril, to reduce interaction of the C-blocks.

The kinetic behavior of our protein polymers with S^{H}_{48} as the self-assembling block seems to be independent of the dimensions of the C-block. For the size range we analyzed this means that we can produce fibrils with any desired C-block density: any incoming $C_mS^{H}_{48}C_n$ molecule, irrespective of the value of m and n, will be incorporated with the same probability. This can be achieved by simply mixing protein polymers with differently sized C-blocks at pre-determined ratios. It also implies that the addition of small functional domains in the C-block (e.g. cell binding or hormonal domains) will not have a large effect on these kinetics. The fact that the size of this repulsive C-block in the size range $C_1 – C_4$ does not lead to a clear increase in the energy barrier for the docking of protein polymer onto an existing fibril is quite surprising, especially since the repulsive nature clearly is visible when looking at fibril-fibril interaction. It seems that folding of a protein polymer can only occur at the end of a growing fibril. The folding protein polymer therefore has to have a high affinity for the end of the fibril; attractive interaction of the silk-like blocks then is likely to be the key factor for the rate of self-assembly. This interaction is of course highly dependent on the size of the silk-like blocks. Exploring this docking and folding mechanism can also greatly benefit from MD simulations.

For biomedical applications, the choice of the pH-responsive amino acid is limited to histidine, as this is the only acidic or basic amino acid that is uncharged under physiological conditions (other amino acids could lead to co-assembly into fibrils with oppositely charged polyelectrolytes under these conditions). It might however be interesting to incorporate different amino acids at the terminal position in the octapeptide. In order to preserve the pH-

responsive nature of the protein polymer, at least a fraction of the octapeptides has to include histidine. A possible new composition of the silk-like block could be $(GAGAGAGH)_n(GAGAGAGX)_m$, with strongly hydrophobic amino acids leucine (L) or isoleucine (I) at position X [19, 20]. This may be a route to control fibril-fibril interaction and thereby obtain controlled bundling into fibers. A key factor in choosing the ratio n:m is to prevent self-assembly under acidic conditions, that is to maintain a high enough charge density of the silk-like block. This is necessary to preserve the pH-responsive character of the protein polymer, as well as its solubility during production. Should these protein polymers self-assemble during the production phase, either inside the host organism *P. pastoris* or in the fermentation broth, this is likely to be highly problematic for the yield of the production.

PERSPECTIVE FOR APPLICATION

Stimulus-responsive protein polymers are promising materials for biomedical applications. Their protein-based structure makes these materials biomimetic and therefore more likely to be biocompatible compared to synthetic materials. Furthermore, the route of genetic engineering to produce these protein polymers gives an unprecedented control over molecular design of these polymers, compared to any chemical synthesis. The fact that our hybrid protein polymers make dilute hydrogels under physiological conditions makes them candidates as basic elements for an ECM-mimicking system. This ExtraCellular Matrix is a complex hydrogel that gets its structural integrity from self-assembled fiber-like protein structures [21-24]. This matrix combines rigidity with an open structure that allows cells to migrate and nutrients to diffuse freely. Hydrogels formed by our protein polymers can achieve a wide range of rigidities; they can deliver structural support for 2D cell cultures [25], but they are not yet porous enough for cells to migrate into the gel and form 3D cell cultures.

Cells and tissues have been successfully grown on multiple 2D substrates. These cells however, fail to mimic cells that grow *in vivo* [24]. Expression of tissue-specific genes differs from that of cells in their natural environment. These 2D grown cells will therefore respond differently to external stimuli compared to their *in vitro* counterparts, a complication when using these cells for e.g. toxicity assays. For tissue engineering, a scaffold that can incorporate 3D cell growth is imperative. Grown tissues should have 3D structures and resemble *in vivo* grown tissues. The development of scaffolds that can facilitate 3D cell cultures is therefore highly desirable.

The combination of high porosity and structural integrity is the main challenge when trying to mimic the ECM [24]. In the natural ECM, this combination is obtained by higher order structures. Micrometer sizes fibrils bundle together into long thick stiff fibers. Also in synthetic polymer gels, bundling of individual fibrils into higher order structures can lead to

very porous, yet rigid hydrogels [26]. To obtain these higher order structures, one has to find the fine balance between attraction of the individual fibrils, while fibers consisting of these bundled fibrils have to have a repulsive nature towards one another in order to prevent macroscopic phase separation.

In our work we have made progress in fine-tuning the interaction between self-assembled fibrils of our pH-responsive silk-like protein polymers. Our self-assembled fibrils attract one another more strongly when the random coil block is decreased in size, leading to a different type of hydrogel. To explore this idea further, a well-defined series of even smaller random coil blocks would be useful. Eventually, these may reveal the switching point between maximum fibril-fibril interaction and macroscopic phase separation, the latter already having been observed for the pure silk-like block. This increased fibril-fibril interaction could lead to a controlled bundling into higher order fiber structure. These fibers will likely be longer, thicker and much stiffer than the individual fibrils; they can therefore yield strong and very porous hydrogels.

The pH-responsive character of our protein polymers is beneficial from an application point of view. If the molecular design of these polymers can be adjusted such, that 3D cell cultures can grow in hydrogels formed by them, they could be used as scaffolds for tissue regeneration. The fact that the proteins are molecularly dissolved at moderately low pH and self-assemble under physiological conditions makes them injectable with a syringe. Locally, due to the pH inside the body, self-assembly will rapidly start and gelation will occur. In this way, a minimally invasive procedure will be required to incorporate this gel *in vivo*.

Just as in the real ECM, any ECM mimic can consist of more than a single component. The complex nature of the ECM makes it challenging to mimic, but it can also be used as an inspiration when designing these mimics. We have observed that our one component hydrogels are rather brittle. Hybrid networks that combine the strength of our silk-like protein

polymers with strain resilience of a second component might prove useful in improving this property [27].

The recombinant nature of our protein polymers makes it relatively easy to incorporate additional functional amino acid based domains. These domains can be cell binding domains (such as RGD), hormonal domains (such as BMP-2), antimicrobial peptide domains, or enzymatic domains. Including these domains gives the hydrogel additional functional properties, thereby stimulating cell development in any required direction.

In conclusion, our recombinant protein polymers are promising candidates as stimulus responsive elements to mimic the ECM. Our improved understanding of their bottom up engineering, from molecular design to macroscopic properties, is a useful tool in designing new amino acid based biomaterials with desirable properties.

REFERENCES

1. Cappello, J.; Crissman, J.; Dorman, M.; Mikolajczak, M.; Textor, G.; Marquet, M.; Ferrari, F., Genetic-Engineering of Structural Protein Polymers. *Biotechnol Progr* **1990**, 6, 198-202.
2. Krejchi, M. T.; Atkins, E. D. T.; Waddon, A. J.; Fournier, M. J.; Mason, T. L.; Tirrell, D. A., Chemical Sequence Control of Beta-Sheet Assembly in Macromolecular Crystals of Periodic Polypeptides. *Science* **1994**, 265, 1427-1432.
3. Krejchi, M. T.; Atkins, E. D. T.; Fournier, M. J.; Mason, T. L.; Tirrell, D. A., Observation of a silk-like crystal structure in a genetically engineered periodic polypeptide. *J Macromol Sci Pure* **1996**, A33, 1389-1398.
4. Krejchi, M. T.; Cooper, S. J.; Deguchi, Y.; Atkins, E. D. T.; Fournier, M. J.; Mason, T. L.; Tirrell, D. A., Crystal structures of chain-folded antiparallel beta-sheet assemblies from sequence-designed periodic polypeptides. *Macromolecules* **1997**, 30, 5012-5024.
5. Altman, G. H.; Diaz, F.; Jakuba, C.; Calabro, T.; Horan, R. L.; Chen, J. S.; Lu, H.; Richmond, J.; Kaplan, D. L., Silk-based biomaterials. *Biomaterials* **2003**, 24, 401-416.
6. Jin, H. J.; Fridrikh, S. V.; Rutledge, G. C.; Kaplan, D. L., Electrospinning Bombyx mori silk with poly(ethylene oxide). *Biomacromolecules* **2002**, 3, 1233-1239.
7. Jin, H. J.; Fridrikh, S.; Rutledge, G. C.; Kaplan, D., Electrospinning bombyx mori silk with poly(ethylene oxide). *Abstr Pap Am Chem S* **2002**, 224, U431-U431.
8. Valluzzi, R.; Gido, S. P.; Zhang, W. P.; Muller, W. S.; Kaplan, D. L., Trigonal crystal structure of Bombyx mori silk incorporating a threefold helical chain conformation found at the air-water interface. *Macromolecules* **1996**, 29, 8606-8614.
9. Schon, P.; Smeenk, J. M.; Speller, S.; Heus, H. A.; van Hest, J. C. M., AFM studies of beta-sheet block copolymers at solid surfaces: High-resolution structures and aggregation dynamics. *Aust J Chem* **2006**, 59, 560-563.
10. Smeenk, J. M.; Otten, M. B. J.; Thies, J.; Tirrell, D. A.; Stunnenberg, H. G.; van Hest, J. C. M., Controlled assembly of macromolecular beta-sheet fibrils. *Angew Chem Int Edit* **2005**, 44, 1968-1971.
11. Smeenk, J. M.; Lowik, D. W. P. M.; van Hest, J. C. M., Peptide-containing block copolymers: Synthesis and potential applications of bio-mimetic materials. *Curr Org Chem* **2005**, 9, 1115-1125.
12. Smeenk, J. M.; Ayres, L.; Stunnenberg, H. G.; van Hest, J. C. M., Polymer protein hybrids. *Macromol Symp* **2005**, 225, 1-8.
13. Martens, A. A.; van der Gucht, J.; Eggink, G.; de Wolf, F. A.; Stuart, M. A. C., Dilute gels with exceptional rigidity from self-assembling silk-collagen-like block copolymers. *Soft Matter* **2009**, 5, 4191-4197.
14. Martens, A. A.; Portale, G.; Werten, M. W. T.; de Vries, R. J.; Eggink, G.; Stuart, M. A. C.; de Wolf, F. A., Triblock Protein Copolymers Forming Supramolecular Nanotapes and pH-Responsive Gels. *Macromolecules* **2009**, 42, 1002-1009.
15. Schor, M.; Martens, A. A.; Dewolf, F. A.; Stuart, M. A. C.; Bolhuis, P. G., Prediction of solvent dependent beta-roll formation of a self-assembling silk-like protein domain. *Soft Matter* **2009**, 5, 2658-2665.
16. Schor, M.; Bolhuis, P. G., The self-assembly mechanism of fibril-forming silk-based block copolymers. *Phys Chem Chem Phys* **2011**, 13, 10457-10467.
17. Schor, M.; Vreede, J.; Bolhuis, P. G., Elucidating the Locking Mechanism of Peptides onto Growing Amyloid Fibrils through Transition Path Sampling. *Biophys J* **2012**, 103, 1296-1304.

18. Ni, R.; Abeln, S.; Schor, M.; Stuart, M. A. C.; Bolhuis, P. G., Interplay between Folding and Assembly of Fibril-Forming Polypeptides. *Phys Rev Lett* **2013**, 111.
19. Thomas, P. D.; Dill, K. A., An iterative method for extracting energy-like quantities from protein structures. *P Natl Acad Sci USA* **1996**, 93, 11628-11633.
20. Dosztanyi, Z.; Csizmok, V.; Tompa, P.; Simon, I., The pairwise energy content estimated from amino acid composition discriminates between folded and intrinsically unstructured proteins. *Febs J* **2005**, 272, 360-360.
21. Baker, E. L.; Bonnecaze, R. T.; Zamao, M. H., Extracellular Matrix Stiffness and Architecture Govern Intracellular Rheology in Cancer. *Biophys J* **2009**, 97, 1013-1021.
22. Tibbitt, M. W.; Anseth, K. S., Hydrogels as Extracellular Matrix Mimics for 3D Cell Culture. *Biotechnol Bioeng* **2009**, 103, 655-663.
23. Forgacs, G.; Newman, S. A.; Hinner, B.; Maier, C. W.; Sackmann, E., Assembly of collagen matrices as a phase transition revealed by structural and rheologic studies. *Biophys J* **2003**, 84, 1272-1280.
24. Geckil, H.; Xu, F.; Zhang, X. H.; Moon, S.; Demirci, U., Engineering hydrogels as extracellular matrix mimics. *Nanomedicine-Uk* **2010**, 5, 469-484.
25. Wlodarczyk-Biegun, M. K.; Werten, M. W.; de Wolf, F. A.; van den Beucken, J. J.; Leeuwenburgh, S. C.; Kamperman, M.; Cohen Stuart, M. A., Genetically engineered silk-collagen-like copolymer for biomedical applications: Production, characterization and evaluation of cellular response. *Acta Biomaterialia* **2014**, 10, 3620-9.
26. Kouwer, P. H. J.; Koepf, M.; Le Sage, V. A. A.; Jaspers, M.; van Buul, A. M.; Eksteen-Akeroyd, Z. H.; Woltinge, T.; Schwartz, E.; Kitto, H. J.; Hoogenboom, R.; Picken, S. J.; Nolte, R. J. M.; Mendes, E.; Rowan, A. E., Responsive biomimetic networks from polyisocyanopeptide hydrogels. *Nature* **2013**, 493, 651-655.
27. Rombouts, W. H.; Colomb-Delsuc, M.; Werten, M. W. T.; Otto, S.; de Wolf, F. A.; van der Gucht, J., Enhanced rigidity and rupture strength of composite hydrogel networks of bio-inspired block copolymers. *Soft Matter* **2013**, 9, 6936-6942.

SAMENVATTING

In dit proefschrift beschrijven wij het ontwerp en de karakterisering van bio-geïnspireerde hybride eiwitpolymeren. Alle verschillende polymeren zijn samengesteld uit twee type bouwblokken. Het eerste type blok is op natuurlijk zijde geïnspireerd en vertoont pH-afhankelijk gedrag. Het blok kan opvouwen en zelf-assembleren in zeer geordende structuren. De elementaire structuur van dit blok is een octapeptide (GAGAGAGX), S^X genoemd. We hebben meerdere eenheden n van dit octapeptide (S^X_n) in onze eiwitpolymeren verwerkt. Het aminozuur X is altijd zwak zuur of zwak basisch. Dit zorgt ervoor dat de pH van de oplossing bepaalt wat de lading van het aminozuur is; in de geladen toestand stoten de zijde-achtige blokken elkaar af en bevinden de eiwitpolymeren zich als individuele moleculen in oplossing. Als de lading geneutraliseerd is, zijn de zijde-achtige blokken hydrofoob en kunnen deze vouwen en op elkaar stapelen. Het tweede type blok is zeer hydrofiel en gedraagt zich als een ongeordende kluwen in waterige oplossingen onder verschillende omstandigheden. De elementaire structuur van dit blok is een sequentie van 99 voornamelijk hydrofiele aminozuren. Deze sequentie bouwen we in als enkel blok of als multimeren, genaamd C_n. De combinatie van beide blokken in één molecuul leidt tot een pH-responsief eiwitpolymeer dat, afhankelijk van de pH van de oplossing, hydrofiel of amfifiel is. Het amfifiele karakter van het ladingsneutrale eiwitpolymeer leidt tot microscopische fasescheiding.

Alle eiwitpolymeren in deze studie zijn ontwikkeld met gebruik van moleculair biologische technieken. De eiwitpolymeren zijn geproduceerd door de genetisch gemodificeerde gist *Pichia pastoris* gedurende een fermentatie. Een simpele ammoniumsulfaat neerslagreactie is voldoende om zeer zuivere eiwitmonsters te verkrijgen.

De types hybride eiwitpolymeren die we hebben geproduceerd en gekarakteriseerd verschillen in 3 aspecten. Ten eerste hebben we 3 verschillende zijde-achtige blokken ontworpen met verschillende aminozuren op positie X in het octapeptide. We hebben het zwak zure aminozuur glutaminezuur (E) gebruikt met een pKa ~ 4, om een blok te verkrijgen dat geladen is bij hoge pH waarden en ongeladen onder zure omstandigheden. We hebben ook zijde-achtige blokken ontworpen met basische aminozuren lysine (K) of histidine (H). Deze blokken zijn positief geladen onder zure omstandigheden, terwijl ze neutraal zijn bij neutrale en basische pH. Lysine, met een pKa ~10, blijft geladen onder licht basische condities en ontlaadt pas bij hoge pH waarden. De pKa van histidine (~6) betekent dat dit het enige aminozuur van de drie is, dat ongeladen is onder fysiologische condities (pH 7.4). Voor biomedische toepassing is histidine daarom het meest interessante aminozuur om in het zijde-achtige blok te verwerken.

Het tweede verschil in ontwerp van de eiwitten is een variatie in relatieve groottes van de twee verschillende blokken. Voor elk amfifiel deeltje is de relatieve grootte van het hydrofiele en het hydrofobe blok essentieel voor de structuur die gevormd wordt bij zelf-assemblage. Het zijde-achtige blok is 8, 16, 24 of 48 octapeptides S^X lang. Het hydrofiele blok is ingebouwd als monomeer C_1, dimeer C_2 of tetrameer C_4.

Als derde variatie in moleculair ontwerp hebben we de volgorde van de twee blokken gebruikt. We hebben twee eiwitpolymeren met een diblokstructuur ontworpen: $C_1S^H_{48}$ en $C_2S^H_{48}$. Alle overige eiwitpolymeren hebben een triblokstructuur. We hebben $C_2S^H_XC_2$ eiwitpolymeren ontworpen, met het zelf-assemblerende zijde-achtige blok centraal in de keten. Daarnaast hebben we $S^X_{24}C_4S^X_{24}$ eiwitpolymeren ontworpen, waar aan elk uiteinde van de keten een zijde-achtig blok aanwezig is. In Tabel 6.1 staat een overzicht van alle eiwitpolymeren die we in dit proefschrift beschrijven.

In hoofdstuk 2 beschrijven we de zelf-assemblage van drie eiwitpolymeren met de structuur $S^{X}_{24}C_4S^{X}_{24}$. We hebben de pH-afhankelijke zelf-assemblage in fibrillen geanalyseerd. Het enige verschil tussen deze drie eiwitpolymeren is het aminozuur op locatie X. We laten zien dat alle eiwitpolymeren zelf-assembleren tot fibrillen bij een pH waarbij aminozuur X ongeladen is. Dit proces is volledig reversibel; als de pH van de oplossing veranderd wordt naar een waarde waarbij het aminozuur X geladen is, vallen de fibrillen onmiddellijk uit elkaar in losse moleculen. De secundaire structuur van alle fibrillen is vergelijkbaar; deze is een combinatie van een ongeordende kluwen (de corona) en een kristallijne gevouwen kern. Zelf-assemblage van deze eiwitpolymeren is een pseudo-eerste orde proces. Initiële snelle (heterogene) nucleatie wordt gevolgd door het groeien van de fibrillen, zonder dat hierna nog nieuwe fibrillen ontstaan. Deze kinetiek leidt tot monodisperse populaties van fibrillen. Fibrillen hebben minstens één levend einde: toevoegen van nieuwe eiwitpolymeren leidt tot verdere groei van deze fibrillen.

In hoofdstuk 3 maken we gebruik van superresolutie fluorescentie microscopie en AFM om zelf-assemblage van het eiwitpolymeer $C_2S^{H}_{48}C_2$ te bestuderen. We hebben, onverwacht, gevonden dat dit proces asymmetrisch is. Fibrillen groeien maar in één richting, ondanks de zeer symmetrische structuur van het eiwitpolymeer waaruit de fibrillen bestaan. We concluderen hierdoor dat nucleatie van fibrillen een heterogeen proces is. We hebben waargenomen dat zodra een eiwitpolymeer deel uitmaakt van een fibril, deze kinetisch vastzit. Op een tijdschaal van 3 dagen vindt er geen uitwisseling plaats van eiwitpolymeren in een fibril met eiwitpolymeren in de oplossing of in andere fibrillen. Eenmaal in een fibril is een eiwitpolymeer te sterk gebonden om los te komen. We tonen ook aan dat nucleatie van deze fibrillen een continu proces is; gedurende de zelf-assemblage worden nieuwe fibrillen gevormd, terwijl bestaande fibrillen groeien door het aansluiten van nieuwe eiwitpolymeren.

Dit leidt tot een mengsel van fibrillen met veel verschillende formaten, een duidelijk verschil met de eiwitpolymeren die we in hoofdstuk 2 beschreven.

In hoofdstuk 4 en 5 bespreken we verscheidene eiwitpolymeren, waarin de groottes van de zijde-achtige blokken en de ongeordende blokken gevarieerd zijn. In hoofdstuk 4 karakteriseren we eiwitpolymeren met zijde-achtige blokken die verschillen in grootte. Al deze eiwitpolymeren hebben de generieke structuur $C_2S^H_nC_2$; de serie bestaat uit n = 8, 16, 24 en 48. De twee kleinste eiwitpolymeren zelf-assembleren tot micellen, als deze ladingsneutraal zijn (pH 8). De twee grootste eiwitpolymeren vormen fibrillen bij deze pH. Bij lage pH, als het zijde-achtige blok sterk geladen is, gedraagt dit blok zich als een (uitgestrekte) ongeordende kluwen, zoals te zien is met circulair dichroisme. Dit gedrag strekt zich uit over de hele serie van blokgroottes. Eenmaal geassembleerd is er een duidelijk verschil in secundaire structuur van het zijde-achtige blok in een micel of in een fibril. De zijde-achtige kern van een micel heeft een structuur die nauwelijks verschilt van de ongeordende toestand van een geladen zijde-achtig blok. In deze kern gedraagt het zijde-achtige blok zich als een (compactere) ongeordende kluwen. De secundaire structuur van het zijde-achtige blok in een fibril verschilt zeer van een ongeordende kluwen. Deze structuur is zeer geordend en interpreteren wij als die van een betaroll.

We tonen aan dat de grootte van het zijde-achtige blok een sterk effect heeft op de kinetiek van zelf-assemblage tot fibrillen. Het grootste eiwitpolymeer $C_2S^H_{48}C_2$ assembleert tot fibrillen met een snelheid die zeker een orde van grootte hoger ligt dan eiwitpolymeer $C_2S^H_{24}C_2$. Deze beide eiwitten kunnen hydrogelen vormen. Er is een duidelijk verschil in stevigheid van beide gelen. De gel die bestaat uit fibrillen van $C_2S^H_{48}C_2$ is ruim 10x zo stevig als de gel van $C_2S^H_{24}C_2$. De sterkere fibril-fibril interactie door de meer blootliggende zijde-achtige kern van fibrillen van $C_2S^H_{48}C_2$ heeft een sterk effect op de macroscopische

eigenschappen van de hydrogel. We gebruiken (gedeeltelijke) enzymatische afbraak van het hydrofiele blok om de invloed van de grootte van dit blok op de zelf-assemblage te onderzoeken. Nadat 80% van dit hydrofiele blok is afgebroken, kunnen beide eiwitpolymeren, die intact micellen vormen, nu wel fibrillen vormen. Dit toont aan dat het zijde-achtige blok de intrinsieke neiging bezit om fibrillen te vormen, zelfs bij een grootte van slechts 64 aminozuren. De fibrillen van $C_2S^H_{24}C_2$ laten een sterk verhoogde interactie zien, nadat een deel van de hydrofiele corona is afgebroken. Individuele fibrillen beginnen lateraal te bundelen. Dit is een aanwijzing dat fibrillen met kleinere hydrofiele blokken stevigere hydrogelen kunnen vormen, door sterkere fibril-fibril interactie.

Gebaseerd op de resultaten in hoofdstuk 4 zijn twee nieuwe eiwitpolymeren ontworpen met kleinere hydrofiele blokken: $C_1S^H_{48}$ en $C_2S^H_{48}$. Met deze eiwitpolymeren bekijken we het verband tussen blootstelling van de zijde-achtige kern van de fibrillen, en de eigenschappen van gevormde hydrogelen. Dit werk presenteren we in hoofdstuk 5. Fibrillen die bestaan uit eiwitpolymeren $C_1S^H_{48}$ verschillen van fibrillen gevormd door $C_2S^H_{48}$ en $C_2S^H_{48}C_2$, doordat ze in de lengterichting beginnen te bundelen. Onverwacht, vinden we dat deze drie verschillende eiwitpolymeren met dezelfde snelheid assembleren tot fibrillen. Blijkbaar is het formaat van het zijde-achtige blok cruciaal voor deze snelheid, en niet het formaat van het hydrofiele blok. De secundaire structuur elk van de drie soorten fibrillen is nagenoeg identiek. De macroscopische eigenschappen van de gevormde hydrogelen op basis van deze eiwitpolymeren verschillen wel sterk. Zowel $C_2S^H_{48}C_2$ als $C_2S^H_{48}$ vormt een hydrogel die zich gedraagt als een gel met zeer weinig (zwakke) crosslinks. Voor beide gels schaalt de elastische modulus met concentratie met een vergelijkbare exponent (1.52 en 1.66). De sterkere aantrekking tussen fibrillen van $C_1S^H_{48}$ leidt tot een ander type hydrogel. De elastische modulus van deze gel is sterk afhankelijk van de concentratie eiwitpolymeer (exponent van 2.8), wat typisch is voor een gel met (fysische) crosslinks. Deze gel is bij

vergelijkbare concentraties veel steviger dan die van $C_2S^H_{48}C_2$ en $C_2S^H_{48}$, maar breekt ook eerder. De porositeit van de gelen (een belangrijke eigenschap voor biomedische toepassingen) neemt toe bij een hydrofiel blok dat afneemt in grootte. Voor de serie eiwitpolymeren die wij hebben onderzocht ligt deze grootte tussen de 10 en 100 nm. Dit is nog te klein voor het gebruik van deze hydrogelen als medium om 3D cel culturen in te laten groeien.

LIST OF PUBLICATIONS

This Thesis

Beun, L.H.; Beaudoux, X. J.; Kleijn, J. M.; de Wolf, F. A.; Cohen Stuart, M. A.; Self-Assembly of Silk-Collagen-Like Triblock Copolymers Resembles a Supramolecular Living Polymerization *ACS Nano* **2012**, 6, (1), 133-140

Beun, L.H.; Storm, I. M.; Werten, M. W. T.; de Wolf, F. A.; Cohen Stuart, M. A.; de Vries, R.; From Micelles to Fibers: Balancing Self-Assembling and Random Coil Domains in pH-Responsive Silk-Collagen-Like Protein-Based Polymers *Biomacromolecules* **2014**, 15, 3349−3357

Beun, L.H.; Albertazzi, L.A.; Cohen Stuart, M.A.; de Vries, R.; Super Resolution Microscopy Shows Asymmetrical Self-Assembly of Highly Symmetrical Protein Based Building Blocks *Manuscript in preparation*

Beun, L.H.; Pham, T.H.T; Werten, M.W.T.; de Wolf, F.A.; Cohen Stuart, M.A.; de Vries, R.; Changing Fibril-Fibril Interaction in Self-Assembled Silk-Like Protein Polymers Leads to a Change in Gel Type *Manuscript in preparation*

Other work

Lemmers, M.; Spruijt, E.; **Beun, L.H**.; Fokkink, R.G.; Leermakers, F.A.M.; Portale, G.; Cohen Stuart, M.A.; Gucht, J. van der; The Influence of Charge Ratio on Transient Networks of Polyelectrolyte Complex Micelles *Soft Matter* **2012**, 8, 104 - 117

ACKNOWLEDGEMENT

This chapter is for everybody that has played an important part in my life in the past 5 years. Without you, the road towards my PhD would have been so much bleaker.

Martien, toen ik als oud-student op het lab langskwam om te vragen naar mogelijke promotieplekken kon ik diezelfde middag nog bij jou terecht. Zo is het eigenlijk altijd gegaan. Als je op het lab was, was je altijd beschikbaar voor vragen. Bedankt daarvoor. Bedankt voor de aansporing en hulp om mijn eerste artikel te schrijven. Dat ik deze worsteling al achter de rug had maakte het schrijven van mijn proefschrift zoveel makkelijker. Bedankt voor het opzetten van de samenwerking met Eindhoven. Mooi dat we eindelijk de vraag over de symmetrie van fibrillen hebben kunnen beantwoorden. En bedankt voor je hulp bij de lange eindsprint die het afronden van mijn proefschrift is geworden. Ook al was je al met emeritaat, of misschien wel dankzij, je was elke keer razendsnel met het bekijken en verbeteren van mijn manuscripten.

Mieke, dank je wel voor je begeleiding in mijn eerste twee jaren. Ik denk dat we een mooi artikel hebben weten te publiceren. En ondanks dat de wetenschappelijke samenwerking daarna is gestopt, is het persoonlijk contact gelukkig altijd goed gebleven. Ik heb dat altijd heel erg gewaardeerd.

Renko, dank je wel voor het reanimeren van mijn onderzoek. Ik waardeer het heel erg hoe je altijd met nieuwe ideeën voor onderzoek kwam. Ik heb veel geleerd van je als het aankomt op het adverteren van mijn werk in introducties. Je hebt me helemaal klaargestoomd voor mijn eindsprint. Vanaf het moment dat je met sabbatical ging, heb ik kunnen doorwerken in het lab, omdat we een gedegen onderzoeksplan hadden liggen. We waren er na een lange worsteling in geslaagd om een mooie rode draad in het experimentele werk te ontwikkelen.

Dit zorgde ervoor dat het schrijven van mijn hoofdstukken een heel stuk overzichtelijker werd en geen zaak van eindeloos nieuwe versies heen en weer sturen. Ik ben erg blij dat we uiteindelijk een mooi wetenschappelijk verhaal hebben kunnen opschrijven in mijn proefschrift.

Liever Mara, wat is het een luxe om jou als collega in het lab te hebben. Als ik iets nodig had van de zolder, uit het glasmagazijn, of dat besteld moest worden: ik hoefde het maar te vragen en je stond klaar om het te regelen. Wat was het gezellig om samen de voorste spinningrij te bemannen en zelfs een hele maand lang onze eigen rit te hebben. Wat was het schandalig luxe dat jij mij altijd inschreef. Ik ben heel blij dat jij als grote steun tijdens mijn promotie ook naast mij op het podium als paranimf zult staan.

Lieve Anita, zonder jou had ik dit proefschrift nooit geschreven. Op het moeilijkste punt van mijn promotietraject hebben we samen gelukkig een oplossing voor de problemen kunnen vinden, dank je wel daarvoor. Op dat moment was voor mij al de keuze gemaakt om jou als paranimf te vragen voor de grote dag. Dank je wel ook voor je inspanningen om mij zoveel tijd te laten meedraaien in het onderwijs. Wat is het al die tijd een voorrecht geweest om op universitair niveau les te mogen staan geven.

Josie, dank je wel voor het boeken van mijn tickets en congressen, het luisteren naar mijn geklaag en vrolijke verhalen, en voor alle kleine en grote zaken die je voor me hebt geregeld. En natuurlijk bedankt dat je zo’n mooie datum en tijd voor mijn verdediging hebt weten te regelen.

Evan, Soumi, Thao, I think we put together a great PhD-trip. Thanks for the nice cooperation. Soumi and Harke, thanks for sharing the office with me all those years. I’m glad we had so many laughs, shared advice about Dutch letters, proper English and programming, and shared our frustrations about referees, colleagues and supervisors. Sabine, Christian,

Armando and Yunus, thanks for taking us to California to visit some of the top universities of the world.

Thao, thanks for helping me with my last two fermentations. Let's hope we can finish the story and get a great publication out of it. Natalia, you were always very helpful with my MALDI-TOF measurements, thank you for that. Inge, gelukkig hebben we onder jouw leiding eindelijk die felbegeerde trofee binnengehaald. Dank je wel dat ik met de zijde-reeks kon werken, we hebben daar een mooi artikel over gepubliceerd en het gaf goede inspiratie voor vervolgonderzoek.

Remco, Hannie, Ronald, Anton, bedankt voor alle snelle hulp met welke apparatuur dan ook in het lab. Bert, bedankt dat je de bak met snoep gevuld hield voor de nodige energie en steun als het een zware dag was. Marc en Frits, bedankt voor jullie waardevolle input bij het ontwerpen en produceren van nieuwe eiwitten. Jullie kritische blikken bij manuscripten, vooral bij de onderdelen die niet typisch fysisch chemisch waren, zijn altijd zeer nuttig gebleken.

Lorenzo, thanks for your help and patience with the STORM-experiments. It has been a privilege to work with such a talented scientist.

René, dank je wel voor het vertrouwen om mij alleen voor groepen studenten te zetten om intensief kennis te kunnen maken met het onderwijsvak. Sabine, dank je wel voor de (achteraf gezien misschien wel dubieuze) carrièretip.

Maarten, het heeft me zo ontzettend goed gedaan om je zo te zien opbloeien. Vergeet niet te blijven bloeien!

Thanks to both Gosia's for the memorable trip to Mexico, including our first bribe experience.

To all my other colleagues at FYSKO and Biont: Evan, Marc, Pascal, Yuan, Junyou, Emilia, Paulina, Monika, Katarzyna, Agata, Frank, Duc, Johan, Ran, Juan, Kamuran, Wolf,

Diane, Merve, Marcel, Hande, Cecilia, Rui, Vittorio, Maria, Dmitry, Helène, Nadia, Antsje, Huanhuan, Tingting, Celine, Jacob, Jeroen, Christine, Kathelijne, Liyakat, Hanne, Ties, Ruben, Jan Bart, Joshua, Joris, Marleen, Frans, Jasper, Aldrick, Herman, Willem, Peter, Jan, Hans: thanks for the endless talks, laughs and cakes in the coffee room, inside and outside offices and labs. In all my years at FYSKO, there has never been a dull and lonely day.

Promoveren gebeurt gelukkig niet alleen maar in het lab. Hans, Mark, Thomas: bedankt voor de klaverjasavonden met bijbehorende wij-zij-discussies. Edwin, Janneke, Joep, Saskia: We zien elkaar niet altijd even frequent, maar als we bij elkaar zijn (al dan niet in het bijzijn van Benjamin Ben) is het altijd erg gezellig. Raymond, ook jij mag natuurlijk een deel van de eer opstrijken. Onze inspiratiesessie heeft geweldig geholpen met het inzetten van mijn eindsprint. Ik hoop dat ik je nog vaak op feestjes en vakanties, en wie weet ooit zelfs als collega, mag meemaken. Lotte, Johan, Anna, Maartje, Marjon, het is altijd mooi om jullie te zien bij al onze hoogtepunten: promoties en bruiloften. Ingi en Ellen, bedankt voor al die uren spinninglessen na het werk. En niet te vergeten voor alle bananen tijdens het rijden van de Marmotte! Wolf, Diane, Maarten, bedankt voor het samen spinnen en quizzen.

Lieve mama, dank je wel voor alle zorg en liefde al die jaren. Ik ben heel blij dat je nu in Boxmeer je plek weer hebt gevonden. Ik hoop dat jij en Han daar nog lang samen gelukkig zullen wonen.

Dear Olli, thanks for sharing the past year and a half with me. Thanks for supporting me when I was feeling that the road to my PhD degree seemed endless. Thank you for encouraging me to go to the lab during weekends and evenings and for your help with the layout. I’m grateful that we can start a new adventure in Den Haag together. I hope this new adventure will turn out great for the both of us. Don’t forget to show your beautiful smile to the world every day!

ABOUT THE AUTHOR

Lennart Harm Beun was born on the 8th of November 1983 in Maastricht, the Netherlands. In 2001 he graduated from the Praedinius Gymnasium in Groningen. At Wageningen University, he obtained both his Bachelor and Master degree in Environmental Sciences, specializing in environmental technology. He obtained his Master degree in March 2009. During his master studies he completed two theses and one internship. His first thesis was performed at the department of Physical Chemistry & Colloid Science, Wageningen University. This thesis focused on the potential of polymer brushes as anti-fouling coatings on membranes in high salt environments. His second thesis was performed at the department of Environmental Technology, Wageningen University. In this thesis he designed a prototype to harvest energy from mixing salt and fresh water using capacitative storage technology. During his internship at BECO Cape Town, in Cape Town, South Africa, he focused on implementing clean technologies in several industries. In July 2009 he started as a PhD candidate at the department of Physical Chemistry & Colloid Science, Wageningen University. He worked in the project Modular Protein Polymers under Prof. Dr. Martien Cohen Stuart, a project financed by the National Research Organisation (NWO). The results of the research within this project are presented in this thesis. During the course of his period as PhD candidate, he worked as a teacher at the department for over a year. Since January 2015, he has been working as a chemistry teacher at Gymnasium Haganum in The Hague, while learning for his teaching degree in the government excellence program Onderwijstraineeship.

TRAINING ACTIVITIES

Discipline specific

Advanced Soft Matter	Wageningen	2009
Han-sur-Lesse Winterschool	Han-sur-Lesse, Belgium	2010
Soft Matter Day	Wageningen	2010
Soft Matter Day	Leiden	2010
Soft Matter Day	Wageningen	2012
Dutch Polymer Days (oral)	Lunteren	2012
Gordon Research Conference (poster)	Davidson, United States	2012
Colloid Science Day (poster)	Wageningen	2013
Dutch Polymer Days	Lunteren	2013

General

PhD competence assessment	Wageningen	2010
VLAG PhD week	Wageningen	2010
Teaching and supervising thesis students	Wageningen	2010
Scientific Writing	Wageningen	2011
Project and Time Management	Wageningen	2012
Theatrical Skills in Education	Wageningen	2013

Optionals

Writing Research Proposal	Wageningen	2009
Organizing PhD-trip	Wageningen	2010-2011
PhD-trip (2x oral)	Singapore, Malaysia, Vietnam	2011
PhD-trip (2x oral)	United States	2013